

AD-A259 040



AFIT/GE/ENC/92D-1

①

Theory and Implementation of Wavelet Analyses
in Rational Resolution Decompositions

THESIS

Bruce P. Anderson
Captain, USAF

AFIT/GE/ENC/92D-1

DTIC
S ELECTE D
JAN 08 1993
B

0/2223
93-00154



162

Approved for public release; distribution unlimited

93 1 04 094

AFIT/GE/ENC/92D-1

Theory and Implementation of Wavelet Analyses
in Rational Resolution Decompositions

THESIS

Presented to the Faculty of the School of Engineering
of the Air Force Institute of Technology
Air University
In Partial Fulfillment of the
Requirements for the Degree of
Master of Science in Electrical Engineering

Bruce P. Anderson, B.S.E.E, M.S.
Captain, USAF

December, 1992

Approved for public release; distribution unlimited

Preface

The *rational resolution analysis* introduced in this thesis is a very small part of the revolutionary mathematical theory of *wavelets*. The *rational resolution analysis* synthesizes the work of Mallat, Daubechies, and Vaidyanathan to present a multiresolution-like analysis which is based on rational dilation factors. It presents a framework within which the multiresolution and integer-resolution analyses exist.

This work was sponsored by the Department of Defense, Ft. Meade MD, under contract number H98230-R5-92-9740.

I would like to thank Dr. Tim Anderson, Dr. Mark Oxley, and Maj Steve Rogers, PhD., who served on my committee and provided useful suggestions in this thesis. I would especially like to thank my advisor, Maj Greg Warhola, PhD., for his exceptional inspiration and guidance. It is not often that I meet someone so dedicated to excellence and adverse to mediocrity. Finally, I would like to thank my fiancé, Julie Phipps, whose humor, patience, support, understanding, and love were key to the successful completion of this thesis.

Bruce P. Anderson

DTIC QUALITY INSPECTED 1

Accession For	
NTIS GRA&I	<input checked="checked" type="checkbox"/>
DTIC TAB	<input type="checkbox"/>
Unannounced	<input type="checkbox"/>
Justification	
By	
Distribution/	
Availability Codes	
Dist	Avail and/or Special
A-1	

Table of Contents

	Page
Preface	ii
Table of Contents	iii
List of Figures	vi
List of Tables	x
Abstract	xii
 I. Introduction	 1-1
1.1 Background	1-1
1.2 Problem Statement	1-1
1.3 Scope	1-2
1.4 Approach/Methodology	1-3
1.5 Objectives	1-3
1.6 Equipment and Materials	1-3
1.7 Notation	1-4
1.8 Preview	1-5
 II. Background	 2-1
2.1 Introduction	2-1
2.2 Mathematical Foundations of Wavelets	2-1
2.3 Multiresolution Analyses	2-3
2.4 Filter Operations and the Multiresolution Analyses	2-8
2.5 Scaling Functions and Wavelets	2-11
2.6 Multirate Discrete-Time Signal Processing	2-13
2.7 Rational Resolution Analysis	2-16

	Page
III. Integer-Based Compactly Supported Scaling Functions and Wavelets . .	3-1
3.1 Introduction	3-1
3.2 Compactly-Supported Scaling Functions	3-1
3.3 Alias-Component Matrix Decomposition	3-5
3.4 Compactly-Supported Wavelets	3-11
IV. Rational Resolution Wavelet Analyses	4-1
4.1 Introduction	4-1
4.2 Rational Resolution Approximation	4-1
4.3 Rational Resolution Reconstruction	4-9
4.4 Scaling functions and Perfect Reconstruction	4-13
4.5 Spline-based Scaling Functions and Perfect Reconstruction .	4-23
4.6 Frequency Domain Interpretation of the RRA	4-28
4.7 Conclusions	4-31
V. Applications	5-1
5.1 Introduction	5-1
5.2 Time-Frequency Characteristics	5-1
5.3 Speech Processing	5-9
5.4 Impulse Response Error Analysis	5-16
5.5 Conclusions	5-19
VI. Conclusions and Recommendations	6-1
6.1 Introduction	6-1
6.2 Major Points and Evaluation of Objectives	6-1
6.3 Recommendations	6-2
6.4 Conclusion	6-4

	Page
Appendix A. Generating Scaling Functions and Wavelets	A-1
A.1 Introduction	A-1
A.2 Mathematical Foundations	A-1
A.3 Scaling Function and Wavelet Support	A-2
A.4 Plotting	A-4
Appendix B. Calculation of Inner Products	B-1
B.1 Introduction	B-1
B.2 Scaling Function Approximations and Integration	B-1
B.3 Inner Products between Scaling Functions with Different Dila- tions	B-2
Appendix C. Compactly-Supported Scaling Function Coefficients	C-1
Appendix D. Plots of Compactly-Supported Scaling Functions	D-1
Vita	VITA-1
Bibliography	BIB-1

List of Figures

Figure		Page
2.1.	Approximation Spaces and Projection Operations	2-5
2.2.	Illustration of the Dyadic Multiresolution Analysis	2-7
2.3.	Multiresolution Analysis 2-Channel Filter Bank	2-14
2.4.	M-Channel Filter Bank	2-14
3.1.	Frequency Response of $M = 3, N = 2$ Approximation Filter and Un- optimized Detail Filters	3-15
3.2.	Frequency Response of $M = 3, N = 2$ Approximation Filter and Detail Filters with Minimum Stop-Band Energy	3-16
3.3.	$M = 3, N = 2$ (Mid-Pass) Wavelet with Minimum Stop-Band Energy ($\psi(t)$ vs. t)	3-16
3.4.	$M = 3, N = 2$ (High-Pass) Wavelet with Minimum Stop-Band Energy ($\psi(t)$ vs. t)	3-17
3.5.	Unoptimized $M = 3, N = 2$ Wavelet ($\psi(t)$ vs. t)	3-17
3.6.	Unoptimized $M = 3, N = 2$ Wavelet ($\psi(t)$ vs. t)	3-18
4.1.	Block Structure of the Inner Product Matrix	4-7
4.2.	Processing diagram for Rational Resolution Approximations	4-9
4.3.	Summary of Rational Resolution Approximation and Reconstruction	4-11
4.4.	Compactly Supported Scaling Function with $p = 3$ and $N = 2$ ($\phi(t)$ vs. t)	4-14
4.5.	Comparison of $M = 3, R = 2$ Scaling Function with Linear Combina- tion of $1/q$ Dilated Scaling Functions for $p = 3$ and $q = 2$ ($\phi(t)$ vs. t)	4-15
4.6.	RRA Reconstruction of Impulse Function	4-20
4.7.	Sample Signal and Approximate Rational Resolution Reconstruction for $M = 3, R = 2$ Scaling Function	4-21
4.8.	Compactly Supported Scaling Function with $p = 3$ and $R = 3$ ($\phi(t)$ vs. t)	4-23

Figure	Page
4.9. Comparison of $M = 3, N = 3$ Scaling Function with Linear Combination of $1/q$ Dilated Scaling Functions for $p = 3$ and $q = 2$ ($\phi(t)$ vs. t)	4-24
4.10. Sample Signal and Approximate Rational Resolution Reconstruction for $M = 3, R = 3$ Scaling Function	4-25
4.11. Frequency Response for Table 4.1	4-30
5.1. Grey Scale Representation of Rect Function Detail Coefficients for $M = 3, N = 2, p = 3, q = 2, 5$ levels. (Wavelet 1)	5-2
5.2. Grey Scale Representation of Rect Function Detail Coefficients for $M = 3, N = 2, p = 3, q = 2, 5$ levels. (Wavelet 2)	5-3
5.3. Grey Scale Representation of Rect Function Detail Coefficients for $M = 2, N = 2, p = 3, q = 2, 5$ levels.	5-3
5.4. Grey Scale Representation of Rect Function Approximation Coefficients for $M = 3, N = 2, p = 3, q = 2, 5$ levels.	5-4
5.5. Grey Scale Representation of Rect Function Approximation Coefficients for $M = 2, N = 2, p = 2, q = 1, 5$ levels.	5-5
5.6. Chirp Signal	5-5
5.7. Grey Scale Representation of Chirp Function Detail Coefficients for $M = 3, N = 2, p = 3, q = 2, 5$ levels. (Wavelet 1)	5-6
5.8. Grey Scale Representation of Chirp Function Detail Coefficients for $M = 3, N = 2, p = 3, q = 2, 5$ levels. (Wavelet 2)	5-7
5.9. Grey Scale Representation of Chirp Function Detail Coefficients for $M = 2, N = 2, p = 2, q = 1, 5$ levels.	5-7
5.10. Grey Scale Representation of Chirp Function Approximation Coefficients for $M = 3, N = 2, p = 3, q = 2, 5$ levels.	5-8
5.11. Grey Scale Representation of Chirp Function Approximation Coefficients for $M = 2, N = 2, p = 2, q = 1, 5$ levels.	5-8
5.12. 5-level RRA Reconstruction Error for 3 Speakers	5-12
5.13. 3-level MRA Reconstruction Error for 3 Speakers	5-12
5.14. 3-level RRA Reconstruction Error for 3 Speakers	5-13

Figure	Page
5.15. Reconstruction Error for Male and Female Speakers versus Dilation Factor and Threshold Level	5-15
5.16. Comparison of Reconstruction Error for Dilation factors with Constant q	5-17
5.17. Comparison of Reconstruction Error for Dilation factors with Constant p	5-18
A.1. Graphical Construction of a 4-Coefficient, $M=2$ Scaling Function . .	A-3
B.1. Graphical Representation of Inner Product Calculation (Integer Dilation)	B-3
B.2. Graphical Representation of Inner Product Calculation (Rational Dilation)	B-3
D.1. Scaling Function (η_7) for $M = 3$ and $N = 2$	D-1
D.2. Scaling Function (η_7) for $M = 3$ and $N = 3$	D-2
D.3. Scaling Function (η_7) for $M = 3$ and $N = 4$	D-2
D.4. Scaling Function (η_7) for $M = 3$ and $N = 5$	D-3
D.5. Scaling Function (η_7) for $M = 3$ and $N = 6$	D-3
D.6. Scaling Function (η_7) for $M = 3$ and $N = 7$	D-4
D.7. Scaling Function (η_5) for $M = 4$ and $N = 2$	D-4
D.8. Scaling Function (η_5) for $M = 4$ and $N = 3$	D-5
D.9. Scaling Function (η_5) for $M = 4$ and $N = 4$	D-5
D.10. Scaling Function (η_5) for $M = 4$ and $N = 5$	D-6
D.11. Scaling Function (η_5) for $M = 4$ and $N = 6$	D-6
D.12. Scaling Function (η_4) for $M = 5$ and $N = 2$	D-7
D.13. Scaling Function (η_4) for $M = 5$ and $N = 3$	D-7
D.14. Scaling Function (η_4) for $M = 5$ and $N = 4$	D-8
D.15. Scaling Function (η_4) for $M = 5$ and $N = 5$	D-8
D.16. Scaling Function (η_4) for $M = 5$ and $N = 6$	D-9

Figure	Page
D.17. Scaling Function (η_4) for $M = 6$ and $N = 2$	D-9
D.18. Scaling Function (η_4) for $M = 6$ and $N = 3$	D-10
D.19. Scaling Function (η_4) for $M = 6$ and $N = 4$	D-10
D.20. Scaling Function (η_4) for $M = 6$ and $N = 5$	D-11
D.21. Scaling Function (η_4) for $M = 6$ and $N = 6$	D-11
D.22. Scaling Function (η_3) for $M = 7$ and $N = 2$	D-12
D.23. Scaling Function (η_3) for $M = 7$ and $N = 3$	D-12
D.24. Scaling Function (η_3) for $M = 7$ and $N = 4$	D-13
D.25. Scaling Function (η_3) for $M = 7$ and $N = 5$	D-13
D.26. Scaling Function (η_3) for $M = 8$ and $N = 2$	D-14
D.27. Scaling Function (η_3) for $M = 8$ and $N = 3$	D-14
D.28. Scaling Function (η_3) for $M = 8$ and $N = 4$	D-15
D.29. Scaling Function (η_3) for $M = 8$ and $N = 5$	D-15
D.30. Scaling Function (η_3) for $M = 9$ and $N = 2$	D-16
D.31. Scaling Function (η_3) for $M = 9$ and $N = 3$	D-16
D.32. Scaling Function (η_3) for $M = 9$ and $N = 4$	D-17
D.33. Scaling Function (η_3) for $M = 9$ and $N = 5$	D-17
D.34. Scaling Function (η_3) for $M = 10$ and $N = 2$	D-18
D.35. Scaling Function (η_3) for $M = 10$ and $N = 3$	D-18
D.36. Scaling Function (η_3) for $M = 10$ and $N = 4$	D-19
D.37. Scaling Function (η_3) for $M = 10$ and $N = 5$	D-19
D.38. Scaling Function (η_3) for $M = 11$ and $N = 2$	D-20
D.39. Scaling Function (η_3) for $M = 11$ and $N = 3$	D-20
D.40. Scaling Function (η_3) for $M = 11$ and $N = 4$	D-21
D.41. Scaling Function (η_3) for $M = 11$ and $N = 5$	D-21

List of Tables

Table		Page
3.1.	Filter Coefficients for $M = 3$ Scaling Filter with 2 Degrees of Regularity	3-4
3.2.	Unoptimized Detail Filter Coefficients for $M = 3$ and $N = 2$	3-13
3.3.	Optimized Detail Filter Coefficients for $M = 3$ and $N = 2$	3-15
4.1.	Rational Approximation Filter Coefficients	4-17
4.2.	Rational Approximation Impulse Response Coefficients with $p = 3$ and $q = 2$	4-17
4.3.	Detail Coefficients	4-17
4.4.	Approximate Reconstruction Filter Coefficients	4-17
4.5.	Comparison of True Approximation Coefficients and Approximate Approximation Coefficients	4-18
4.6.	Impulse Response Coefficients for a Rational Resolution Using the $M = 3$, $R = 2$ Scaling Function	4-19
4.7.	Impulse Response Coefficients for a Rational Resolution Using the $M = 3$, $R = 3$ Scaling Function	4-22
C.1.	$M = 3$ Scaling Function Coefficients	C-2
C.2.	$M = 4$ Scaling Function Coefficients	C-3
C.3.	$M = 5$ Scaling Function Coefficients	C-4
C.4.	$M = 5$ Scaling Function Coefficients (continued)	C-5
C.5.	$M = 6$ Scaling Function Coefficients	C-6
C.6.	$M = 6$ Scaling Function Coefficients (continued)	C-7
C.7.	$M = 7$ Scaling Function Coefficients	C-8
C.8.	$M = 7$ Scaling Function Coefficients (continued)	C-9
C.9.	$M = 8$ Scaling Function Coefficients	C-10
C.10.	$M = 8$ Scaling Function Coefficients (continued)	C-11

Table	Page
C.11. $M = 9$ Scaling Function Coefficients	C-12
C.12. $M = 9$ Scaling Function Coefficients (continued)	C-13
C.13. $M = 10$ Scaling Function Coefficients	C-14
C.14. $M = 10$ Scaling Function Coefficients (continued)	C-15
C.15. $M = 10$ Scaling Function Coefficients (continued)	C-16
C.16. $M = 11$ Scaling Function Coefficients	C-17
C.17. $M = 11$ Scaling Function Coefficients (continued)	C-18
C.18. $M = 11$ Scaling Function Coefficients (continued)	C-19

Abstract

The multiresolution analysis (MRA) developed by Mallat and Meyer and further discussed by Daubechies is a useful tool in the analysis of sampled signals such as images and speech. This thesis develops the theory and implementation of a rational-resolution analysis (RRA) as an extension of the dyadic MRA for arbitrary rational dilation factors. We present a method to calculate families of compactly-supported scaling functions and wavelets based on arbitrary integer dilation factors and provide examples. The perfect-reconstruction properties of the RRA are discussed and it is demonstrated that the compactly-supported scaling functions and wavelets do not yield perfect-reconstruction. However, the approximate-reconstruction is demonstrated and families of basis functions which do lead to perfect reconstruction are characterized. Finally, comparisons are made between RRAs and conventional MRAs and illustrated with speech signals.

Theory and Implementation of Wavelet Analyses in Rational Resolution Decompositions

I. Introduction

1.1 Background

In recent years a revolutionary mathematical theory, that of wavelets, has emerged and promises to significantly change the face of information processing as it exists today. The theory of wavelets was pioneered by French geophysicist Jean Morlet in the early part of the previous decade as a tool to aid in the signal processing associated with oil exploration. Most practical uses of wavelets in recent years have been based on the work of Stephane Mallat of the Courant Institute. His "multiresolution analysis" provides an efficient mathematical framework for decomposing discrete-time signals at various resolution levels. Multiresolution analyses have begun to take their place beside traditional Fourier techniques as tools in the world of information processing. From these beginnings, wavelets, and multiresolution analyses in particular, have spread to the areas of image processing, pattern recognition, speech processing, information coding, and a myriad of others. While the applications are far reaching in scope, we believe the potential of the theory has yet to be realized.

1.2 Problem Statement

A multiresolution analysis (MRA) is a technique wherein a signal is decomposed into successive approximations. It is related to resolution in the sense that each approximation represents the signal "seen" at a particular resolution. The dilation factor associated with an MRA determines the ratio between the resolutions of adjacent approximations.

Currently, most multiresolution analyses are implemented with dilation factors of 2. The theory of MRAs with other integer and rational dilation factors is also well known[8], though these are not commonly seen in implementation. The desire for a rational resolution analysis (RRA) in which the dilation factor is a non-integer rational number has become apparent in the past decade to aid in the processing of biologically motivated data. For instance, it is now well known that the human ear processes frequency on a logarithmic scale[18]. Although MRAs have a logarithmic frequency interpretation, the RRA may allow the spectrum to be divided into bands which correspond better to those effectively used by the human ear.

This thesis will present a theory of multiresolution analyses based on arbitrary integer and rational dilation factors. Practical implementations of the rational resolution theory will be designed. A comparison of the rational resolution analysis and the dyadic MRA will be made and demonstrated on representative test signals as well as real-world speech signals.

1.3 Scope

This thesis is limited to the following:

1. A brief description of the mathematical theory of wavelets and multiresolution analyses.
2. A development of integer resolution and rational resolution analysis theory.
3. A description of the implementation of integer and rational resolution analyses. This includes a description of scaling functions and wavelets.
4. Development of the tools (design methodology, software, etc...) necessary to implement integer and rational resolution analyses.

5. A comparison between rational and dyadic resolution analyses to demonstrate the features of the RRA.

1.4 Approach/Methodology

The RRA will be developed as an extension of the integer resolution analysis. The integer resolution analysis is presented as a synthesis of the current state of the art in compactly supported scaling functions and wavelets, dyadic MRAs, and multirate signal processing. Once the RRA is developed and implemented, we will demonstrate its use by comparing it to the dyadic case over a range of test signals including human speech.

1.5 Objectives

The four specific objectives of this research are to answer the following questions:

1. Can the theory of dyadic multiresolution analyses be extended for arbitrary integer dilation factors?
2. Can the theory of multiresolution analyses for arbitrary rational dilation factors be developed? Are there any limitations on its implementation?
3. Is the implementation of the rational resolution theory feasible and is it applicable to real-world problems?
4. How does the rational resolution case compare to that of the dyadic? How do they contrast?

1.6 Equipment and Materials

Being mostly theoretical in nature, this thesis requires no special materials or equipment. SPARC 2 workstations are used to support general purpose programming. More specifically, \LaTeX is used to typeset this document. Mathematica is used for numeric

calculations and to generate some of the figures and plots. Gnuplot is also used for some plots. Matlab is used for optimization and minimization. Finally, all general programming is done in the ANSI C programming language.

1.7 Notation

We use the following notation throughout this thesis:

- \mathbb{C} for the set of complex numbers.
- \mathbb{Z} for the set of integers.
- \mathbb{Z}^+ for the set of non-negative integers.
- \mathbb{R} for the set of real numbers.
- \mathbb{Q} for the set of rational numbers.
- $L^2(\mathbb{R})$ for the space of measurable, square-integrable functions:

$$L^2(\mathbb{R}) = \{f : f \text{ is Lebesgue-measurable and } \int_{-\infty}^{+\infty} |f(x)|^2 dx < \infty\}.$$

If $f \in L^2(\mathbb{R})$, f is sometimes referred to as a finite-energy function.

- The inner product of $f, g \in L^2(\mathbb{R})$ will be denoted by

$$\langle f, g \rangle = \int_{-\infty}^{+\infty} f(x)g^*(x)dx,$$

where the asterisk represents complex conjugation.

- $l^2(\mathbb{Z})$ for the space of square-summable sequences:

$$l^2(\mathbb{Z}) = \left\{ a = (\dots, a_{-1}, a_0, a_1, \dots) : a_k \in \mathbb{C}, \sum_{k=-\infty}^{+\infty} |a_k|^2 < \infty \right\}.$$

For matrices and operators \mathbf{A} , we use the following notation:

- $\mathbf{A} = [a(i, j)]_{ij}$ defines a matrix \mathbf{A} whose element in the i -th row and j -th column is given by $a(i, j)$, where a is a function on $\mathbb{Z}^+ \times \mathbb{Z}^+$.
- \mathbf{A}^T for the transpose of the matrix \mathbf{A} .
- \mathbf{A}^* for the complex conjugate of \mathbf{A} . The asterisk will also be used to denote the adjoint operator. The distinction between matrices and operators will be clear from the context.
- \mathbf{A}^\dagger for the transposed conjugate of \mathbf{A} .
- $\tilde{\mathbf{H}}(z)$ denotes $\mathbf{H}^T(z^{-1})$.
- \sum_n will denote the sum over all $n \in \mathbb{Z}$ unless specific limits are given.
- The Fourier transform of f will be denoted by either \hat{f} or F . It is defined as $\hat{f}(\nu) = \int_{-\infty}^{+\infty} f(x) e^{-i2\pi\nu x} dx$ for $f \in L^2(\mathbb{R})$ and as $\hat{f}_k = \sum_n f_n e^{-i2\pi kn}$ for $f \in l^2(\mathbb{Z})$.

1.8 Preview

This thesis is organized as follows: the next chapter presents background material on wavelets and scaling functions, multiresolution analyses, perfect reconstruction multirate filter banks, and rational resolution approximations. While not intended as a tutorial, it will provide a working understanding of the concepts needed to understand integer and rational resolution analyses. It will describe the current state of rational resolution approximations in the literature.

The following chapter presents a development of compactly-supported scaling functions and wavelets based on arbitrary integer dilation factors. It is presented as an extension of the work by I. Daubechies[6] and P.P. Vaidyanathan[26]. It will also discuss the generation of spline-based scaling functions.

In Chapter IV, we present a design for a rational resolution analysis for which we can get perfect reconstruction under certain conditions. We develop the approximation

and reconstruction operations and discuss the role of the scaling function. We conclude the chapter with a discussion of the frequency domain characteristics of the RRA.

Chapter V presents a comparison of the rational resolution analysis to the dyadic multiresolution analysis. Comparisons to the dyadic case are demonstrated in several examples including human speech signals.

We conclude the thesis with a summary of its major points and accomplishments. We draw some conclusions and, of course, make recommendations for future research.

The appendices contain useful information on the techniques used to calculate various numerical values. They also contain scaling function coefficients and the corresponding scaling function graphs.

II. Background

2.1 Introduction

This chapter serves two purposes. First, it is intended to provide background material for the development of the rational resolution analysis and second, it provides a literature review for the many topics discussed later. While not intended as a tutorial, the background material will be discussed in enough detail to give the reader a reasonable understanding of the development.

The chapter is outlined as follows: we first discuss the early beginnings of wavelet analysis, its mathematical foundations, and the continuous wavelet transform. From there we describe the discrete wavelet transform and present the multiresolution analysis. We also discuss compactly supported scaling functions and wavelets. Next, we turn to discrete-time signal processing and its relationship to the multiresolution analysis. This is followed by a description of multirate filter banks and how they are related to integer resolution analyses. Finally, we review the current state of the art for rational resolution analyses. We present the work of two individuals whose research in this area is most applicable.

2.2 Mathematical Foundations of Wavelets

Wavelet theory has a short but rich history. In 1984, Alexander Grossman and Jean Morlet[9] showed that any finite energy function could be decomposed into families of constant-shape wavelets. For $f \in L^2(\mathbb{R})$ the continuous wavelet transform is

$$(Wf)(a, b) = \int_{-\infty}^{\infty} f(t) \psi_{a,b}^*(t) dt, \quad (2.1)$$

where

$$\psi_{a,b}(t) = a^{-1/2} \psi\left(\frac{t-b}{a}\right) \quad (2.2)$$

and the "mother wavelet" ψ is subject to

$$\int_{-\infty}^{\infty} |\xi|^{-1} |\hat{\psi}(\xi)|^2 d\xi < \infty. \quad (2.3)$$

These wavelets are so called because they generally have some oscillatory behavior since Equation 2.3 implies they are zero-mean functions and decay at infinity. These families of wavelets are formed by dilations and translations of the mother wavelet. Morlet was trying to develop a method by which he could analyze non-stationary seismic signals. Fourier analysis was inadequate because of its inability to localize frequencies in time[5] [10]. The short-time Fourier transform (STFT) is only a little better because its time localization properties are poor[19]. The fundamental difference between the STFT and the wavelet transform can be understood in the frequency domain. The STFT effectively divides the frequency spectrum into equal-bandwidth regions while the wavelet transform divides the spectrum into bands which have a constant bandwidth on a logarithmic frequency scale. That is, the wavelet transform uses a small bandwidth for low frequencies and a larger bandwidth for higher frequencies. This is equivalent to having a STFT with a variable sized window, a small window for good time resolution and a large window for good frequency resolution.

We can also describe the continuous wavelet transform by considering the wavelets as basis functions. Equation 2.1 is an inner product which effectively measures the similarity between f and the particular wavelet $\psi_{a,b}$. While the wavelets are a basis for $L^2(\mathbb{R})$, they are not orthogonal and they redundantly represent the signal. However, by discretizing the values of the shift and scale parameters in Equation 2.1, we can define an orthonormal set of wavelets. If we let $a = a_0^m$ and $b = nb_0 a_0^m$ for $m, n \in \mathbb{Z}$, then we can find an orthonormal wavelet basis for some choice of a_0 and b_0 provided certain conditions on ψ are met[7][14][19]. The choice most commonly made is for $a_0 = 2$ and $b_0 = 1$; a_0 is known as the dilation factor.

2.3 Multiresolution Analyses

The discretization of the continuous wavelet transform and the generation of mother wavelets whose dilations and integer translations form an orthonormal basis of $L^2(\mathbb{R})$ naturally leads to the multiresolution analysis (MRA). The multiresolution analysis developed by Mallat[13][12] and Meyer[15] was triggered by the Laplacian pyramid schemes of Burt and Adelson[4]. However, Mallat is primarily given the credit because he developed the fast algorithm which implements it.

An MRA is a set of embedded subspaces V_m such that

$$\cdots \subset V_2 \subset V_1 \subset V_0 \subset V_{-1} \subset V_{-2} \subset \cdots \quad (2.4)$$

These spaces, known as approximation spaces, further satisfy the conditions

$$\bigcap_{m \in \mathbb{Z}} V_m = \{0\} \quad \text{and} \quad \overline{\bigcup_{m \in \mathbb{Z}} V_m} = L^2(\mathbb{R}), \quad (2.5)$$

and with the dilation factor of 2,

$$f \in V_m \iff f(2 \cdot) \in V_{m-1}. \quad (2.6)$$

Furthermore, there must exist a scaling function $\phi \in V_0$ such that $\{\phi_{mn}\}_{n \in \mathbb{Z}}$ forms an unconditional basis for V_m ; i.e.,

$$V_m = \overline{\text{span}\{\phi_{mn}\}_{n \in \mathbb{Z}}}, \quad (2.7)$$

where

$$\phi_{mn}(x) = 2^{-m/2} \phi(2^{-m}x - n). \quad (2.8)$$

The integer translations of ϕ are not necessarily orthogonal, but Daubechies[6] shows that given an unconditional basis, we can find an orthogonal basis with no loss of generality. For simplicity, we will assume orthogonality in this thesis.

Given this definition, we want to demonstrate the role of wavelets. First, we define the detail space W_m as the orthogonal complement of V_m in V_{m-1} . This means

$$W_m \perp V_m, \quad (2.9)$$

$$W_m \subset V_{m-1}, \quad (2.10)$$

and

$$V_m \oplus W_m = V_{m-1}. \quad (2.11)$$

The wavelets are an orthonormal basis for the detail spaces:

$$W_m = \overline{\text{span}\{\psi_{mn}\}_{n \in \mathbb{Z}}}, \quad (2.12)$$

where

$$\psi_{mn}(x) = 2^{-m/2} \psi(2^{-m}x - n). \quad (2.13)$$

The constant $2^{-m/2}$ in the above and in Equation 2.8 normalizes the energy of the corresponding scaling function or wavelet.

Now, we want to describe how a function $f \in L^2(\mathbb{R})$ can be represented as a series of the discretized wavelets ψ_{mn} . Suppose we want to find the approximation of f at the m -th resolution level. This is equivalent to finding the orthogonal projection of f onto V_m . We write

$$P_m f \in V_m \Rightarrow P_m f(t) = \sum_n c_{mn} \phi_{mn}(t), \quad (2.14)$$

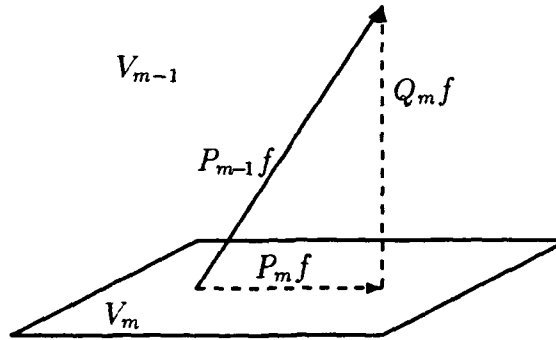


Figure 2.1. Approximation Spaces and Projection Operations

where P_m is the orthogonal projection operator, $P_m : L^2(\mathbb{R}) \rightarrow V_m$, and

$$c_{mn} = \langle f, \phi_{mn} \rangle \quad (2.15)$$

are known as the approximation coefficients. The approximation at level m is entirely characterized by c_{mn} for $n \in \mathbb{Z}$. We can define a similar projection operator to project f onto W_m :

$$Q_m f \in W_m \Rightarrow Q_m f(t) = \sum_n d_{mn} \psi_{mn}(t), \quad (2.16)$$

where the d_{mn} are known as detail coefficients and are defined similarly to the c_{mn} . From these two projections, we can reconstruct the approximation of f at the $m-1$ level by

$$Q_m f + P_m f = P_{m-1} f. \quad (2.17)$$

This is illustrated graphically in Figure 2.1. It is shown in [13] that

$$\bigoplus_m W_m = L^2(\mathbb{R}) \quad (2.18)$$

which implies that all dyadic dilations and translations of the mother wavelet ψ form an orthonormal basis for $L^2(\mathbb{R})$. The multiresolution framework provides an efficient and

elegant algorithm to find the approximation and detail coefficients at each resolution level by using discrete filters on the approximation coefficients of the next higher level. Each successive set of approximation and detail coefficients can be calculated from the previous set of approximation coefficients and this calculation is independent of level.

To see this, consider the scaling function $\phi_{10}(t)$. Because we have $V_1 \subset V_0$, we can express $\phi_{10}(t)$ as a linear combination of ϕ_{0n}

$$2^{-1/2}\phi(t/2) = \sum_n h(n)\phi(t-n), \quad (2.19)$$

where

$$h(n) = \langle \phi_{10}, \phi_{0n} \rangle. \quad (2.20)$$

Taking the Fourier transform of both sides of Equation 2.19 yields

$$\hat{\phi}(2f) = H(f)\hat{\phi}(f), \quad (2.21)$$

where $H(f)$ is the 1-periodic function defined by

$$H(f) = 2^{-1/2} \sum_n h(n) e^{-i2\pi n f}. \quad (2.22)$$

This filter has a great deal of significance in the multiresolution analysis. Mallat demonstrates in [13] that approximation coefficients c_{mn} at one level can be easily calculated from the approximation coefficients of the previous level by using the coefficients of filter H ; specifically,

$$c_{mk} = \sum_n h(n-2k)c_{m-1,n}. \quad (2.23)$$

Notice that the approximation coefficients c_{mn} , which completely characterize the approximation, can be calculated without having to calculate the inner product of f with ϕ_{mn} directly. This is the elegance of Mallat's algorithm.

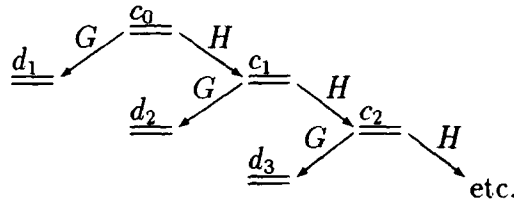


Figure 2.2. Illustration of the Dyadic Multiresolution Analysis

The detail coefficients d_{mn} can also be calculated from the $c_{m-1,n}$ in a similar way.

If we define

$$g(n) = \langle \psi_{10}, \phi_{0n} \rangle, \quad (2.24)$$

then, taking Fourier transforms, we get

$$\hat{\psi}(2f) = G(f)\hat{\phi}(f), \quad (2.25)$$

with $G(f)$ defined similarly to $H(f)$. Now, at each resolution level in a multiresolution decomposition, we get a set of detail coefficients. This is illustrated in Figure 2.2. As the number of decompositions grows without bound, the entire function will be represented by the sets of detail coefficients.

Using the approximation and detail coefficients at a particular resolution level m , we can reconstruct the approximation at the $m-1$ level by using the same filter coefficients:

$$c_{m-1,n} = \sum_k h(n-2k)c_{mk} + \sum_k g(n-2k)d_{mk}. \quad (2.26)$$

This is a consequence of $P_{m-1}f = P_m f + Q_m f$.

2.4 Filter Operations and the Multiresolution Analyses

The filters H and G are very important. However, as Daubechies points out in [6], Mallat's algorithm deals only with sequences; the underlying multiresolution analysis is only used in the computation of the filters H and G . Daubechies studied the filters and determined they had certain properties which allowed Mallat's discrete algorithm to be "weaned" from its multiresolution parent.

By defining \mathbf{H} and \mathbf{G} as bounded operators from $l^2(\mathbb{Z})$ to itself:

$$\begin{aligned} (\mathbf{H}a)_k &= \sum_n h(n-2k)a_n, \\ (\mathbf{G}a)_k &= \sum_n g(n-2k)a_n, \end{aligned} \quad (2.27)$$

Daubechies showed that for these operators, necessary conditions for Mallat's algorithm to work could be expressed as

$$\begin{aligned} \sum_n |h(n)| &< \infty, \\ \sum_n |g(n)| &< \infty. \end{aligned} \quad (2.28)$$

In terms of discrete-time signal processing, this condition is equivalent to requiring the discrete filters defined using the coefficients above to be stable. We want to perfectly reconstruct a sequence from its decomposition, so with the adjoint operators

$$\begin{aligned} (\mathbf{H}^*a)_n &= \sum_k h(n-2k)a_k, \\ (\mathbf{G}^*a)_n &= \sum_k g(n-2k)a_k, \end{aligned} \quad (2.29)$$

we also require

$$\mathbf{H}\mathbf{H}^* + \mathbf{G}\mathbf{G}^* = \mathbf{1}, \quad (2.30)$$

where $\mathbf{1}$ is the identity operator. Similar to the requirement that the detail and approximation spaces be orthogonal, we require

$$\mathbf{H}\mathbf{G}^* = \mathbf{0}. \quad (2.31)$$

Finally, we assign approximation and detail roles to the operators by requiring

$$\begin{aligned} \sum_n h(n) &= \sqrt{2}, \\ \sum_n g(n) &= 0. \end{aligned} \quad (2.32)$$

The four properties described above are identified by Daubechies[6] as the essence of Mallat's algorithm. They are the conditions which allow you to separate the algorithm from the multiresolution analysis (MRA).

These conditions can be restated in many different forms, some of which are more useful for specific applications. One way we will find useful when relating Daubechies' work to others in the discrete-time signal processing field is that of the polyphase representation[25]. The conditions on the operators \mathbf{H} and \mathbf{G} can be rewritten in terms of the coefficients $h(n)$ and $g(n)$. The normality and orthogonality conditions expressed above in Equations 2.30–2.32 can be combined and rewritten as

$$\begin{aligned} \sum_k [h(m-2k)h(n-2k) + g(m-2k)g(n-2k)] &= \delta_{mn}, \\ \sum_n [h(n-2k)g(n-2l)] &= 0, \end{aligned} \quad (2.33)$$

where δ_{mn} is the Kroenecker delta function defined as

$$\delta_{mn} = \begin{cases} 1 & m = n \\ 0 & m \neq n. \end{cases} \quad (2.34)$$

To eliminate the factors of 2, we can define

$$\begin{aligned}
 a_{00}(n) &= h(2n), \\
 a_{01}(n) &= h(2n+1), \\
 a_{10}(n) &= g(2n), \\
 a_{11}(n) &= g(2n+1).
 \end{aligned} \tag{2.35}$$

so that the conditions on the coefficients in Equation 2.33 can be restated as

$$\begin{aligned}
 \sum_k [a_{00}(m-k)a_{00}(n-k) + a_{10}(m-k)a_{10}(n-k)] &= \delta_{mn}, \\
 \sum_k [a_{01}(m-k)a_{01}(n-k) + a_{11}(m-k)a_{11}(n-k)] &= \delta_{mn}, \\
 \sum_k [a_{00}(m-k)a_{01}(n-k) + a_{10}(m-k)a_{11}(n-k)] &= 0, \\
 \sum_n [a_{00}(n-k)a_{10}(n-l) + a_{01}(n-k)a_{11}(n-l)] &= 0.
 \end{aligned} \tag{2.36}$$

In the Fourier domain, these conditions become

$$\begin{aligned}
 |\alpha_{00}(f)|^2 + |\alpha_{10}(f)|^2 &= 1, \\
 |\alpha_{01}(f)|^2 + |\alpha_{11}(f)|^2 &= 1, \\
 \alpha_{00}(f)\overline{\alpha_{01}(f)} + \alpha_{10}(f)\overline{\alpha_{11}(f)} &= 0, \\
 \alpha_{00}(f)\overline{\alpha_{10}(f)} + \alpha_{01}(f)\overline{\alpha_{11}(f)} &= 0,
 \end{aligned} \tag{2.37}$$

where

$$\alpha_{jk}(f) = \sum_n a_{jk}(n)e^{-i2\pi n f} \tag{2.38}$$

for $j, k \in \{0, 1\}$. If we define the matrix \mathbf{E} such that

$$\mathbf{E}^T = \begin{bmatrix} \alpha_{00}(f) & \alpha_{10}(f) \\ \alpha_{01}(f) & \alpha_{11}(f) \end{bmatrix}, \quad (2.39)$$

then it is easy to check that the four conditions on the α_{ij} stated above are equivalent to requiring \mathbf{E} to be unitary. With a little manipulation, we can relate this requirement back to Mallat's original filters $H(f)$ and $G(f)$. Requiring \mathbf{E} to be unitary is equivalent to

$$\begin{bmatrix} H(f) & G(f) \\ H(f + \frac{1}{2}) & G(f + \frac{1}{2}) \end{bmatrix} \quad (2.40)$$

being unitary¹. It is important to note at this point that the conditions expressed above are necessary and sufficient conditions for the Mallat's algorithm to work. However, Mallat originally defined the filter coefficients h and g in terms of the scaling function ϕ and wavelet ψ , respectively, which is to say that placing requirements on the filter coefficients will affect the corresponding basis functions. In general, we want these functions to look reasonably "nice" (continuous, differentiable, etc.) which implies that we want them to have some degree of regularity. In the next section, we further examine the relationship between filters and basis functions and examine regularity considerations.

2.5 Scaling Functions and Wavelets

We saw in the previous section that the scaling functions and wavelets were related respectively to the approximation and detail filters H and G . We developed conditions on these filters which allow Mallat's algorithm to work. Now we want to investigate how these conditions affect the scaling functions and wavelets.

¹Mallat and Daubechies define $h(n)$ differently which leads to some discrepancies when trying to relate their work. Mallat defines $h(n) = 1/2(\phi(\cdot/2), \phi(\cdot - n))$ whereas Daubechies defines $h(n)$ with a normalization factor of $2^{-1/2}$ instead of $1/2$. Conceptually the filters do the same operation, but the difference in the scale factors can cause some apparent inconsistencies when expressing the conditions on the filters.

Equations 2.21 and 2.25 express the relationship between the filters and the corresponding basis functions. We iterate Equation 2.21 to get

$$\hat{\phi}(f) = \hat{\phi}(0) \prod_{k=1}^{\infty} H(2^{-k}f). \quad (2.41)$$

From this expression, we can see that the scaling function will be determined by the iterated product of the approximation filter. Consequently, given an approximation filter which satisfies the conditions for an MRA, we can calculate ϕ via Equation 2.41 or its discrete time equivalent. See Appendix A for details. The wavelet can be found by substituting the expression for $\hat{\phi}$ above into Equation 2.25 and changing variables to get

$$\hat{\psi}(f) = \hat{\phi}(0)G(f/2) \prod_{k=2}^{\infty} H(2^{-k}f). \quad (2.42)$$

We mentioned earlier that we want the scaling functions and wavelets to look relatively “nice” (continuous, differentiable, etc.) which implies they are somewhat regular. Daubechies[6] has shown that a necessary condition for the iterated scaling function in Equation 2.41 to converge to a regular function is that the filter $H(f)$ have zeros of sufficiently high degree at $f = k + 1/2$ for $k \in \mathbb{Z}$. This causes the zeroes of one dilation of H in Equation 2.41 to attenuate the peaks of the previous dilation. As H is successively dilated and multiplied in the infinite product, the high frequency peaks will be attenuated. The greater the degree of the zero, the more attenuation occurs in the high frequencies and the time-domain function is more regular. Consequently, for a regular scaling function, we must have $H(f)$ of the form

$$H(f) = (1 + e^{-i2\pi f})^N \mathcal{L}(f) \quad (2.43)$$

which implies that the sequence $h(n)$ is formed by N discrete convolutions of the sequence

$$\epsilon(n) = \begin{cases} 1 & n = 0, 1 \\ 0 & \text{otherwise} \end{cases} \quad (2.44)$$

with the sequence l , where

$$\mathcal{L}(f) = \sum_n l(n) e^{-i2\pi n f}. \quad (2.45)$$

This will be important in the next chapter. The most significant contribution of Daubechies' work in [6] is the development of a set of scaling functions (and thus wavelets via Equation 2.42) which are compactly supported and have an arbitrary degree of regularity. Equivalently, an approximation filter is found which has the form of Equation 2.43 and also satisfies the conditions of an MRA. If the sequence l is finite, then $h(n)$ will be finite and the scaling function generated by iterating $H(f)$ will be compactly supported[6].

2.6 Multirate Discrete-Time Signal Processing

Multiresolution analysis has many connections with discrete-time signal processing. Mallat's algorithm deals only with sequences and Daubechies has shown that it depends on the sequences h and g . In this section we discuss the relationships between the MRA as implemented by Mallat and maximally-decimated perfect-reconstruction filter banks. We show that this interpretation leads to the development of MRAs which have integer dilation factors other than 2. These MRAs have a single scaling function and two or more mutually orthogonal wavelets. All dilations and translations of these wavelets form an orthogonal basis for $L^2(\mathbb{R})$.

Mallat's algorithm can be interpreted as a 2-channel maximally-decimated filter bank as in Figure 2.3. We say the filter bank has perfect reconstruction (PR) when $\tilde{x}(n) = x(n - n_0)$ for $n_0 \in \mathbb{Z}^+$. The constant n_0 accounts for the delay inherent in non-causal

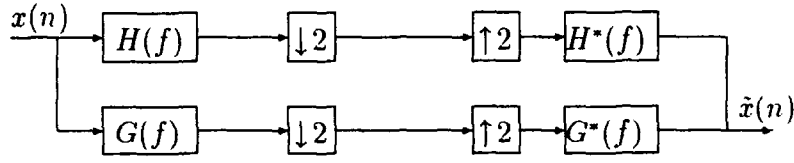


Figure 2.3. Multiresolution Analysis 2-Channel Filter Bank

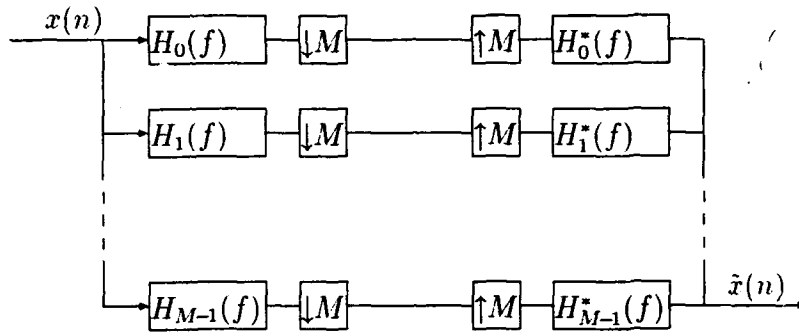


Figure 2.4. M-Channel Filter Bank

filters. The conditions on the filters H and G as stated in Equation 2.40 are necessary for perfect reconstruction and they were identified by Smith and Barnwell in [20].

The 2-channel filter bank can be generalized to an arbitrary M -channel filter bank. The conditions for perfect reconstructions have been studied by many [16][21][23][27] and they can also be seen as a generalization of those in Equation 2.40. The M -channel filter bank shown in Figure 2.4 has perfect reconstruction if

$$\mathbf{H}(f) = \begin{bmatrix} H_0(f) & H_1(f) & H_2(f) & \cdots & H_{M-1}(f) \\ H_0(f + \frac{1}{M}) & H_1(f + \frac{1}{M}) & H_2(f + \frac{1}{M}) & \cdots & H_{M-1}(f + \frac{1}{M}) \\ H_0(f + \frac{2}{M}) & H_1(f + \frac{2}{M}) & H_2(f + \frac{2}{M}) & \cdots & H_{M-1}(f + \frac{2}{M}) \\ \vdots & \vdots & \vdots & \ddots & \vdots \\ H_0(f + \frac{M-1}{M}) & H_1(f + \frac{M-1}{M}) & H_2(f + \frac{M-1}{M}) & \cdots & H_{M-1}(f + \frac{M-1}{M}) \end{bmatrix} \quad (2.46)$$

is unitary. This matrix is referred to in the literature as the alias-component matrix[21][24]. Vaidyanathan focuses on finding unitary alias component matrices in [16] and [26]. He has developed a technique whereby a unitary alias component matrix can be found given one of the filters. We will discuss this technique in the next chapter and use it to find compactly-supported wavelets.

We can now relate the M -channel PR filter banks back to multiresolution analyses. In the dyadic multiresolution case, we had each approximation space composed of two mutually orthogonal subspaces: a lower resolution approximation space and a detail space. With the MRA based on the M -channel filter bank, which we will call the integer resolution analysis (IRA), we will have each approximation space composed of M mutually orthogonal subspaces: a lower resolution approximation space and $M - 1$ detail spaces. This is significant because we now have $M - 1$ wavelets as basis functions for the $M - 1$ detail spaces!

When implementing an IRA, we must be careful in rushing too quickly to find a set of M filters whose alias component matrix is unitary. This is only a necessary condition. The idea is to be able to develop a set of filters that satisfy the perfect reconstruction property, but at the same time, ensure the filters satisfy the conditions required for approximation and detail operators. The relationships in Equations 2.21 and 2.25 are generalized for the IRA so that

$$\begin{aligned}\hat{\psi}^{(k)}(Mf) &= H_k(f)\hat{\phi}(f), \quad k = 1 \dots M - 1, \\ \hat{\phi}(Mf) &= H_0(f)\hat{\phi}(f),\end{aligned}\tag{2.47}$$

where we have arbitrarily chosen H_0 to correspond to the approximation filter. We also want to impose some regularity on the scaling functions. This will be the topic of the next chapter. Furthermore, we will want a method to find a set of perfect reconstruction filters which satisfy the conditions for an IRA. We also discuss this in the next chapter.

2.7 Rational Resolution Analysis

The rational resolution analysis (RRA), the main topic of this thesis, is a relatively new concept and has little or no literature currently available. However, there are two notable items which are related to the research at hand and it is appropriate to mention them here.

The first is the work of Pascal Auscher in both [2] and [3]. Auscher has shown that multiresolution analyses with rational dilation factors are possible and that the corresponding wavelets form an orthonormal basis for $L^2(\mathbb{R})$. However, the wavelets are neither compactly supported nor do they have exponential decay. We can allow non-compactly supported wavelets, but if they do not have sufficient decay, their usefulness diminishes. We want a wavelet to decay relatively quickly so that it has good localization in time (or position). Without good localization, the wavelets' usefulness in analyzing non-stationary signals is limited. Recall this is why wavelets were developed in the first place.

The second item is not as important as the first but has some relevance. Kovačević and Vetterli have done some work in [11] on perfect reconstruction filter banks which have rational sampling rate changes. This is encouraging from an intuitive standpoint because of the effect rational sampling rate changes have on the spectrum of a signal. Furthermore, the RRA we develop later involves the concept of rational sampling rate changes. More will be said on this in the discussion of the RRA. First, we must discuss the integer-resolution case since it is a necessary component for reconstructions in the RRA.

III. Integer-Based Compactly Supported Scaling Functions and Wavelets

3.1 Introduction

In this chapter we extend the work of Daubechies and Vaidyanathan to produce compactly supported scaling functions and wavelets which correspond to the integer resolution analysis (IRA) described in the previous chapter. These scaling functions and wavelets can be generated with an arbitrary degree of regularity, although regularity is traded for support width. We apply a technique developed by Vaidyanathan to calculate the detail filters (and thus the wavelets) once the approximation filter is given. The technique also allows the wavelets to be selected in some optimum way. We present an example where the wavelets of a particular IRA have been optimized so that the stop-band energy of the corresponding detail filters is minimized.

3.2 Compactly-Supported Scaling Functions

The theory of compactly-supported scaling functions for dyadic multiresolution analyses is well developed in [6]. Compactly-supported scaling functions which have some degree of regularity can be generated from approximation filters which satisfy the conditions

$$\begin{aligned} |H(f)|^2 + |H(f + 1/2)|^2 &= 1, \\ H(0) &= 1, \end{aligned} \tag{3.1}$$

where H has the form of Equation 2.43. For compactly-supported scaling functions, we also require that for the filter $H(f) = 2^{-1/2} \sum_n h(n)e^{-i2\pi nf}$, a finite number of the coefficients $h(n)$ are non-zero. In signal processing terms, we say $H(f)$ must be an FIR filter.

These are two conditions on the approximation filter that must hold for the dyadic MRA. The conditions can be generalized for integer-resolution analyses with dilation factors other than 2. The first condition in Equation 3.1, above, is a result of the orthogonality

of the family $\{\phi_{0n}\}_{n \in \mathbf{Z}}$ expressed by

$$\sum_n |\hat{\phi}(f+n)|^2 = 1 \quad (3.2)$$

via the Poisson summation formula[12]. It is also a restatement that the first column of the matrix given in Equation 2.40 has unit norm, which is required for a unitary matrix. The corresponding condition for an IRA with dilation factor M is that the first column of the alias component matrix in Equation 2.46 have unit norm so that

$$\sum_{k=0}^{M-1} |H(f+k/M)|^2 = 1. \quad (3.3)$$

The second condition in Equation 3.1 is independent of dilation factor and thus remains the same.

In order to have a scaling function with some degree of regularity, we must impose additional constraints on the form of the filter as we saw for the dyadic case in Equation 2.43. The spectral factors, $(1 + e^{-i2\pi f})$, are necessary to attenuate repeated spectra in the construction of the scaling function via Equation 2.41. Analogously, we require that an approximation filter for an IRA with dilation factor M have the form

$$H(f) = \left(\sum_{k=0}^{M-1} e^{-i2\pi k f} \right)^N \mathcal{L}(f), \quad (3.4)$$

where

$$\mathcal{L}(f) = \sum_{n=0}^{L-1} l(n) e^{-i2\pi n f}. \quad (3.5)$$

This is equivalent to requiring the sequence $h(n)$ be equivalent to N discrete convolutions of the sequence

$$e(n) = \begin{cases} 1 & n \in \{0, 1, \dots, M-1\} \\ 0 & \text{otherwise} \end{cases} \quad (3.6)$$

with the sequence l . Because we require scaling functions with compact support, $\mathcal{L}(f)$ is such that l has a finite number of non-zero terms.

To calculate the approximation filter coefficients, it is helpful to rewrite the conditions on the approximation filter in terms of its coefficients. The two conditions above can be combined into a single condition on the coefficients of the approximation filter:

$$\sum_n h(n - Mk)h(n - Ml) = \delta_{lk}, \quad (3.7)$$

which is derived by expressing Equation 3.3 in terms of the $h(n)$ and combining like terms. The incorporation of the second condition, $H(0) = 1$, is forced by the structure of the filter. If N is chosen so the corresponding scaling function has as much regularity as its support will allow, ($N = L$), then the second condition will be satisfied. This is illustrated by the following example.

Example 3-1 Suppose we want to find an approximation filter H for $M = 3$ such that there are 6 non-zero terms in $h(n)$ (6 taps). We want to impose maximum regularity which implies $N = 2$ because any larger would generate at least a 7-tap filter. This means that $h(n)$ is composed of a convolution of the sequence $r(n) = \{1, 2, 3, 2, 1\}$ with a two element sequence $\{l(0), l(1)\}$. We perform this discrete convolution and find the following expressions for the $h(n)$:

$$\begin{aligned} h(0) &= l(1), \\ h(1) &= 2l(1) + l(0), \\ h(2) &= 3l(1) + 2l(0), \\ h(3) &= 2l(1) + 3l(0), \\ h(4) &= l(1) + 2l(0), \\ h(5) &= l(0). \end{aligned}$$

With the filter constraints as:

$$\sum_{n=0}^5 |h(n)|^2 = 1,$$

$$\sum_{n=0}^2 h(n)h(n+3) = 0.$$

We determine $l(0) = \pm 1.01516$ and $l(1) = \mp 0.43781$ so that the resulting $h(n)$ are shown in Table 3.1.

Table 3.1. Filter Coefficients for $M = 3$ Scaling Filter with 2 Degrees of Regularity

n	$h(n)$
0	0.3383860972838639
1	0.5308361870137393
2	0.7232862767436145
3	0.2389641719057618
4	0.0465140821758866
5	-0.1459360075539887

□

We can generalize the technique illustrated in this previous example to find scaling functions for arbitrary M dilation factors. For higher regularity, we simply increase N . We also find that l will have N non-zero terms, there will be N constraints on h , and the length of h will be NM .

Coefficients for various approximation filters and graphs of their corresponding scaling functions are contained in the appendices. In general, the coefficients were found using root-finding software. It is interesting to note that the scaling filter coefficients are not unique and that the result depends upon the initial guess at the solutions. The choices given in Appendix C were chosen to generally correspond to those published by Daubechies in [6] so that the scaling functions generated would be comparable in shape. This shape

similarity is very important to the RRA and we will comment more on this in the following chapter.

3.3 Alias-Component Matrix Decomposition

We have seen the relationship between integer resolution analyses and perfect reconstruction filter banks. A unitary alias-component matrix satisfies the majority of the conditions for an integer resolution analysis. In the previous section, we have shown how the constraints for an approximation filter can be satisfied so that one column in the alias-component matrix is now fixed. Note that the second condition for the wavelet filters

$$\sum_n h^{(k)}(n), k = 1 \dots M - 1 \quad (3.8)$$

is also satisfied now as a consequence of satisfying both conditions on the approximation filter. The task now is to find $M - 1$ filters such that the alias-component matrix is unitary.

Vaidyanathan[26] has developed a technique with which the other filters of an M -channel perfect reconstruction filter bank can be found once one of the filters is specified. This technique is easily adapted to finding the $M - 1$ wavelet filters once the approximation filter has been calculated as in the last section.

In order to describe its implementation, we need to introduce some notation from multirate digital signal processing. Reference [24] provides a good background. We introduce the z -domain notation for the description of our filters:

$$H(z) = M^{-1/2} \sum_n h(n) z^{-n}. \quad (3.9)$$

This filter is related to the previously defined $H(f)$ by $z = e^{i2\pi f}$. We say that $H(z)$ is causal if the sequence $h(n) = 0$ for $n < 0$. Substituting the z -domain notation for $H(f)$

into the alias-component matrix we get

$$\mathbf{H}(z) = \begin{bmatrix} H_0(z) & H_1(z) & \cdots & H_{M-1}(z) \\ H_0(W^{-1}z) & H_1(W^{-1}z) & \cdots & H_{M-1}(W^{-1}z) \\ \vdots & \vdots & \ddots & \vdots \\ H_0(W^{-(M-1)}z) & H_1(W^{-(M-1)}z) & \cdots & H_{M-1}(W^{-(M-1)}z) \end{bmatrix}, \quad (3.10)$$

where $W = z^{1/M} = e^{i2\pi/M}$. Because we have only changed notation, requiring \mathbf{H} to be unitary is equivalent to requiring the alias-component matrix (Equation 2.46) to be unitary.

A filter $H_k(z) = \sum_n h_k(n)z^{-n}$ can be expressed in the following polyphase form:

$$H_k(z) = \sum_{l=0}^{M-1} z^{-l} E_{kl}(z^M), \quad (3.11)$$

where

$$E_{kl}(z) = \sum_n h_k(Mn + l)z^{-n}. \quad (3.12)$$

The $E_{kl}(z)$ are known as the polyphase components of $H(z)$ [26]. We define the polyphase matrix $\mathbf{E}(z)$ such that the k -th row and l -th column is given by $E_{kl}(z)$ for $k, l \in \{0, 1, \dots, M-1\}$. The polyphase matrix $\mathbf{E}(z)$ is related to the alias-component matrix by

$$\mathbf{H}(z) = \mathbf{W}^\dagger \mathbf{D}(z) \mathbf{E}^T(z^M), \quad (3.13)$$

where \mathbf{W} is the $M \times M$ discrete Fourier Transform (DFT) matrix defined by $[W^{kl}]_{kl}$ and \mathbf{D} is given by

$$\mathbf{D} = \text{diag}[1 \ z^{-1} \ \cdots \ z^{-(M-1)}]. \quad (3.14)$$

One thing to notice in this expression for $\mathbf{H}(z)$ is that both \mathbf{W}^\dagger and \mathbf{D} are unitary matrices. Consequently, $\mathbf{E}(z)$ must be unitary if $\mathbf{H}(z)$ is unitary and vice versa. Thus, requiring $\mathbf{E}(z)$

to be unitary is equivalent to requiring $\mathbf{H}(z)$ to be unitary. We will find it more convenient to deal with unitary polyphase matrices than alias-component matrices.

Suppose we have a unitary polyphase matrix. Because the product of unitary matrices is also unitary, it makes sense to decompose a polyphase matrix into several smaller, less complicated matrices. The reverse is also true: we can construct a unitary polyphase matrix using those same building-block matrices. However, we need to be able to specify those matrices so that the resulting polyphase matrix satisfies the additional conditions for an IRA. We want one of the columns in the polyphase matrix to correspond to the approximation filter—the other filters will automatically correspond to wavelet filters.

The degree of a unitary alias-component matrix $\mathbf{H}(z)$ is defined as the degree of its determinant. Perfect reconstruction (or lossless) systems have determinants of the form

$$\det \mathbf{H}(z) = cz^{-(N-1)} \quad (3.15)$$

so that the degree is simply $N - 1$. Vaidyanathan demonstrates in [26] that any $M \times M$ causal FIR system $\mathbf{H}_{N-1}(z)$ is lossless if and only if it can be expressed as

$$\mathbf{H}_{N-1}(z) = \mathbf{V}_{N-1}(z)\mathbf{V}_{N-2}(z) \cdots \mathbf{V}_1(z)\mathbf{H}_0. \quad (3.16)$$

where the subscript on \mathbf{H} indicates its degree so that \mathbf{H}_0 is a constant $M \times M$ unitary matrix and $\mathbf{V}_k(z)$ are $M \times M$ FIR unitary matrices of degree one. Each \mathbf{V}_k has the form

$$\mathbf{V}_k = [\mathbf{I} - \mathbf{v}_k \mathbf{v}_k^\dagger + \mathbf{v}_k \mathbf{v}_k^\dagger z^{-1}] \quad (3.17)$$

so that the entire system can be characterized as a set of $N - 1$ unit-norm vectors, \mathbf{v}_k , and the unitary matrix, \mathbf{H}_0 . Furthermore, Vaidyanathan demonstrates that any $M \times 1$ column

vector of the form

$$\mathbf{P}_{N-1}(z) = \sum_{n=0}^{N-1} \mathbf{p}(n)z^{-n} \quad (3.18)$$

is lossless¹ if and only if it can be expressed as

$$\mathbf{P}_{N-1}(z) = \mathbf{U}_{N-1}(z)\mathbf{U}_{N-2}(z) \cdots \mathbf{U}_1(z)\mathbf{P}_0 \quad (3.19)$$

where again the subscript on \mathbf{P} indicates its degree so that \mathbf{P}_0 is a constant $M \times 1$ column vector with unit norm. Here, the degree of a vector \mathbf{P} is defined as $N-1$ from its definition in terms of \mathbf{p} . The definition requires $\mathbf{p}(N-1) \neq 0$. The \mathbf{U}_k are $M \times M$ degree-one lossless FIR matrices and they have a form similar to \mathbf{V}_k :

$$\mathbf{U}_k = [\mathbf{I} - \mathbf{u}_k \mathbf{u}_k^\dagger + \mathbf{u}_k \mathbf{u}_k^\dagger z], \quad (3.20)$$

where \mathbf{u}_k are constant $M \times 1$ unit-norm vectors.

We want to find the \mathbf{U}_k which will decompose \mathbf{P}_{N-1} as in Equation 3.19. The choice of \mathbf{u}_k is critical. We want to choose \mathbf{u}_k such that \mathbf{U}_k reduces the degree of \mathbf{P}_k . That is, we want to choose \mathbf{U}_k so that $\mathbf{U}_k \mathbf{P}_k = \mathbf{P}_{k-1}$. (Note that only the subscript on \mathbf{P} denotes its degree; the subscript k on \mathbf{U} denotes the matrix that reduces \mathbf{P}_k to \mathbf{P}_{k-1} .) In order to do this, two things must happen. First, the coefficients $\mathbf{p}_k(k)$ of z^{-k} must be "zeroed out" and second, the system must remain causal, i.e. no positive powers of z can result from the operation. From the definition of \mathbf{U}_k , this implies that

$$[\mathbf{I} - \mathbf{u}_k \mathbf{u}_k^\dagger] \mathbf{p}_k(k) = 0 \quad (3.21)$$

and

$$[\mathbf{u}_k \mathbf{u}_k^\dagger] \mathbf{p}_k(0) = 0, \quad (3.22)$$

¹For vectors, "lossless" means the vector has unit-norm or $\hat{\mathbf{P}}\mathbf{P} = 1$

for $k = 1, 2, \dots, N-1$. A property of lossless vectors $\mathbf{P}_k(z)$, is that $\mathbf{p}_k^\dagger(0)\mathbf{p}_k(k) = 0$. This can easily be seen by multiplying $\tilde{\mathbf{P}}\mathbf{P}$ and equating powers of z . With this in mind, we choose

$$\mathbf{u}_k = \frac{\mathbf{p}_k(k)}{\|\mathbf{p}_k(k)\|} \quad (3.23)$$

which satisfies Equations 3.21 and 3.22. The resulting \mathbf{U}_k will reduce the degree of \mathbf{P}_k . It is clear we can successively reduce the degree of \mathbf{P}_{N-1} by choosing the appropriate $\mathbf{U}_k(z)$ at each step. Furthermore, the factorization

$$\mathbf{P}_{N-1}(z) = \mathbf{U}_{N-1}(z)\mathbf{U}_{N-2}(z) \cdots \mathbf{U}_1(z)\mathbf{P}_0 \quad (3.24)$$

is unique. At every step in the factorization, there is only one choice (to a scale factor) of \mathbf{u}_k that will result in a $\mathbf{U}_k(z)$ that reduces the degree of $\mathbf{P}_k(z)$. Each of the $\mathbf{U}_k(z)$ is then unique as is the final vector \mathbf{P}_0 . This is in contrast to the factorization of the matrix

$$\mathbf{H}_{N-1}(z) = \mathbf{V}_{N-1}(z)\mathbf{V}_{N-2}(z) \cdots \mathbf{V}_1(z)\mathbf{H}_0. \quad (3.25)$$

The $\mathbf{V}_k(z)$ are not unique in general. However, the final matrix \mathbf{H}_0 is unique and so is the product $\mathbf{V}(z) = \mathbf{V}_{N-1}(z)\mathbf{V}_{N-2}(z) \cdots \mathbf{V}_1(z)$ [26]. This uniqueness will be useful later in finding sets of orthonormal detail filters which correspond to wavelets. The following example illustrates a simple decomposition.

Example 3-2 Consider the lossless vector $\mathbf{P}_1(z)$:

$$\mathbf{P}_1(z) = \begin{bmatrix} 0.022876 - 0.577124z^{-1} \\ -0.016176 - 0.816176z^{-1} \end{bmatrix}.$$

To decompose $P_1(z)$ we choose

$$\begin{aligned} u_1 &= \frac{p_1(1)}{\|p_1(1)\|} \\ &= \frac{1}{0.999607} \begin{bmatrix} -0.577124 \\ 0.816176 \end{bmatrix} \\ &= \begin{bmatrix} -0.577351 \\ 0.816497 \end{bmatrix}, \end{aligned}$$

so that

$$\begin{aligned} U_1 &= I - u_k u_k^\dagger + u_k u_k^\dagger z \\ &= \begin{bmatrix} 0.6667 + 0.3333z & -0.471405 + 0.471405z \\ -0.471405 + 0.471405z & 0.6667 + 0.3333z \end{bmatrix}. \end{aligned}$$

Then

$$U_1 P_1 = P_0 = \begin{bmatrix} 0.6 \\ 0.8 \end{bmatrix},$$

which is equivalent to

$$\begin{aligned} P_1(z) &= \begin{bmatrix} 0.022876 - 0.577124z^{-1} \\ -0.016176 - 0.816176z^{-1} \end{bmatrix} \\ &= \begin{bmatrix} 0.6667 + 0.3333z^{-1} & -0.471405 + 0.471405z^{-1} \\ -0.471405 + 0.471405z^{-1} & 0.6667 + 0.3333z^{-1} \end{bmatrix} \begin{bmatrix} 0.6 \\ 0.8 \end{bmatrix}. \end{aligned}$$

□

Having gone through this development, it is useful to provide a summary. We have shown an IRA requires a unitary alias-component matrix. We related this requirement to

a z -domain representation of the alias-component matrix and to the polyphase representation. From there, we demonstrated that the unitary system matrix (or vector depending upon your representation) of any lossless system can be factored into a set of degree-one unitary matrices and a constant (degree-zero) unitary matrix (or vector). The next step is to describe how we use such factorizations to implement an IRA.

3.4 *Compactly-Supported Wavelets*

Suppose we have the approximation filter of an IRA found, perhaps, using the technique described earlier in this chapter. We express it in polyphase form and treat it as one column of the polyphase matrix $\mathbf{E}^T(z)$. We can then factor this column like we factored $\mathbf{P}_{N-1}(z)$ and find the unique

$$\mathbf{U}(z) = \mathbf{U}_{N-1}(z)\mathbf{U}_{N-2}(z) \cdots \mathbf{U}_1(z) \quad (3.26)$$

that decomposes the approximation filter. We can then specify the other filters (columns in $\mathbf{E}^T(z)$) by simply letting the \mathbf{P}_0 be one column in \mathbf{H}_0 (Equation 3.25) and finding the other columns such that the matrix is unitary. The transformation matrix $\mathbf{U}(z)$ will transform each column independently so that the resulting \mathbf{H}_{N-1} matrix is guaranteed to be lossless because it has two unitary matrices $\mathbf{U}(z)$ and \mathbf{H}_0 as its only factors.

It is interesting to note that the number of different filters that result from this scheme is equivalent to the number of ways you can specify a constant unitary matrix with one column fixed. For an arbitrary M , there are degrees of freedom in the choice of the other columns which means that the detail filters are not unique and so the corresponding wavelets are not unique.

Because we have flexibility in the choice of wavelets, we can apply some design criteria in their selection. One choice of design criteria is to minimize the stop-band energy of the filters. We define the pass-band of the approximation filter as the lower $(1/M)$ -th of the

normalized frequency range ($f \in [0, 1/(2M)]$) and we define the pass-bands of the other wavelet filters as continuous non-overlapping regions of width $1/(2M)$. We optimize the filters so that the energy outside of their pass-bands is minimized. This is important if we want the wavelets to correspond to good bandpass filters. We illustrate this with the following example:

Example 3-3 In Example 3-1 we calculated the approximation filter coefficients for the $M = 3, N = 2$ scaling function. Decomposing this filter, we find

$$\begin{bmatrix} h_0 + h_3 z^{-1} \\ h_1 + h_4 z^{-1} \\ h_2 + h_5 z^{-1} \end{bmatrix} = \mathbf{U}(z) \cdot \begin{bmatrix} \frac{1}{\sqrt{3}} \\ \frac{1}{\sqrt{3}} \\ \frac{1}{\sqrt{3}} \end{bmatrix},$$

where

$$\mathbf{U}(z) = \begin{bmatrix} 1 - h_3^2 + h_3^2 z^{-1} & -h_3 h_4 + h_3 h_4 z^{-1} & -h_3 h_5 + h_3 h_5 z^{-1} \\ -h_4 h_3 + h_4 h_3 z^{-1} & 1 - h_4^2 + h_4^2 z^{-1} & -h_4 h_5 + h_4 h_5 z^{-1} \\ -h_5 h_3 + h_5 h_3 z^{-1} & -h_5 h_4 + h_5 h_4 z^{-1} & 1 - h_5^2 + h_5^2 z^{-1} \end{bmatrix}.$$

The h_n above are given in Table 3.1. Notice that the constant vector has repeated entries of the same value. As it turns out, scaling functions constructed in this way will all have the value $M^{-1/2}$ as the only unique value in the constant vector. This is a result of imposing regularity on the filters and is independent of N .

With the $\mathbf{U}(z)$ given above, the next step is to find two more constant vectors such that they are orthogonal to the constant vector above and orthogonal to each other. We need to find the h_{ij} so that

$$\mathbf{H}_0 = \begin{bmatrix} \frac{1}{\sqrt{3}} & h_{10} & h_{20} \\ \frac{1}{\sqrt{3}} & h_{11} & h_{21} \\ \frac{1}{\sqrt{3}} & h_{12} & h_{22} \end{bmatrix}$$

Table 3.2. Unoptimized Detail Filter Coefficients for $M = 3$ and $N = 2$

n	$h_1(n)$	$h_2(n)$
0	-0.1001669566712731	0.4082482904638631
1	-0.1571348402636774	-0.816496580927726
2	-0.2141027238560812	0.4082482904638631
3	0.8072737378578210	0.0
4	0.1571348402636774	0.0
5	-0.4930040573304665	0.0

is unitary. We could choose

$$\mathbf{h}_1 = [\sqrt{1/2} \quad 0 \quad -\sqrt{1/2}]^T$$

and

$$\mathbf{h}_2 = [\sqrt{1/6} \quad -\sqrt{2/3} \quad \sqrt{1/6}]^T.$$

This would give us the coefficients given in Table 3.2. The frequency responses of the detail filters given by these coefficients is shown in Figure 3.1². The approximation filter is also shown in the same figure for reference.

We optimize the choice of the two remaining columns to yield detail filter coefficients which correspond filters with minimum stop-band energy. For the $M = 3$ case, we assign the pass-bands to be successive thirds of the spectrum. The approximation filter is assigned the lowest third, and the two detail filters are assigned the middle and upper thirds. The energy density of a filter is given by

$$S(f) = H(f)H^*(f) = |H(f)|^2.$$

²The coefficients for $h_2(n)$ are not in error. This particular set of coefficients is unchanged by multiplication with $U(z)$ and can be considered an eigenvector of the matrix.

In terms of the filter coefficients:

$$\begin{aligned} S(f) &= \sum_n R(n) e^{i2\pi n f} \\ &= R(0) + 2 \sum_{n=1}^{\infty} R(n) \cos(2\pi n f) \end{aligned}$$

where R is the autocorrelation sequence given by

$$R(\tau) = \sum_n h(n) h(n - \tau).$$

The energy in the stop-band of a filter is found by integrating $S(f)$ over the stop-band. In this example, we want to minimize the energy in the stop-bands of the two detail filters with respect to their coefficients, so the objective function is given by

$$J(f) = \int_0^{\frac{1}{6}} S_1(f) df + \int_{\frac{1}{3}}^{\frac{1}{2}} S_1(f) df + \int_0^{\frac{1}{3}} S_2(f) df$$

where S_1 and S_2 are the filter energies of the respective detail filters. We only need to integrate over stop-bands for $f \in [0, 1/2]$ because $|H(f)|$ is symmetric about $f = 1/2$ for filters with real coefficients.

J will be a function of the six remaining coefficients in \mathbf{H}_0 . We minimize³ J subject to \mathbf{H}_0 being unitary and we find

$$\mathbf{h}_1 = [-0.812690 \quad 0.338143 \quad 0.474546]^T$$

and

$$\mathbf{h}_2 = [0.078752 \quad -0.743186 \quad 0.664434]^T$$

³Matlab's *constr* function (Optimization Toolbox) was used.

with the corresponding detail filter coefficients given in Table 3.3. The frequency response of the approximation filter and the two optimized detail filters are shown in Figure 3.2.

The corresponding wavelets are shown in Figures 3.3 and 3.4. For comparison, the

Table 3.3. Optimized Detail Filter Coefficients for $M = 3$ and $N = 2$

n	$h_1(n)$	$h_2(n)$
0	-0.07789569612441	0.41307668343873
1	0.48116523128534	-0.67811359291308
2	0.02581048126453	0.46026129761925
3	-0.73479360808553	-0.33431907117540
4	-0.14302667214182	-0.06507479604830
5	0.44874026380189	0.20416947907880

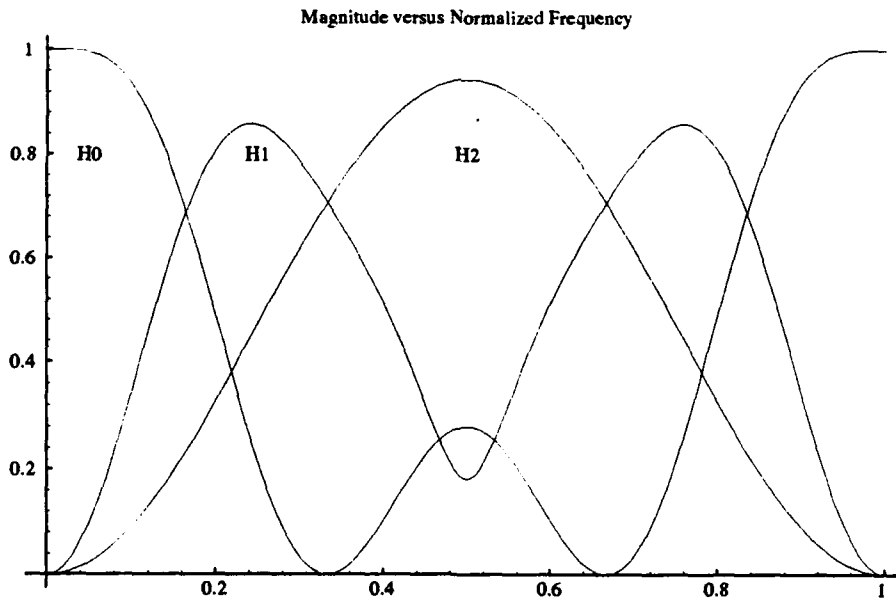


Figure 3.1. Frequency Response of $M = 3$, $N = 2$ Approximation Filter and Unoptimized Detail Filters

wavelets corresponding to the unoptimized detail filter coefficients (Table 3.2) are shown in Figures 3-3 and 3-3.

□

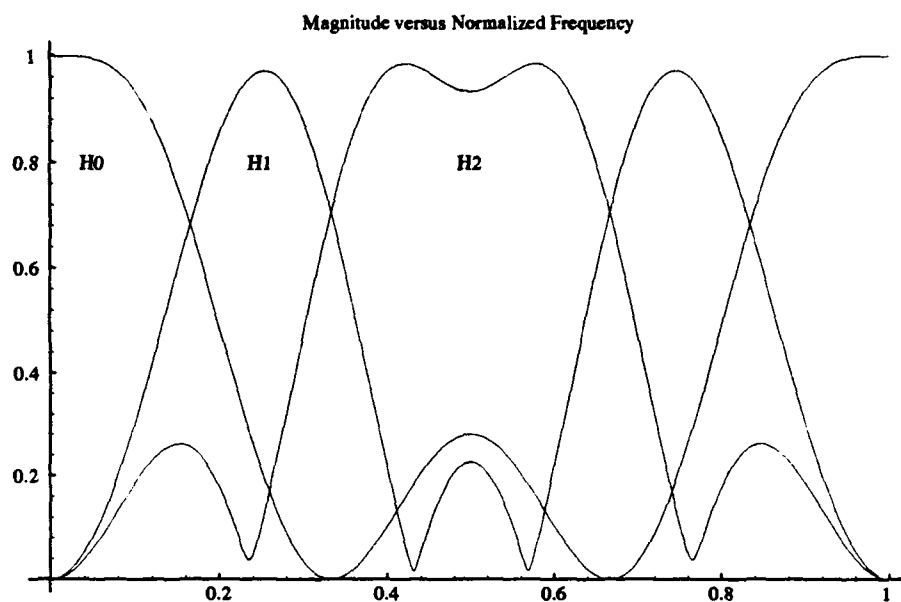


Figure 3.2. Frequency Response of $M = 3$, $N = 2$ Approximation Filter and Detail Filters with Minimum Stop-Band Energy

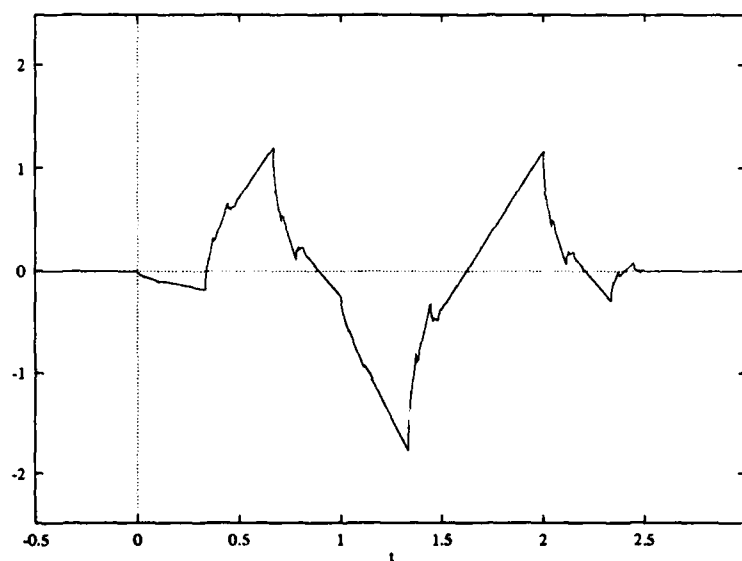


Figure 3.3. $M = 3$, $N = 2$ (Mid-Pass) Wavelet with Minimum Stop-Band Energy ($\psi(t)$ vs. t)

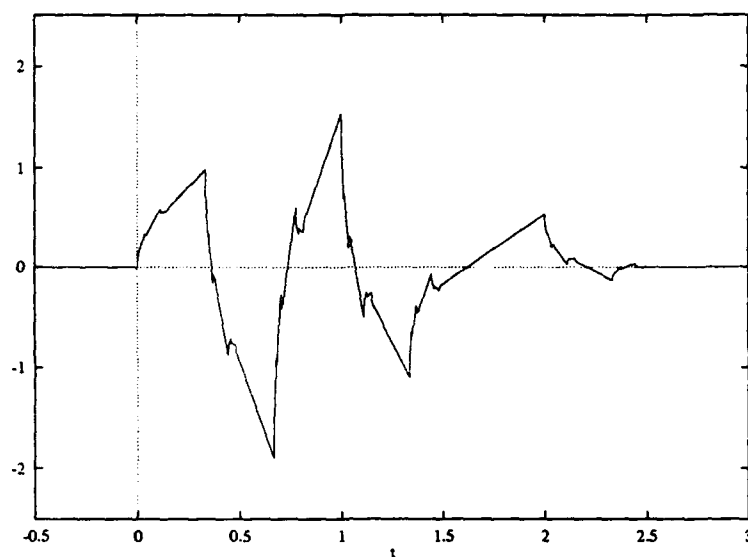


Figure 3.4. $M = 3, N = 2$ (High-Pass) Wavelet with Minimum Stop-Band Energy ($\psi(t)$ vs. t)

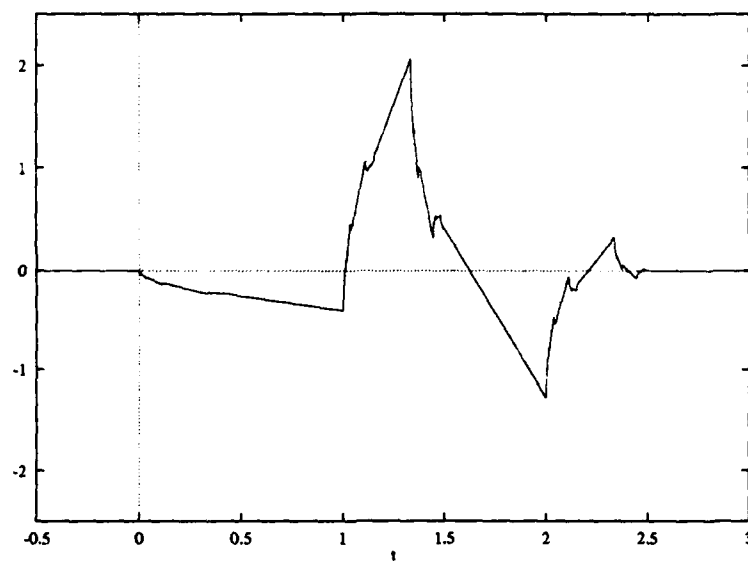


Figure 3.5. Unoptimized $M = 3, N = 2$ Wavelet ($\psi(t)$ vs. t)

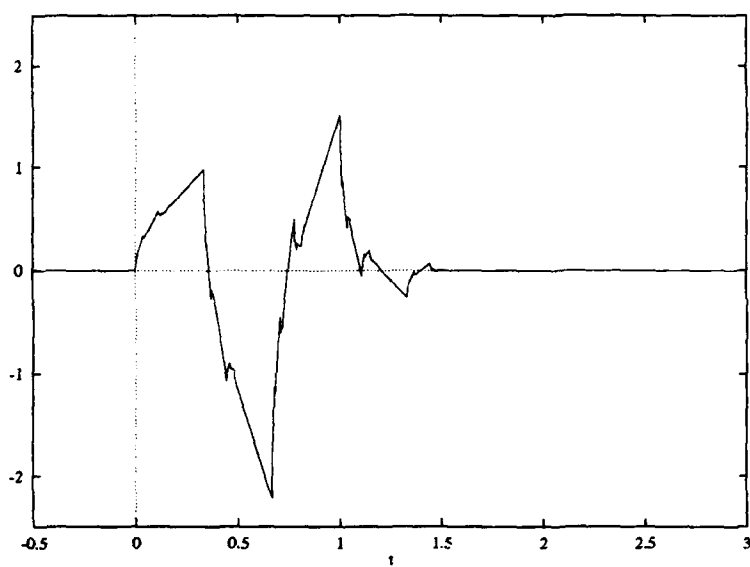


Figure 3.6. Unoptimized $M = 3, N = 2$ Wavelet ($\psi(t)$ vs. t)

IV. Rational Resolution Wavelet Analyses

4.1 Introduction

This chapter introduces a rational resolution analysis (RRA). A rational resolution analysis is similar to the integer resolution analyses except the approximation and reconstruction operations are generally more complicated because the approximation spaces are not embedded, as in the integer resolution analyses. We begin with a definition which is similar to the integer resolution analysis followed by a description of the decomposition and reconstruction operations. We study the approximate reconstruction obtained with compactly supported scaling functions and wavelets. We derive the necessary conditions for perfect reconstruction. In particular, we show that the spline-based wavelets and scaling functions will give perfect reconstruction. Finally, we provide a description of the frequency characteristics of the rational resolution analysis.

4.2 Rational Resolution Approximation

Recall the approximation spaces V_m for integer resolution analyses were defined as the spaces spanned by orthonormal integer translations of a single dilated scaling function:

$$V_m = \overline{\text{span}\{\phi_{mn}\}_{n \in \mathbb{Z}}}. \quad (4.1)$$

The integer resolution analysis restricted the dilation factor M to be an integer greater than 1. Now, for the rational resolution case, we relax this restriction and allow $M = p/q$ for $p, q \in \mathbb{Z}^+$, $p > q$, and $q \neq 0$. In general, the rational dilation factors of most interest will lie between 1 and 2.

Like the integer resolution case, we define the rational resolution approximation operation as an orthogonal projection onto an approximation space V_m . We define

$$_{p/q}\phi_{mn}(t) = (p/q)^{-m/2} \phi((p/q)^{-m}t - n) \quad (4.2)$$

and

$$V_m = \overline{\text{span}\{_{p/q}\phi_{mn}\}_{n \in \mathbb{Z}}}, \quad (4.3)$$

where ϕ_{0n} for $n \in \mathbb{Z}$ is an orthonormal basis of V_0 . For $f \in V_{m-1}$, the approximation of f in V_m is given by

$$(P_m^{p/q} f)(t) = \sum_n c_{mn} \, _{p/q}\phi_{mn}(t), \quad (4.4)$$

where now

$$c_{mn} = \langle f, \, _{p/q}\phi_{mn} \rangle. \quad (4.5)$$

This is slightly different than the integer-resolution case in that the operator projects from one approximation space to the next instead of from $L^2(\mathbb{R})$ to an approximation space. This implies that the projection from $L^2(\mathbb{R})$ to some V_m has been found. This difference will be further explained later.

The p/q forescript is used to explicitly denote the dilation factor. We will generally omit the forescript throughout this chapter except in cases where it is necessary for clarity.

The approximation at a given level m is entirely characterized by the approximation coefficients c_{mn} for $n \in \mathbb{Z}$. To cast this approximation into a multi-level decomposition scheme so we can relate $f \in V_{m-1}$ to its approximation in V_m , we need to describe the relationships between the approximation coefficients at adjacent levels. We want to develop operators on those coefficients which will effectively project a function from one space to the next. To do this, we need to look at the relationship between the c_{mn} and $c_{m-1,n}$.

Given a function $f \in V_0$, we write

$$f(t) = \sum_n c_{0n} \phi_{0n}(t). \quad (4.6)$$

The first level approximation of f is given by

$$(P_1^{p/q} f)(t) = \sum_k c_{1k} \phi_{1k}(t). \quad (4.7)$$

We express the $\{c_{1k}\}_{k \in \mathbf{Z}}$ in terms of the coefficients of the expansion of $f \in V_0$:

$$c_{1k} = \sum_n c_{0n} \langle \phi_{0n}, \phi_{1k} \rangle \quad (4.8)$$

which relates the two sets of approximation coefficients. We can express this relationship by defining a filter matrix \mathbf{H}^1 such that its k -th row and n -th column is $\langle \phi_{0n}, \phi_{1k} \rangle$. If we write the approximation coefficients as vectors \mathbf{c}_0 and \mathbf{c}_1 , then we have

$$\mathbf{c}_1 = \mathbf{H} \mathbf{c}_0. \quad (4.9)$$

This development is identical to the integer resolution case thus far, but the similarity ends here.

Recall that for the IRA, the approximation spaces are embedded. This allows us to express the basis function of one approximation space as a linear combination of the basis functions of the previous approximation space:

$$\phi(t/M) = \sum_n h(n) \phi(t - n) \quad (4.10)$$

¹We also defined \mathbf{H} earlier to be the alias component matrix. Its use will be clear from the context.

where M is the familiar integer dilation factor and $h(n) = \langle \phi_{10}, \phi_{0n} \rangle$. We will show that for the rational resolution analysis defined above, the approximation spaces are not embedded and so the relationship between approximation coefficients at adjacent levels is not so straightforward.

To see that the approximation spaces are not embedded for rational dilation factors, let ϕ be an orthonormal basis for V_0 and r be an arbitrary rational dilation factor. Now consider the function $r^{-1}\phi(t/r) \in V_1$. If we assume embedding of the approximation spaces, we write

$$r^{-1}\phi(t/r) = \sum_n c(n)\phi(t - n). \quad (4.11)$$

Now consider the function $r^{-2}\phi(t/r^2) \in V_2$. Since $V_2 \subset V_1 \subset V_0$, this function also has an expansion in terms of ϕ :

$$r^{-2}\phi(t/r^2) = \sum_n d(n)\phi(t). \quad (4.12)$$

Taking the Fourier transforms of these two expressions, we find

$$\begin{aligned} \hat{\phi}(rf) &= C(f)\hat{\phi}(f) \\ \hat{\phi}(r^2f) &= D(f)\hat{\phi}(f) \end{aligned} \quad (4.13)$$

with $D(f) = \sum_n d(n)e^{-i2\pi nf}$ and $C(f)$ defined similarly. This leads to

$$D(f) = C(f)C(rf). \quad (4.14)$$

Now, we know $D(f)$ and $C(f)$ are both 1-periodic in f from their definitions. However, $C(rf)$ is $1/r$ -periodic. Therefore, the product $C(f)C(rf)$ is 1-periodic if and only if r is an integer. Consequently, the approximation spaces are embedded for, and only for, integer dilation factors.

This is why we express the projection operators as projections from one approximation space to the next instead of from $L^2(\mathbb{R})$ to an approximation space. When the approximation spaces are not embedded, the projection from $L^2(\mathbb{R})$ onto V_m is not equivalent to the projection from $L^2(\mathbb{R})$ onto V_{m-1} and then to V_m .

The relationship between the approximation coefficients at adjacent resolution levels can now be derived. We demonstrate the relationship in two ways. The first involves the inner product filter matrix \mathbf{H} . Consider the following examples:

Example 4-1 Consider the rational dilation case with $p = 2$ and $q = 1$ and scaling function $\phi = \chi_{[0,1]}$, the characteristic function. This integer resolution case is a special case of a rational dilation. The scaling function of the first approximation level is $\phi_{1k} = \sqrt{1/2}\chi_{[0,2]}$. The inner product matrix is then

$$\mathbf{H} = \begin{bmatrix} \ddots & 0 & 0 & 0 & 0 & 0 \\ 0 & \sqrt{1/2} & \sqrt{1/2} & 0 & 0 & 0 \\ 0 & 0 & 0 & \sqrt{1/2} & \sqrt{1/2} & 0 \\ 0 & 0 & 0 & 0 & 0 & \ddots \end{bmatrix}. \quad (4.15)$$

The approximation operation is expressed by $\mathbf{c}_m = \mathbf{H}\mathbf{c}_{m-1}$ where \mathbf{c}_m represents a column vector of approximation coefficients corresponding to the m -th approximation level. The values of \mathbf{H} are calculated from the definition of the inner product:

$$\langle \phi_{0n}, \phi_{1k} \rangle = \sqrt{1/2} \int_{-\infty}^{\infty} \chi_{[n,n+1)}(t) \chi_{[2k,2(k+1))}(t) dt. \quad (4.16)$$

□

Notice for this simple example that the rows of \mathbf{H} are identical except for column shifts. This allows us to write the relationship between the c_{0n} and c_{1k} in the form with which we

are most familiar:

$$c_{1k} = \sum_n h(n - Mk) c_{0n}, \quad (4.17)$$

where

$$h(n) = \begin{cases} \sqrt{1/2} & n = 0, 1 \\ 0 & \text{otherwise} \end{cases}. \quad (4.18)$$

Also notice for \mathbf{H} corresponding to integer dilation factors, we have

$$\mathbf{H}\mathbf{H}^* = \mathbf{I} \quad (4.19)$$

which encapsulates many of the orthogonality conditions on the approximation filters discussed earlier[28]. Now consider a rational approximation case.

Example 4-2 Consider the integer dilation case with $p = 3$ and $q = 2$ and scaling function $\phi = \chi_{[0,1)}$. Now, the scaling function of the first approximation level is $_{p/q}\phi_{1k} = (3/2)^{-1/2} \chi_{[0,3/2)}$. The inner product matrix is now

$$\mathbf{H} = \begin{bmatrix} \ddots & 0 & 0 & 0 & 0 & 0 & 0 & 0 \\ 0 & \sqrt{2/3} & \sqrt{1/6} & 0 & 0 & 0 & 0 & 0 \\ 0 & 0 & \sqrt{1/6} & \sqrt{2/3} & 0 & 0 & 0 & 0 \\ 0 & 0 & 0 & 0 & \sqrt{2/3} & \sqrt{1/6} & 0 & 0 \\ 0 & 0 & 0 & 0 & 0 & \sqrt{1/6} & \sqrt{2/3} & 0 \\ 0 & 0 & 0 & 0 & 0 & 0 & 0 & \ddots \end{bmatrix} \quad (4.20)$$

where the values are calculated from the definition of the inner product:

$$\langle \phi_{0n}, \phi_{1k} \rangle = (3/2)^{-1/2} \int_{-\infty}^{\infty} \chi_{[n, n+1)}(t) \chi_{[\frac{2}{3}k, \frac{2}{3}(k+1))}(t) dt. \quad (4.21)$$

□

The inner product matrices in both the previous examples have similar block structures. That is, the matrices consist solely of non-overlapping shifted versions of some elementary submatrix, called a block, along their main diagonal. This is caused by the periodic behavior of the inner product:

$$\langle \phi_{1k}, \phi_{0n} \rangle = \langle \phi_{0k-lq}, \phi_{1n-lp} \rangle, \text{ for each } l \in \mathbf{Z}. \quad (4.22)$$

The dimensions of the block will depend on the rational dilation factor and the support of the scaling function. There will be q rows and each block will be offset from the next by p columns. This is shown in Figure 4.1(a). Another interpretation of the structure is to

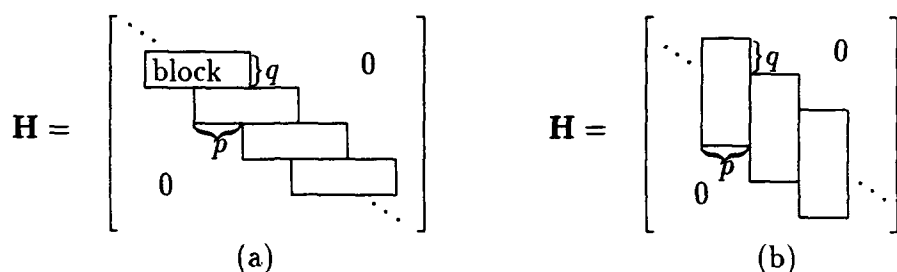


Figure 4.1. Block Structure of the Inner Product Matrix

define the block to have p columns with each block offset from the next by q rows. This interpretation is shown in Figure 4.1(b). With this interpretation, H can be considered as a filter operator and the impulse response of the filter can be found by directly looking at a particular column of the elemental block. Notice that the filter will generally have p different impulse responses depending on the location of the single non-zero value in the input sequence.

Figure 4.1 suggests the elemental blocks have finite dimensions. This is true when compactly-supported scaling functions are used. The width (Figure 4.1(a)) or height (Figure 4.1(b)) of the fundamental block will depend upon the support of the scaling function. The matrix entry will be non-zero only for row k and column n corresponding to shifts of

ϕ_{0n} and ϕ_{1k} which result in some overlapping support. For scaling functions which are not compactly-supported, the blocks will have infinite dimensions. However, the inner product matrix as a whole will still have structure in the sense that rows and columns will regularly repeat because Equation 4.22 will still hold.

The second description of the relationship between the approximation coefficients at adjacent levels is presented in the Fourier domain. By Parseval's relationship

$$\langle \phi_{1k}, \phi_{0n} \rangle = \langle \widehat{\phi_{1k}}, \widehat{\phi_{0n}} \rangle. \quad (4.23)$$

Now with

$$\begin{aligned} \widehat{\phi_{0n}}(f) &= e^{-i2\pi n f} \hat{\phi}(f), \\ \widehat{\phi_{1k}}(f) &= (p/q)^{1/2} e^{-i2\pi \frac{p}{q} k f} \hat{\phi}(f), \end{aligned} \quad (4.24)$$

we have

$$\langle \widehat{\phi_{0n}}, \widehat{\phi_{1k}} \rangle = \sqrt{pq} \int_{-\infty}^{\infty} \hat{\phi}(qf) \hat{\phi}(pf) e^{i2\pi(nq - kp)f} df. \quad (4.25)$$

By defining $H(f) = \hat{\phi}(qf)\hat{\phi}(pf)$, Equation 4.25 defines the inverse Fourier transform, h , of H so that

$$\langle \phi_{0n}, \phi_{1k} \rangle = h(nq - kp). \quad (4.26)$$

By defining

$$\tilde{H}(f) = \sum_n \tilde{h}(n) e^{-i2\pi n f}, \quad (4.27)$$

where $\tilde{h}(n) = h(-n)$, the operation $\mathbf{c}_1 = \mathbf{H}\mathbf{c}_0$ can be viewed as a filter operation where the $\{c_{0n}\}$ are upsampled by q , filtered with \tilde{H} , and downsampled by p . Figure 4.2 illustrates this. This leads to the following relationship between the approximation coefficients:

$$c_{1k} = \sum_n h(nq - kp) c_{0n}. \quad (4.28)$$

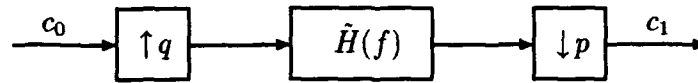


Figure 4.2. Processing diagram for Rational Resolution Approximations

Notice the case where $q = 1$. The dilation factor becomes simply p and the same expression as the integer resolution case results. The integer resolution analysis is simply a rational resolution analysis with $q = 1$. This is intuitive considering the integers are a subset of the rational numbers.

4.3 Rational Resolution Reconstruction

The previous section dealt with the approximation operation of a rational resolution analysis. This section will discuss reconstruction. Like the approximation operation, rational resolution reconstruction is more complicated than the integer resolution case because the approximation spaces are not embedded. Embedding implies each approximation space can be expressed as the direct sum of a lower-resolution approximation space and one or more detail spaces. Any information not carried into the next approximation is retained in the detail space(s). Consequently, reconstruction is simply the recombination of information contained in the approximation and detail spaces and no information is lost because the direct sum of the subspaces equals the original space. The orthogonality of the subspaces ensures no redundant information is obtained in the approximation space.

When the approximation spaces are not embedded, it is not clear how the detail information can be represented. We could define a detail space which is orthogonal to the rational approximation space. A space whose orthogonal basis is an equivalently-dilated wavelet would qualify. However, this space cannot be the orthogonal complement of V_m in V_{m-1} . This is a consequence of the approximation spaces not being embedded. Hence, we do not have wavelets which represent the detail information in the same way as the

integer resolution wavelets so we must find another way to recover the information lost during rational approximation.

Suppose we have a function $f \in V_{m-1}$ which has been projected onto V_m via a rational approximation operator $P^{p/q}$. Our goal is to reconstruct f from the approximated version $(P^{p/q} f)$. First we approximate $(P^{p/q} f)$ by projecting it onto a space V'_m defined such that

$$V'_m = \overline{\text{span}\{D^{1/q}_{p/q}\phi_{ml}\}_{l \in \mathbb{Z}}}, \quad (4.29)$$

where D is defined as the dilation operator such that $(D^\theta f)(t) = f(\theta t)$. Notice that the $\{D^{1/q}_{p/q}\phi_{ml}\}_{l \in \mathbb{Z}}$ span the same space as the p -dilated basis functions of V_{m-1} . In other words, we also have

$$V'_m = \overline{\text{span}\{D^{1/p}_{p/q}\phi_{m-1,l}\}_{l \in \mathbb{Z}}}. \quad (4.30)$$

Consequently, if ϕ is defined so that it satisfies the integer dilation equation

$$\hat{\phi}(pf) = H(f)\hat{\phi}(f) \quad (4.31)$$

for some $H(f) = \sum_n h(n)e^{-i2\pi nf}$, it follows that we have $V'_m \subset V_{m-1}$. If V'_m is an embedded subspace of V_{m-1} based on an integer dilation factor of p , then it will have $p-1$ mutually orthogonal detail spaces. From this point, the reconstruction is the same as an integer resolution analysis based on p . Define the following projection operators on $L^2(\mathbb{R})$:

$$\begin{aligned} P^{p/q}_m f &= \sum_k \langle f, \phi_{mk} \rangle_{p/q} \phi_{mk}, \\ P^q_m f &= (1/q) \sum_l \langle f, D^{1/q}_{p/q}\phi_{ml} \rangle D^{1/q}_{p/q}\phi_{ml}, \\ P^p_m f &= (1/p) \sum_l \langle f, D^{1/p}_{p/q}\phi_{m-1,l} \rangle D^{1/p}_{p/q}\phi_{m-1,l}, \\ Q^p_m f &= \sum_l \langle f, D^{1/p}_{p/q}\psi_{m-1,l} \rangle D^{1/p}_{p/q}\psi_{m-1,l}. \end{aligned} \quad (4.32)$$

The notation $D^{1/p}_{p/q}\psi_{m-1,l}$ denotes the wavelets which form the orthogonal complement of V'_m in V_{m-1} . The RRA approximation and reconstruction scheme is illustrated in Figure 4.3.

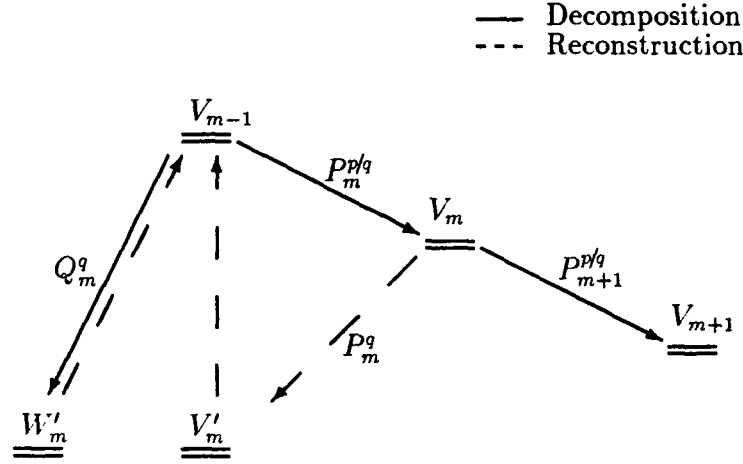


Figure 4.3. Summary of Rational Resolution Approximation and Reconstruction

We cannot assume this scheme yields perfect reconstruction unless we start with the correct approximation in V'_m . So, we need to study the projection onto V'_m from V_m .

In order to get perfect reconstruction, the projection onto V'_m must be the same regardless whether we project from V_{m-1} or V_m . This implies that for $f \in V_m$ we must show

$$P_m^q P_m^{p/q} f = P_m^p f. \quad (4.33)$$

To show this, we start with

$$P_m^{p/q} f = \sum_k \langle f, p/q \phi_{mk} \rangle p/q \phi_{mk}. \quad (4.34)$$

Projecting this function onto V'_m gives:

$$\begin{aligned} P_m^q P_m^{p/q} f &= \sum_l \sum_k \langle f, p/q \phi_{mk} \rangle \langle p/q \phi_{mk}, D^{1/q} p/q \phi_{ml} \rangle D^{1/q} p/q \phi_{ml} \\ &= \sum_l \left\langle f, \sum_k \langle p/q \phi_{mk}, D^{1/q} p/q \phi_{ml} \rangle p/q \phi_{mk} \right\rangle D^{1/q} p/q \phi_{ml}, \end{aligned} \quad (4.35)$$

where we have used the fact that all the functions are real. Now, consider the projection of f directly onto V'_m :

$$P_m^p f = \sum_l \langle f, D^{1/p} p/q \phi_{m-1,l} \rangle D^{1/p} p/q \phi_{m-1,l}. \quad (4.36)$$

Substituting

$$D^{1/p} p/q \phi_{m-1,l} = (p/q)^{1/2} D^{1/q} p/q \phi_{ml}, \quad (4.37)$$

we find that in order to show the equivalence of the two projections, it is necessary and sufficient to show

$$D^{1/q} p/q \phi_{ml} = \sum_k \langle p/q \phi_{mk}, D^{1/q} p/q \phi_{ml} \rangle p/q \phi_{mk}. \quad (4.38)$$

This simply says $D^{1/p} p/q \phi_{ml}$ is a linear combination of the $D^{1/q} p/q \phi_{mk}$, from which it follows that these spaces must also be embedded. So, in order to get perfect reconstruction, we must define the space V'_m such that $V'_m \subset V_{m-1}$ and $V'_m \subset V_m$.

The projection from V_m to V'_m is interesting. Dilating both sides of Equation 4.38 by $(p/q)^m$ gives

$$\phi_{1l} = \sum_k \langle p/q \phi_{1k}, p/q \phi_{1l} \rangle \phi_{0k}. \quad (4.39)$$

By substituting $\langle p/q \phi_{mk}, D^{1/q} p/q \phi_{ml} \rangle = \sqrt{q} \langle \phi_{0k}, \phi_{1l} \rangle$ in this expression, we arrive at the condition:

$$\phi_{1l} = \sum_k \langle \phi_{0k}, \phi_{1l} \rangle \phi_{0k}. \quad (4.40)$$

This implies that the approximation operator which projects from V_m to V'_m is based on an integer dilation factor of q . That is, given a function $f \in V_m$, we have $P^q f \in V'_m$. This is significant because integer-based projection operations are generally easier to implement than rational ones.

As a summary of this section and the previous one, consider Figure 4.3. From this figure, the processing scheme suggests that the rational resolution analysis is superimposed upon an integer resolution analysis. The reconstruction procedure exactly corresponds to an integer resolution analysis except the approximation in V'_m is found by way of an intermediate space V_m rather than by direct projection from V_{m-1} . We have also established that perfect reconstruction is obtainable only if the V'_m spaces are defined to be embedded subspaces of both V_m and V_{m-1} . The next section discusses the role of the scaling function in this requirement.

4.4 Scaling functions and Perfect Reconstruction

For perfect reconstruction, the choice of scaling function plays a key role in the rational resolution analysis. The scaling functions are intrinsically related to the approximation spaces. Thus, placing requirements on the approximation spaces will have repercussions in the choice of scaling functions. We have already seen one constraint in Equation 4.31.

In this section, we show by example that the compactly supported scaling functions which were described in the previous chapter do not lead to approximation spaces which allow perfect reconstruction using the scheme described in the previous section. However, we demonstrate that the reconstruction obtained from these scaling functions is still very good. We conclude with a description of a class of scaling functions which lead to embedded approximation spaces and provide an example.

We want to show by example that the compactly-supported scaling functions defined previously do not satisfy the perfect reconstruction scheme of the previous section. To do

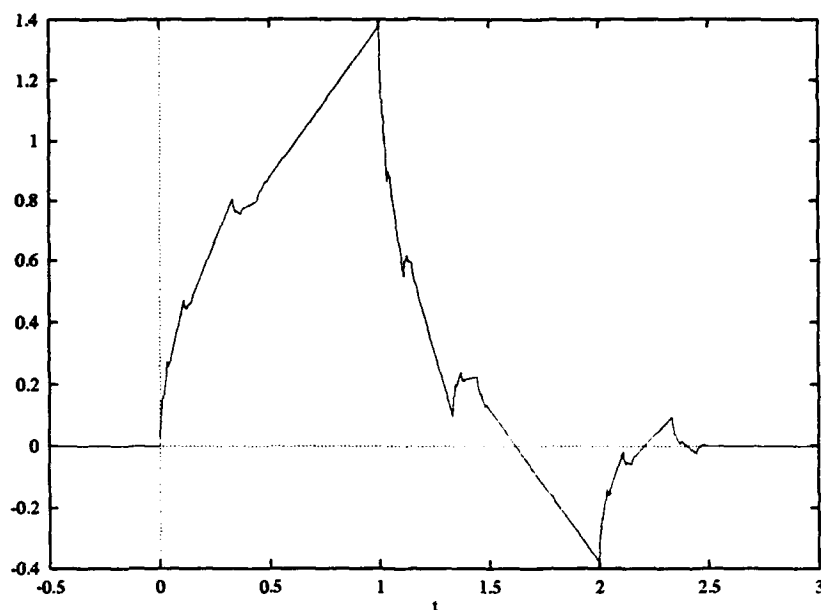


Figure 4.4. Compactly Supported Scaling Function with $p = 3$ and $N = 2$ ($\phi(t)$ vs. t)

this, consider Equation 4.40 again. Suppose we are using a compactly supported scaling function based on an integer $p = M$ dilation. We can calculate the sum in Equation 4.40, dilate it by $1/q$, and compare it to the original scaling function. Consider the following example.

Example 4-3 Consider the $M = 3, N = 2$ compactly supported scaling function ϕ shown in Figure 4.4. Define the approximation space V_0 to be the span of its orthonormal integer translates. Now suppose $q = 2$. With $p = 3$, we calculate the inner products required in Equation 4.40 (See Appendix B for details). If this equation holds, then the scaling function dilated by 2 is in V_0 . Conversely, ϕ_{00} should be in the space spanned by $D^2\phi_{0n}$ for $n \in \mathbb{Z}$. In Figure 4.5, we graphically compare ϕ_{00} and its projection onto the space spanned by $D^2\phi_{0n}$ for $n \in \mathbb{Z}$. Although the two scaling functions have the same basic shape, they are

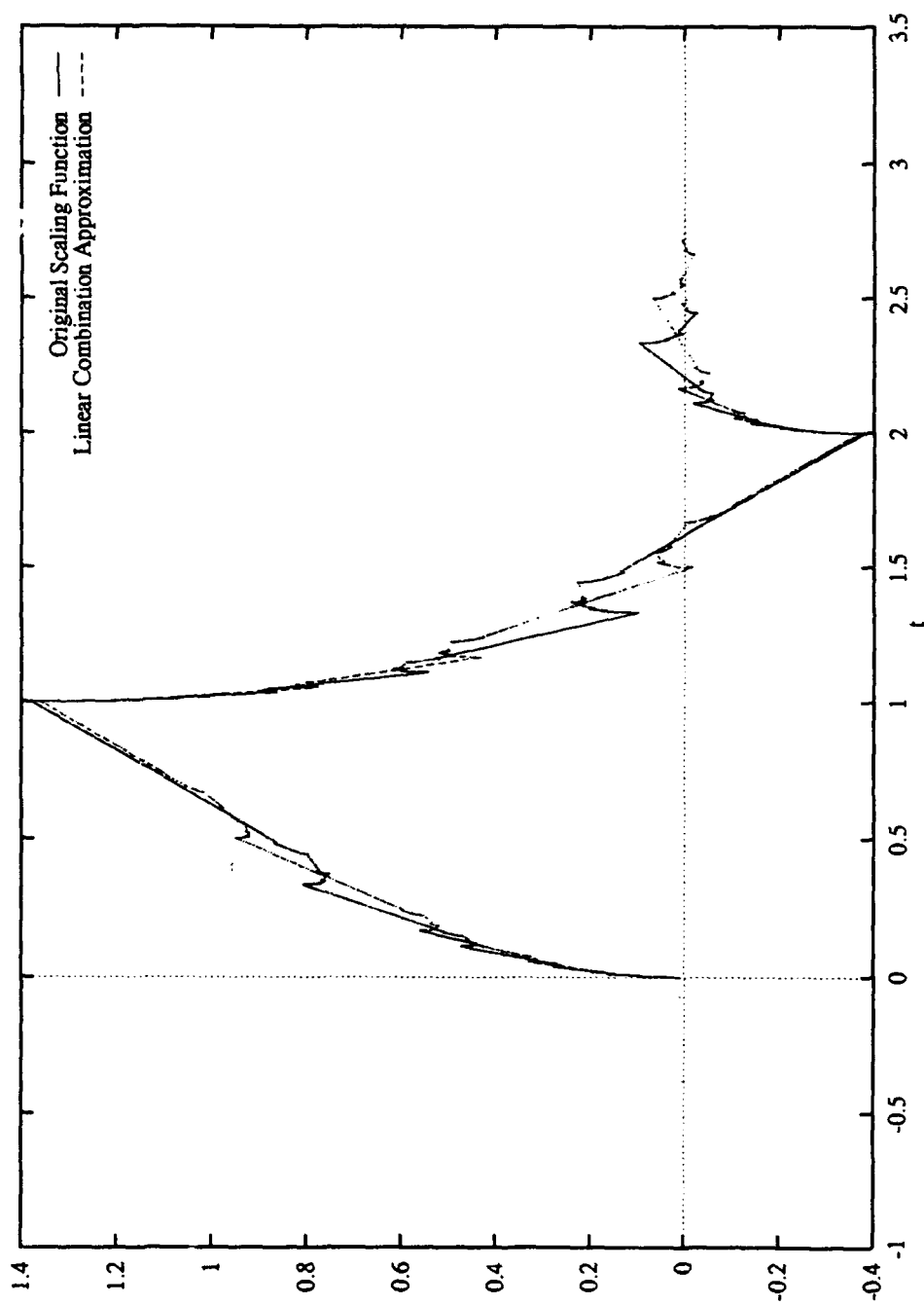


Figure 4.5. Comparison of $M = 3$, $R = 2$ Scaling Function with Linear Combination of $1/q$ Dilated Scaling Functions for $p = 3$ and $q = 2$ ($\phi(t)$ vs. t)

obviously not equivalent. For instance, they have unequal supports. From this we conclude the approximation spaces V_1 and V'_1 are not embedded.

□

Because the approximation spaces based on compactly-supported scaling functions are not embedded, we cannot hope to obtain perfect reconstruction. However, because the shapes of the two scaling functions in the previous example are similar, we can expect a reasonable reconstruction. In order to see this effect of this approximation, we return to approximation coefficients and discrete filter operations.

The multiresolution analysis, rational or otherwise, is a linear transformation. As with most discrete processing systems, the impulse response is very important in that it provides a great deal of information about the characteristics of the system. Consider the following example.

Example 4-4 Suppose we have a set of approximation coefficients

$$c_{0n} = \begin{cases} 1 & n = 0 \\ 0 & \text{otherwise} \end{cases} \quad (4.41)$$

and we want to rationally approximate these coefficients and then reconstruct. Assume that $p = 3$ and $q = 2$ and the scaling function associated with the analysis is the one given in the previous example (Figure 4.4). We decompose this set of approximation coefficients using the coefficients in Table 4.1 which were calculated as in Appendix B. The resulting approximation coefficients are shown in Table 4.2. The detail coefficients are generated using the optimized detail filter coefficients of Example 3-3. These detail coefficients generated from the c_{0n} are shown in Table 4.3.

Now, the c_{1k} are filtered via the coefficients in Equation 4.40 for the scaling function given shown in Figure 4.4. These filter coefficients are given in Table 4.4. The result-

Table 4.1. Rational Approximation Filter Coefficients

n	$h(n)$
-4	-0.000287420672395512
-3	-0.0440663791657491
-2	0.00572865007567187
-1	0.305000213846163
0	0.734891371897753
1	0.908269395408422
2	0.582716289665621
3	0.126436376018966
4	-0.0975392317518494
5	-0.0709325019117585
6	-0.000764787823073089
7	3.77671951090657e-05

Table 4.2. Rational Approximation Impulse Response Coefficients with $p = 3$ and $q = 2$

k	c_{1k}
-2	-0.000764787823073
-1	0.126436376018966
0	0.734891371897753
1	-0.044066379165749

Table 4.3. Detail Coefficients

l	d_l^1	d_l^2
-1	-0.73479360808553	-0.33431907117540
0	-0.07789569612441	0.41307668343873

ing coefficients are approximate approximation coefficients and we denote them by \tilde{c}'_{1l} . The true approximation coefficients, c'_{1l} , are found by filtering the c_{0n} with the $M = p$

Table 4.4. Approximate Reconstruction Filter Coefficients

n	$h(n)$
-2	-0.000258795002995204
-1	0.0051580987167051
0	0.487272389375389
1	0.830841375288264
2	0.220942569573341
3	-0.128892692818564
4	-0.000849382759163267

integer-resolution approximation filter. Both sets of coefficients are given in Table 4.5. The similarity of the two sets of coefficients is a good indication of the degree of perfect reconstruction which is obtainable in this case. Combining the \tilde{c}'_{1l} in Table 4.5 with the detail coefficients in Table 4.3, we obtain \tilde{c}_{0n} which is an approximation of the original c_{0n} . The \tilde{c}_{0n} are given in Table 4.6 and shown graphically in Figure 4.6. The values of the \tilde{c}_{0n} are identically zero outside the range of n shown in the figure and listed in the table. The impulse response shown in Figure 4.6 is non-causal (has non-zero values for $n < 0$) because the filters used to obtain it are non-causal. In practice, we would be constrained to causal filters and would naturally expect a delay in the impulse response.

Table 4.5. Comparison of True Approximation Coefficients and Approximate Approximation Coefficients

l	c_{1l}	c'_{1l}
-3	0.0	6.495975913362887e-07
-2	0.0	-0.017089903223261
-1	0.2389641719057618	0.2727245348859523
0	0.3383860972838639	0.3221324728780859
1	0.0	-0.0004174849486161193

Table 4.6. Impulse Response Coefficients for a Rational Resolution Using the $M = 3$,
 $R = 2$ Scaling Function

n	\tilde{c}_{0n}
-9	2.198147937372851e-07
-8	3.448299084782647e-07
-7	4.698450232192443e-07
-6	-0.00578283042412773
-5	-0.009071908848033937
-4	-0.01236098727194014
-3	0.007340162900056513
-2	0.0171263011937004
-1	0.02691243948734121
0	1.002567516653402
1	-0.00705767970676463
2	-0.01668287606694384
3	-0.004025304999031559
4	-0.0009776385395248652
5	0.002070027919981815
6	-9.976394502917046e-05
7	-1.941892920712597e-05
8	6.092608661491856e-05

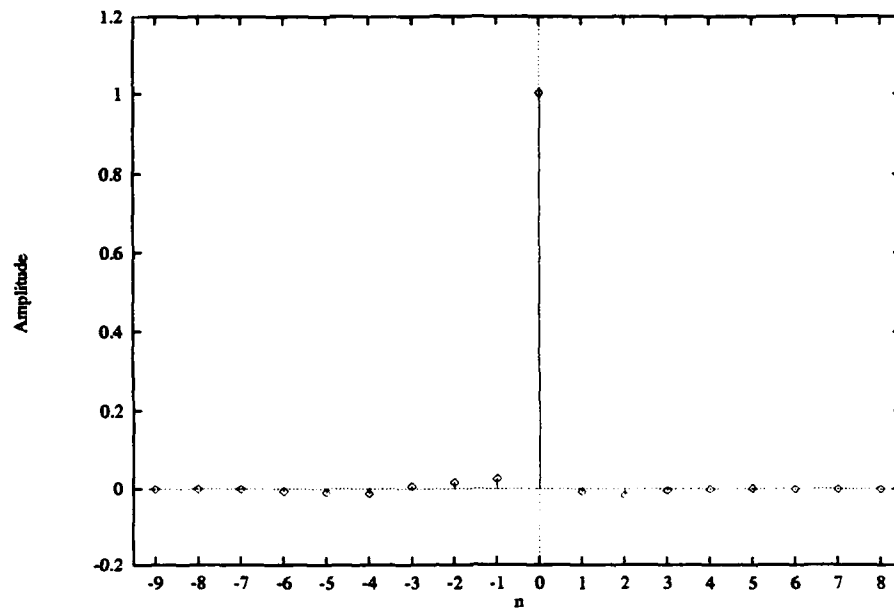


Figure 4.6. RRA Reconstruction of Impulse Function

Although the approximation coefficients have significant differences, the effect on the reconstruction is minimal in this case. To illustrate this point, Figure 4.7 shows a sample signal and its reconstruction using the coefficients given above. Any differences between the two are not graphically detectable.

□

We mentioned earlier that the rational resolution approximation will generally have more than one impulse response. For simplicity, we demonstrated only one of the three in the previous example. Figure 4.7 indicates that the other two responses are similar to the one demonstrated in the example.

For the particular choice of scaling function in the previous example, the quality of the approximate reconstruction is comparable to the exact reconstruction. cursory inspection of the actual values of the sample signal indicate exact agreement to 6 decimal places. To

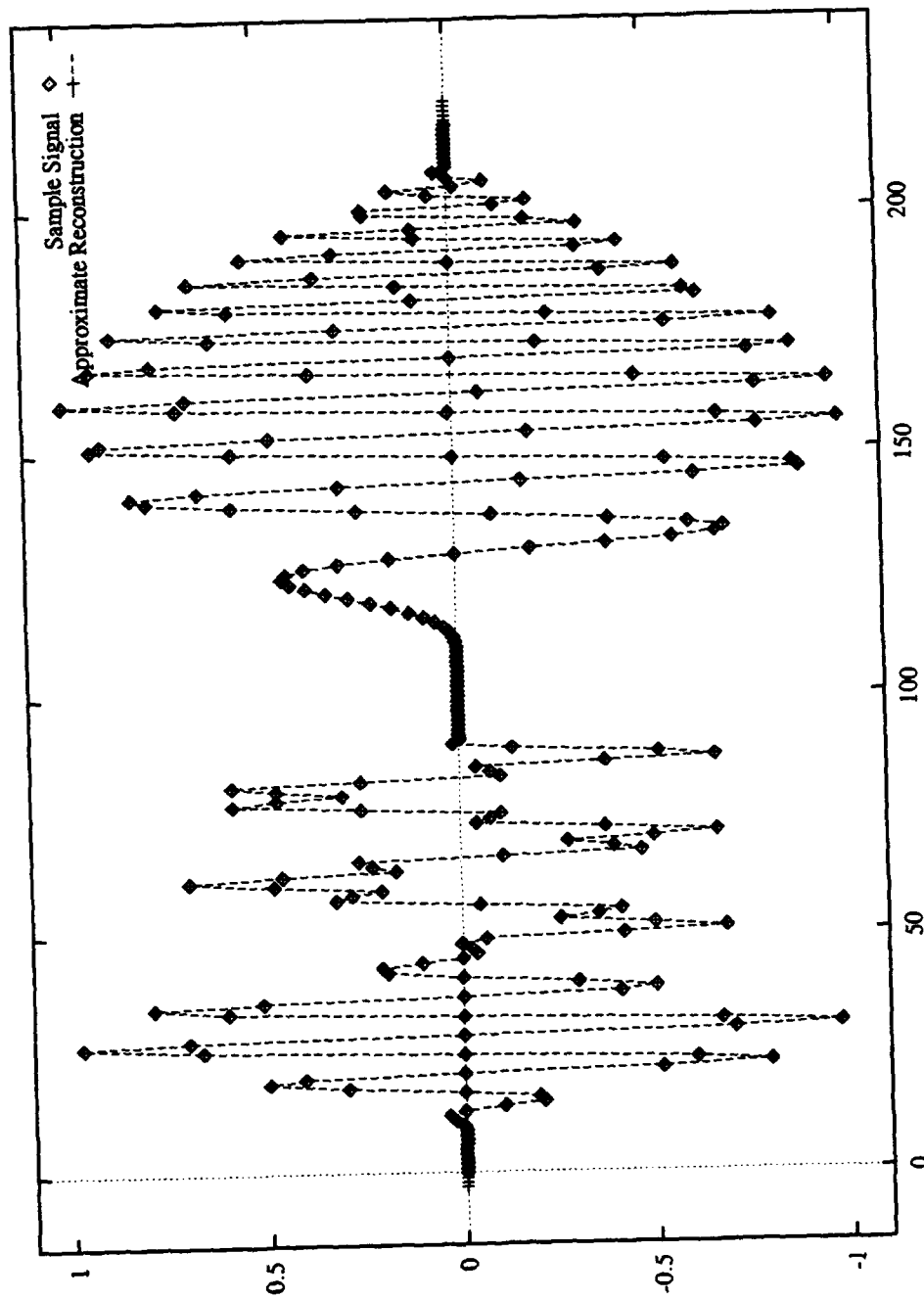


Figure 4.7. Sample Signal and Approximate Rational Resolution Reconstruction for $M = 3$, $R = 2$ Scaling Function

investigate whether the choice of scaling function has any effect on this performance, the same experiment was performed with the $M = 3$, $R = 3$ scaling function, which is more regular than the one in Example 4-4. The scaling function is shown in Figure 4.8 and the comparison between it and the $1/2$ -dilated linear combination given by the inner product calculations of Equation 4.40 is shown in Figure 4.9. The impulse response reconstruction is given in Table 4.7 and the sample signal reconstruction is shown in Figure 4.10.

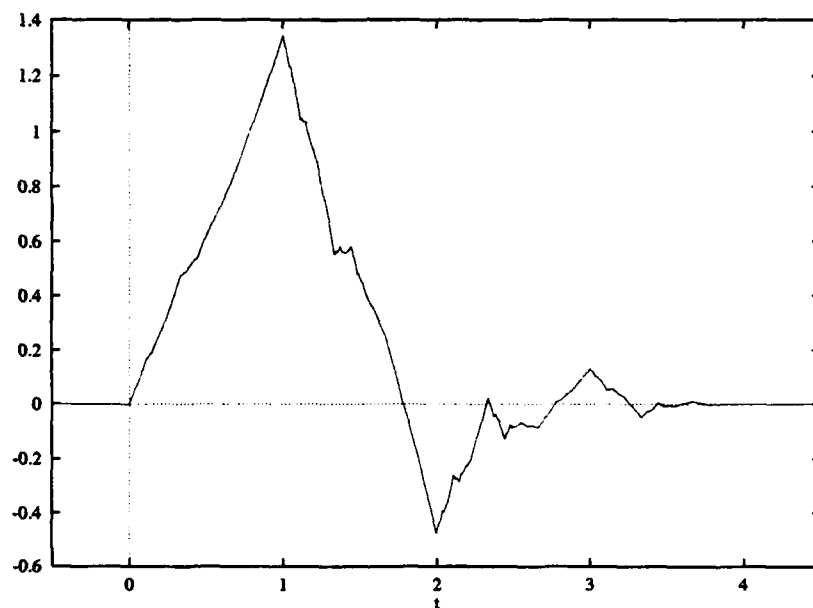


Figure 4.8. Compactly Supported Scaling Function with $p = 3$ and $R = 3$ ($\phi(t)$ vs. t)

When impulse response coefficients in Table 4.6 and Table 4.7 are compared, it is apparent that the coefficients in Table 4.6 are closer to a true impulse response. This would seem to indicate that the approximation is better with the lower regularity scaling functions. A quick inspection of the actual reconstructed samples in Figure 4.10 reveals that this is true. The approximate values differ somewhat from the actual values although these differences are not detectable in Figure 4.10.

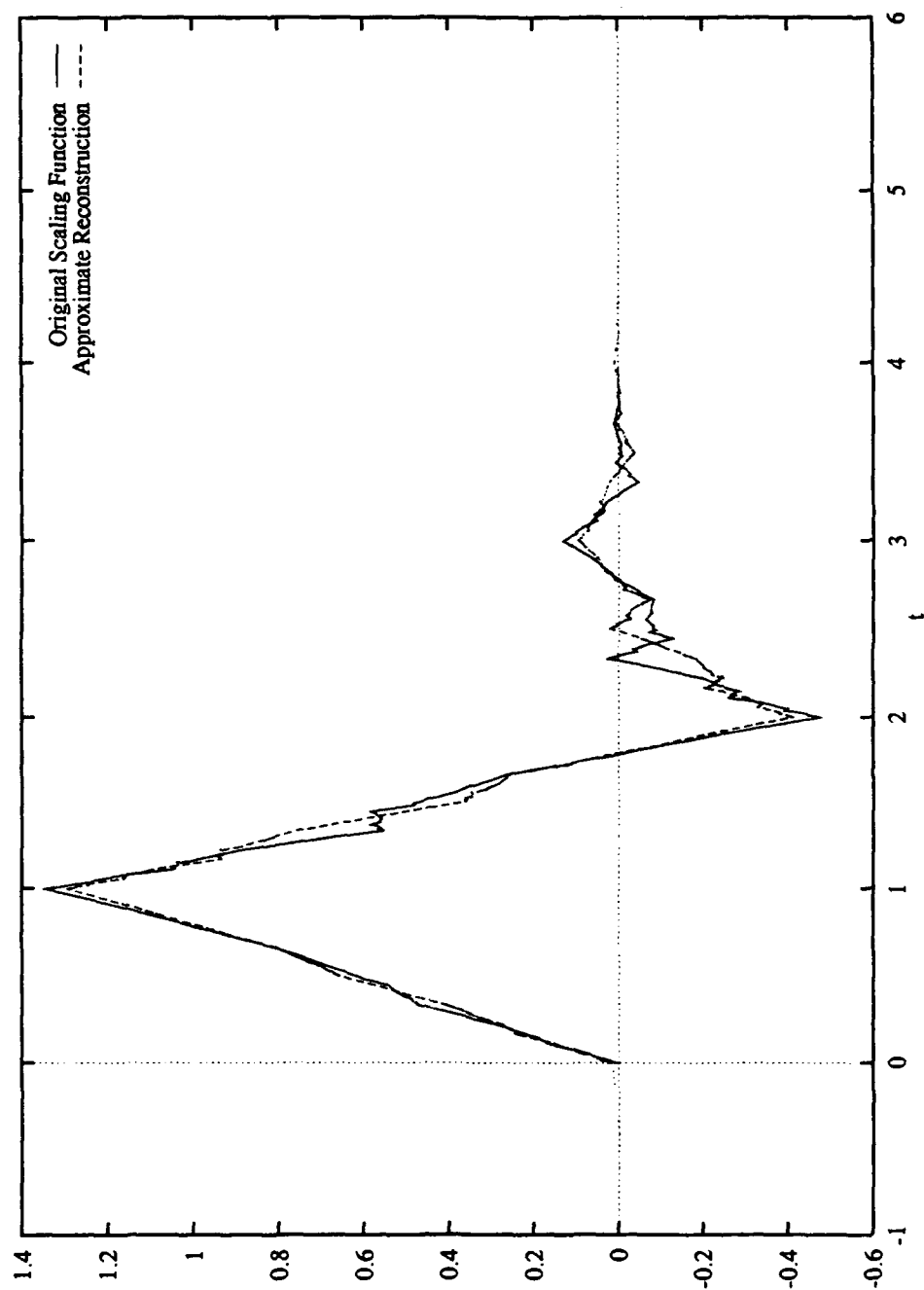


Figure 4.9. Comparison of $M = 3$, $N = 3$ Scaling Function with Linear Combination of $1/q$ Dilated Scaling Functions for $p = 3$ and $q = 2$ ($\phi(t)$ vs. t)

Table 4.7. Impulse Response Coefficients for a Rational Resolution Using the $M = 3$, $R = 3$ Scaling Function

n	\tilde{c}_{0n}
-15	2.521503816700972e-08
-14	5.252538602629477e-08
-13	8.779863683804167e-08
-12	2.364535890286332e-05
-11	4.916486647168172e-05
-10	8.211815480890592e-05
-9	0.002455484054276105
-8	0.005030148725821753
-7	0.00834900132830889
-6	-0.001828456187451866
-5	-0.01244507728606293
-4	-0.0268146562922356
-3	-0.009806152342156149
-2	0.006368699629402036
-1	0.02988496789836725
0	1.015390801838894
1	0.004469421168744825
2	-0.0134326466588571
3	-0.006385114138053594
4	-0.00366493783613446
5	0.002158128377207594
6	4.950872631421729e-05
7	0.0001268319880036728
8	-0.0001776711990643005
9	9.029619674973409e-05
10	5.573695713435322e-05
11	-5.928195953517768e-05
12	5.267473524307781e-09
13	3.251115519546015e-09
14	-3.457748942040833e-09

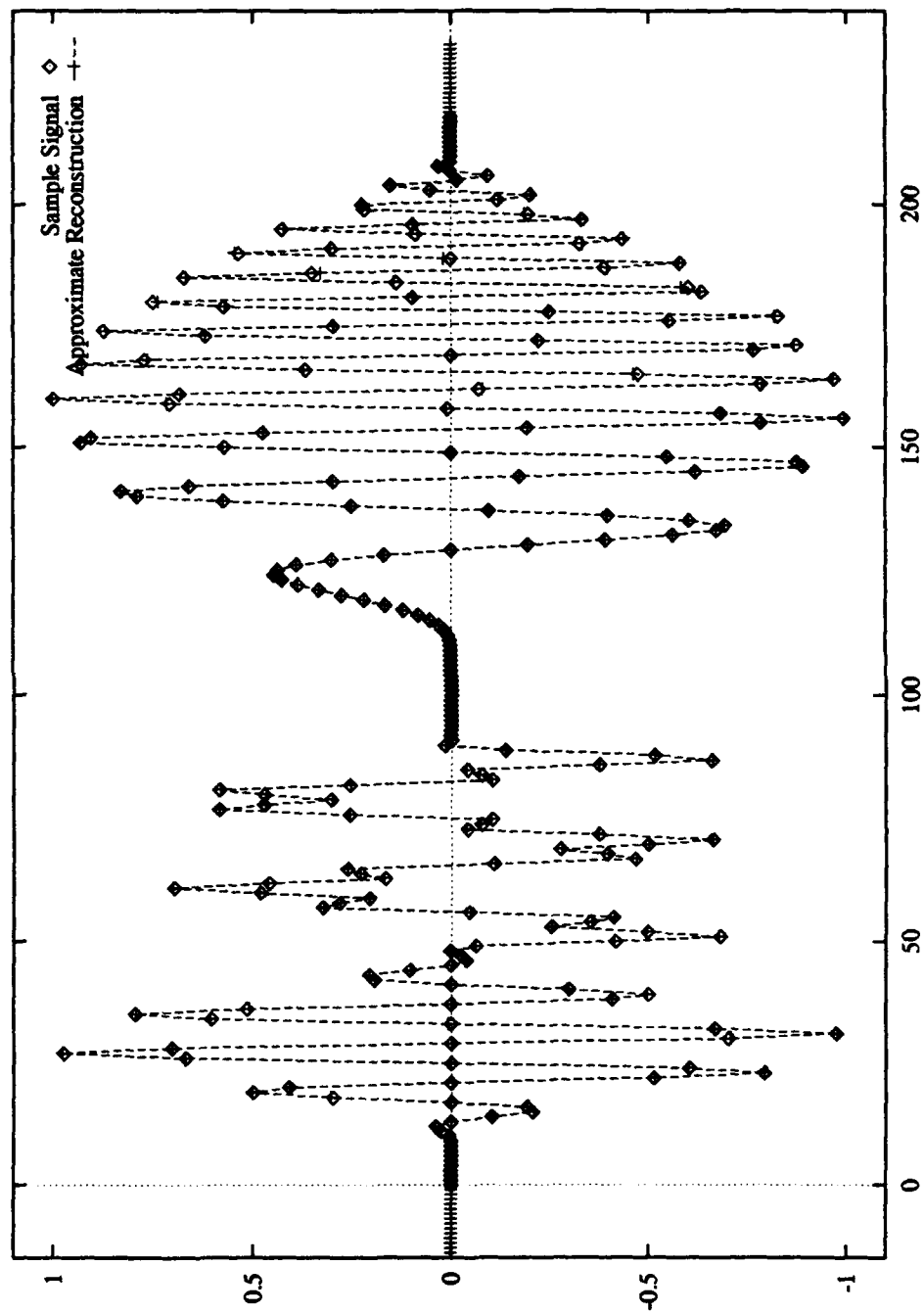


Figure 4.10. Sample Signal and Approximate Rational Resolution Reconstruction for $M = 3$, $R = 3$ Scaling Function

While the analysis of the reconstruction properties using compactly supported scaling functions is a topic for further investigation, we suggest that the reconstruction quality decreases with regularity of the scaling functions. The actual choices for the rational dilation factor p/q might also affect the reconstruction quality and it, too, is a topic for further investigation.

4.5 Spline-based Scaling Functions and Perfect Reconstruction

In the previous section we generally discussed the class of compactly supported scaling functions and showed we could get reasonable reconstruction results using the scheme we developed earlier. In this section, we want to further comment on the perfect reconstruction conditions and discuss the class of spline-based scaling functions which are suitable for achieving perfect reconstruction.

When the approximation spaces are defined as in Figure 4.3, we have shown it is necessary to have V'_m as an embedded subspace of both V_{m-1} and V_m for perfect reconstruction. For the compactly supported scaling functions in this thesis, this condition is not met. The exception to this is the scaling function which is the characteristic function $\chi_{[0,1)}$. We cannot say categorically that there are no other compactly supported scaling functions which lead to perfect reconstruction but such an investigation is beyond the scope of this thesis.

Recall how the compactly-supported scaling functions were developed. We needed to develop a set of projection operators which satisfied certain orthonormality conditions. We cast the projection operators in terms of discrete filters and from these the scaling functions were generated. The approximation spaces were then defined in terms of the scaling functions. That is, we defined an approximation space as the closed linear span of integer translates of the scaling function we had defined. In all cases, the scaling function was defined before the approximation space.

But the constraints for perfect reconstruction in the rational resolution scheme are placed on the approximation spaces, not directly on the scaling functions. Hence, if we want to satisfy conditions on the approximation spaces, we can start with those spaces and not with the scaling functions. In other words, we can define the approximation spaces to satisfy the rational resolution perfect reconstruction constraints, then find the corresponding scaling functions, not vice versa. Consider the following simple example:

Example 4-5 Consider the space of piecewise constant functions. An orthonormal basis for this space is the familiar characteristic function $\chi_{[0,1)}$. If we let

$$V_0 = \overline{\text{span}\{\chi_{[n,n+1)}\}_{n \in \mathbb{Z}}} \quad (4.42)$$

then for all rational dilation factors p/q , it is easy to see that the space embedding condition for RR perfect reconstruction will hold because we can write

$$\chi_{[pl, p(l+1))} \approx \sum_{n=pl}^{p(l+1)} \chi_{[n, n+1)} \quad (4.43)$$

and

$$\chi_{[ql, q(l+1))} \approx \sum_{n=ql}^{q(l+1)} \chi_{[n, n+1)}. \quad (4.44)$$

□

As a general class of functions, consider the B -splines. A B -spline is a piecewise polynomial function such that at its nodes (or knots), only $B - 2$ continuous derivatives exist. Further consider the B -splines which have knots at the integers. For instance, the linear splines (2-splines) are continuous at the integers, but its first derivative generally does not exist. Example 4-5 illustrates the simplest case of B -spline functions: the piecewise constant functions. These functions are not even continuous at the integers. The B -spline

spaces are interesting because they satisfy the RR perfect reconstruction conditions. To see this, consider the following example:

Example 4-6 *Define the approximation space V_0 to be the space of all linear splines in $L^2(\mathbb{R})$. Assume we have a function ϕ such that the integer translations of ϕ form an orthonormal basis of V_0 . For any rational dilation factor p/q , it is clear that we can write $\phi(t/p)$ and $\phi(t/q)$ as a sum of $\phi(t - n)$ because the p and q -dilated versions of ϕ will also be piecewise linear except their nodes (or knots) will occur at integer multiples of p and q respectively instead of at every integer. Hence, conditions for RR perfect reconstruction will be satisfied because the approximation spaces are embedded.*

□

This example extends to any space of spline functions, but while the scaling function ϕ can be found in a straightforward manner, it generally does not have compact support. Hence, the approximation filter will not have compact support. Thus its implementation will introduce errors because we would have to represent an infinite length filter with a finite length approximation. Additionally, we cannot produce the spline wavelets by Vaidyanathan's technique described in the previous chapter. This is a topic for future investigation.

4.6 Frequency Domain Interpretation of the RRA

In this section, we detach ourselves from the mathematics of the rational resolution analysis to investigate its discrete-time signal processing characteristics. Throughout this thesis we have cast the approximation and reconstruction operations in both the integer and rational multiresolution analyses as discrete filter operations. We have discussed the

frequency characteristics of the filters for integer resolution analyses; this section discusses the frequency domain interpretation of those for the rational resolution analysis.

We expressed the rational resolution approximation processing as an upsampling by q , then filtering by h , followed by downsampling by p (see Figure 4.2). This sort of scheme is typically used in discrete-time signal processing to do rational sampling rate changes. The filter is used to prevent aliasing. See [17] for more details on rational sampling rate changes.

For the integer resolution analysis based on a dilation of p , each successive approximation had the effect of a low-pass filtering operation. In terms of the frequency spectrum, each approximation was effectively the lowest $1/p$ -th of the frequency spectrum of the previous approximation. For the rational resolution case, we can extend this idea and say that each approximation is effectively the lower q/p of the spectrum of the previous approximation. It is easy to see the effects of a $1/p$ low-pass filter operation for the integer case, but the rational p/q case takes a bit more explanation because of the upsampling.

When a discrete-time signal is upsampled by q , the sampling rate is effectively increased by q . In terms of the actual signal, upsampling inserts $q - 1$ zeros between each sample so that the sampling period T is effectively decreased to T/q . Compressing the discrete-time axis by q has the effect of dilating the frequency axis by the same amount. This is important when you consider the effect of the anti-aliasing filter $h^{(p/q)}$.

Suppose we have a discrete-time signal with sample period T_1 which is band-limited to its Nyquist frequency $f_s = 1/(2T_1)$. If we define normalized frequency ω such that

$$\omega = 2\pi fT \quad (4.45)$$

where T is the sample period, then $\omega_s = \pi$ results². Suppose we upsample this signal by q so that the new sample period is $T_2 = T_1/q$. The signal will be still be bandlimited to f_s , but now, the corresponding normalized frequency will be $\omega_s = \pi/q$.

If $h^{(p/q)}$ is a lowpass filter with a cutoff frequency $\omega_c = \pi/p$, then the effective cutoff of the signal in continuous frequency will be

$$f_c = \frac{\omega_c}{T_2} = \frac{q\omega_c}{T_1}. \quad (4.46)$$

Substituting for ω_c in terms of f_s , we find

$$f_c = \frac{q}{p} f_s. \quad (4.47)$$

This implies that the approximation filter has an "effective" cutoff frequency of q times that of $h^{(1/q)}$ so that we can interpret the entire rational approximation operation as keeping the lower q/p of the input spectrum via a lowpass filter with cutoff at $\omega_c = \pi(q/p)$. To verify that the approximation filter $h^{(p/q)}$ is indeed a π/p lowpass filter, consider Figure 4.11 which is the frequency response of the filter given in Table 4.1. The "extra" gain in the filter (indicated by the magnitude at $f = 0$ being $\sqrt{6}$ and not 1) is to compensate for the loss which occurs in the upsample operation. See [17] for details.

Compare this frequency interpretation with that of the integer resolution analysis. For an integer dilation of p , the approximation filter is lowpass in that it passes the lowest $1/p$ of the input spectrum. For the rational dilation case, we see that the approximation filter is again lowpass, but it tries to pass the lowest p/q of the input spectrum because of the upsampling. Once again we see how the integer resolution analysis is just a special case of the rational resolution analysis corresponding to $q = 1$.

²We use f here to denote continuous frequency. We have used f previously in this thesis to denote both continuous and normalized frequency because we assumed a unit sample period. We introduce ω here to avoid confusion and to be consistent with discrete-time processing literature.

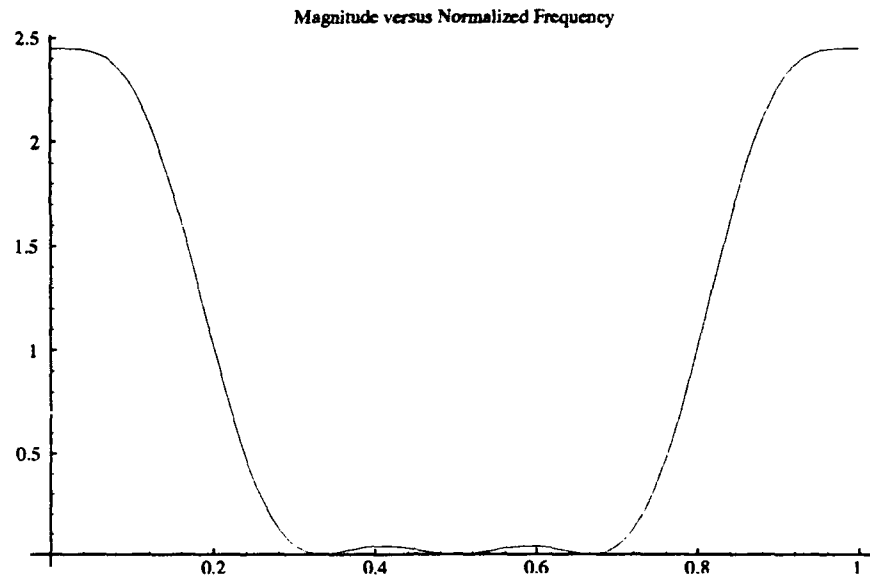


Figure 4.11. Frequency Response for Table 4.1

4.7 Conclusions

We conclude this chapter with a summary of its major points. We described the rational resolution approximation as a series of projections onto a set of non-embedded approximation spaces. The basis function of one approximation space is simply a p/q dilation of the basis function of the previous space. In this respect, the RRA is similar to the IRA. We saw how the filtering operation for rational dilation factors was an upsampling by q , a discrete filter operation, followed by downsampling by p . Reconstruction is more complicated because the spaces are not embedded.

The reconstruction scheme involves a further projection of the rational approximation onto a newly defined lower resolution approximation space V_m'' . This space was defined to be an embedded subspace of the original higher-resolution space so that the integer resolution reconstruction technique could be used to reconstruct the function. We showed that a necessary condition for perfect reconstruction was that the approximation space V_m'' be an embedded subspace of V_m and of V_{m-1} .

We demonstrated that the compactly supported scaling functions of previous chapters did not in general lead to perfect reconstruction in the rational resolution scheme. However, we presented examples which demonstrated that the approximate reconstruction was very good for two particular compactly supported scaling functions. Thus, although we could not get perfect reconstruction, compactly-supported scaling functions were still useful with rational resolution analyses.

We described a set of approximation spaces which satisfied the RR perfect reconstruction condition. The spaces of B -splines satisfy the conditions because they represent functions whose break points or "knots" are defined at the integers. Integer dilations of these functions will still have knots at integer values so that the approximation spaces defined by the b -splines are embedded for all integer dilations, not necessarily restricted to the integer dilation used to generate the scaling function. However, the scaling functions generally do not have compact support and it is unclear at this time how the corresponding B -spline wavelets can be generated.

The final section presented an interpretation of the rational resolution analysis in terms of its frequency characteristics. We showed that the rational approximation is a low-pass filtering operation like the integer approximations. The cutoff frequency is roughly defined by the dilation factor. We use some of the frequency domain characteristics in practical applications of the rational resolution analysis in the next chapter.

V. Applications

5.1 Introduction

In this chapter we present some practical applications of the Rational Resolution Analysis. Our main goal is to compare and contrast the RRA developed in previous chapters with the conventional dyadic MRA on a variety test signals including human speech. We want to investigate the time-frequency localization characteristics, the coding potential, and sources of errors for the RRA with respect to the dyadic case. We find areas where the RRA has advantages over the MRA and also identify areas where it falls short.

5.2 Time-Frequency Characteristics

Wavelet analysis was primarily developed to aid in the processing of non-stationary signal-signals whose frequency characteristics are not constant with respect to the independent variable (usually time or position). This section qualitatively investigates the time-frequency processing characteristics of the RRA and compares it to the dyadic MRA. We are specifically interested in the two methods' ability to localize frequency and whether or not we can determine if one is better than the other in this respect.

Define a rectangular input sequence

$$\text{rect}(n) = \begin{cases} 1 & |n - 200| < 100 \\ 0 & \text{otherwise.} \end{cases} \quad \text{for } n \in \{0, 1, \dots, 399\}$$

We decompose this sequence with both a dyadic MRA and an RRA with dilation factor of $3/2$. We use regularity based on $N = 2$ for both. The results of the decompositions are presented in Figures 5.1–5.11; these require some explanation. The independent variable n is increasing left to right along the bottom edge these images. The vertical axis indicates increasing levels of decomposition and, thus, coarser resolution. Each horizontal band

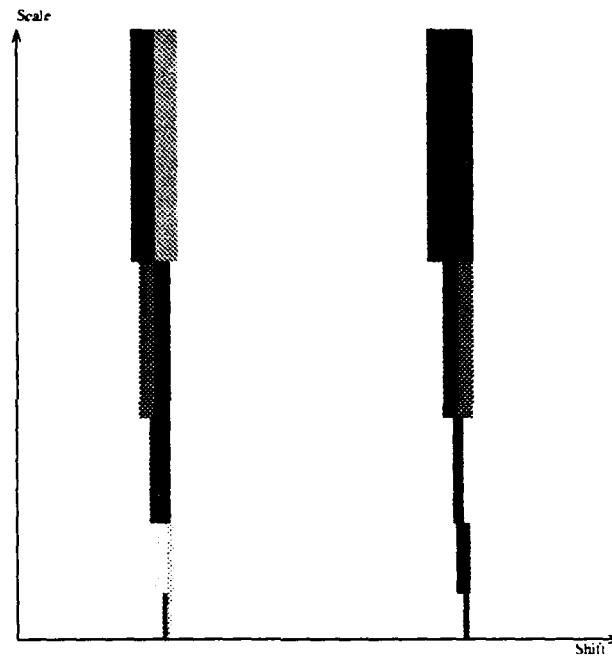


Figure 5.1. Grey Scale Representation of Rect Function Detail Coefficients for $M = 3$, $N = 2$, $p = 3$, $q = 2$, 5 levels. (Wavelet 1)

represents the approximation or detail coefficients at that level, depending upon what is being illustrated. The darker the block, the greater the magnitude of the coefficient. White corresponds to zero and solid black corresponds to the coefficient with the greatest magnitude at each resolution level. All other values at that level are linearly scaled between zero and this value. The height of each band is individually scaled to correspond to the dilation of the basis function at that level. If we were to express the vertical axis logarithmically, the bands would have equal height. The ratio between widths of adjacent bands is determined by the dilation factor.

Figures 5.1 and 5.2 are the detail coefficients for a rational resolution decomposition of the rect function with $p/q = 3/2$ and $N = 2$. The detail filters used in the decomposition are the same stop-band optimized filters developed in Example 3-3. The decomposition of the dyadic case is shown in Figure 5.3. We can observe several things about these figures. First, it is apparent that the wavelets in both the RRA and MRA highlight the



Figure 5.2. Grey Scale Representation of Rect Function Detail Coefficients for $M = 3$, $N = 2$, $p = 3$, $q = 2$, 5 levels. (Wavelet 2)

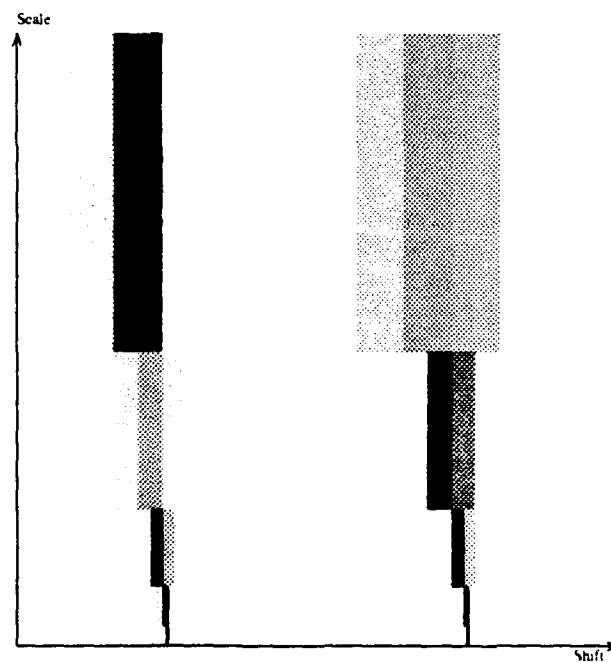


Figure 5.3. Grey Scale Representation of Rect Function Detail Coefficients for $M = 2$, $N = 2$, $p = 3$, $q = 2$, 5 levels.

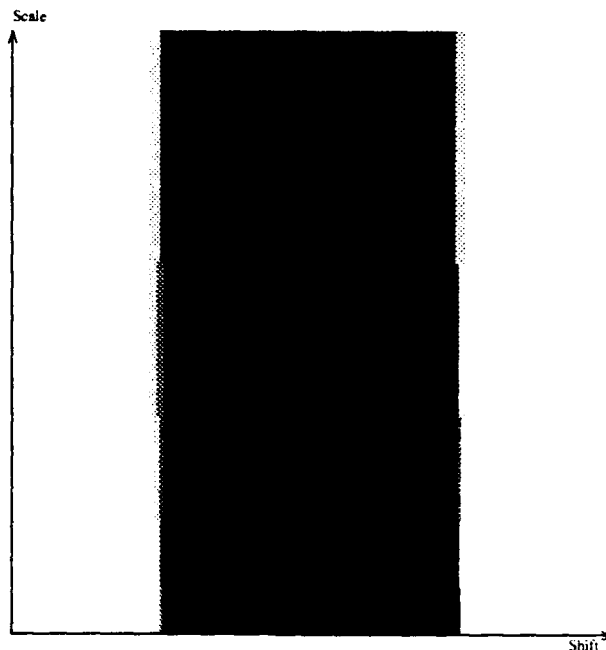


Figure 5.4. Grey Scale Representation of Rect Function Approximation Coefficients for $M = 3$, $N = 2$, $p = 3$, $q = 2, 5$ levels.

high-frequency edges of the input signal. This verifies the high-pass nature of the scaling filters. Second, it is not apparent whether one representation or the other better localizes the edges of the input.

Before moving on, consider the RRA and MRA approximation coefficients which result from processing the rect input signal. These are shown in Figures 5.4 and 5.5 respectively. They show similar behavior in that the edges begin to blur as the decomposition level increases.

Now consider a non-stationary signal such as a chirp. Define an input signal

$$\text{chirp}(n) = \begin{cases} \sin(2\pi((n - 100)/100)^3) & n \in \{100, 101, \dots, 299\} \\ 0 & \text{otherwise} \end{cases} \quad (5.1)$$

This signal is shown in Figure 5.6. Although the signal is a set of discrete points, the signal shown is continuous so that its structure is apparent. This signal has time-varying

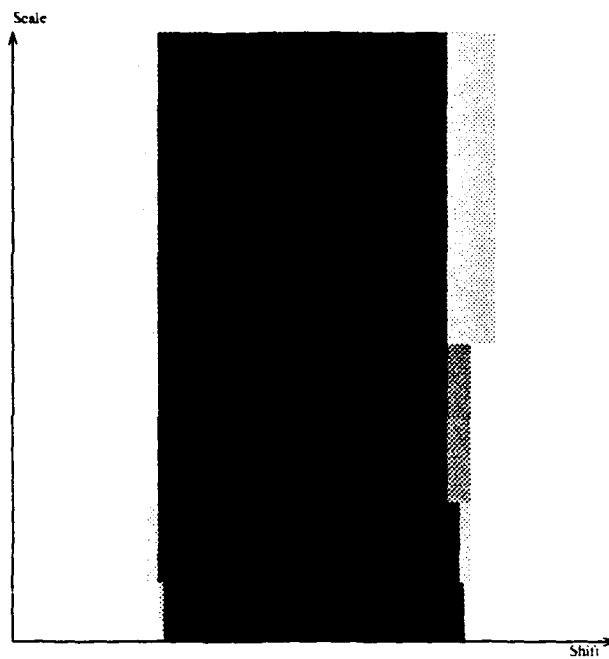


Figure 5.5. Grey Scale Representation of Rect Function Approximation Coefficients for $M = 2$, $N = 2$, $p = 2$, $q = 1, 5$ levels.

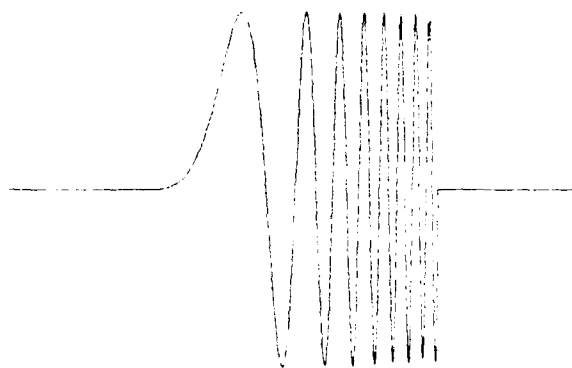


Figure 5.6. Chirp Signal

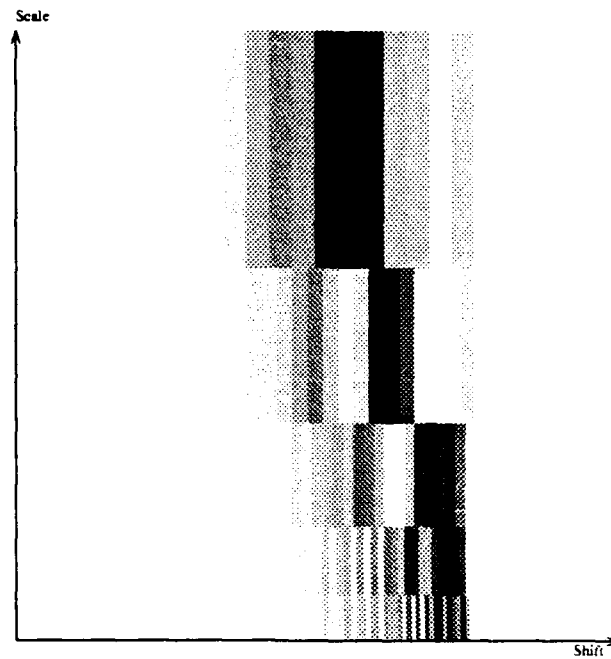


Figure 5.7. Grey Scale Representation of Chirp Function Detail Coefficients for $M = 3$, $N = 2$, $p = 3$, $q = 2, 5$ levels. (Wavelet 1)

frequency so we would expect this feature to appear in the detail and approximation coefficients shown in Figures 5.7 - 5.11. Recall the wavelets used in the rational resolution decomposition correspond to detail filters which have been chosen to have minimum stop-band energy. This implies they have maximum pass-band energy and, thus, have maximum response to specific bands of the spectrum. Also, recall that these pass-bands were defined to be adjacent to each other in the spectrum. Thus, since the chirp has monotonically increasing frequency, we expect to see the two wavelets responding to parts of the chirp which are next to each other at each resolution level. This is indeed the case as seen in the third and fourth level coefficients in Figures 5.7 and 5.8. The image of the second wavelet responds (more black) to the higher frequencies and the first wavelet responds more to the lower frequencies. If the two images are overlaid, it is evident that the two wavelets are responding to adjacent parts of the chirp.

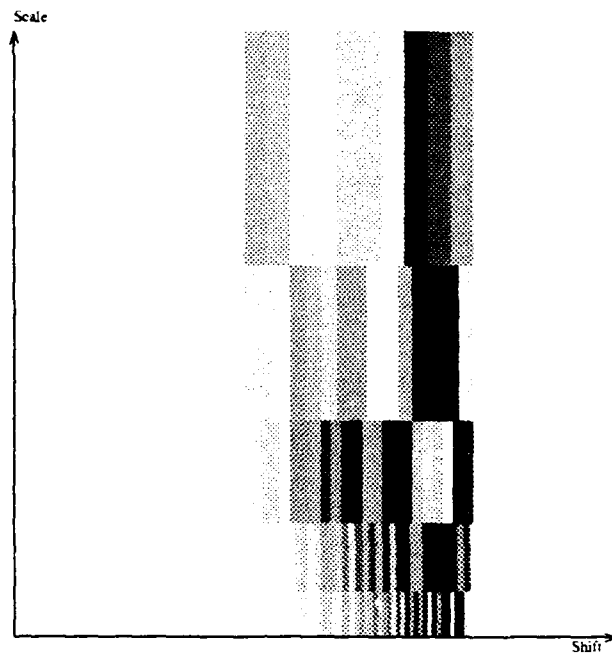


Figure 5.8. Grey Scale Representation of Chirp Function Detail Coefficients for $M = 3$, $N = 2$, $p = 3$, $q = 2$, 5 levels. (Wavelet 2)

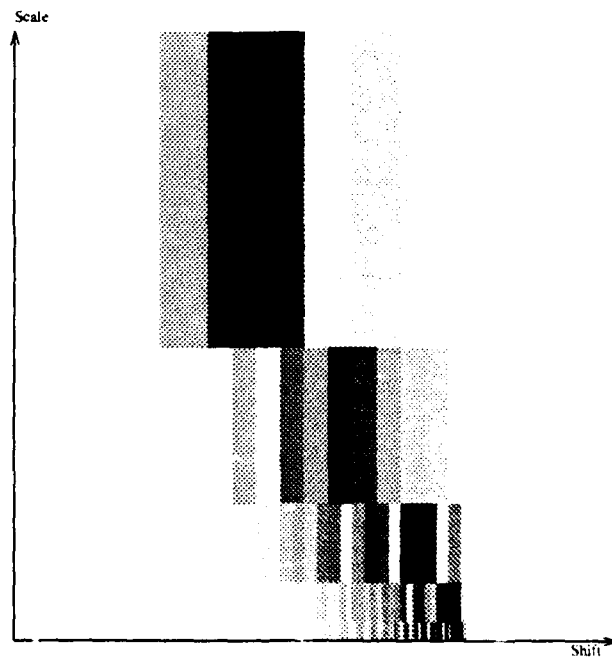


Figure 5.9. Grey Scale Representation of Chirp Function Detail Coefficients for $M = 2$, $N = 2$, $p = 2$, $q = 1$, 5 levels.

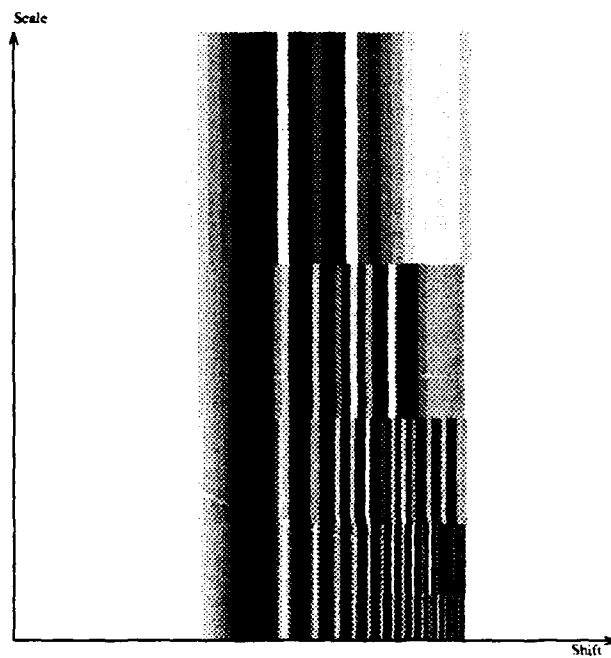


Figure 5.10. Grey Scale Representation of Chirp Function Approximation Coefficients for $M = 3$, $N = 2$, $p = 3$, $q = 2$, 5 levels.

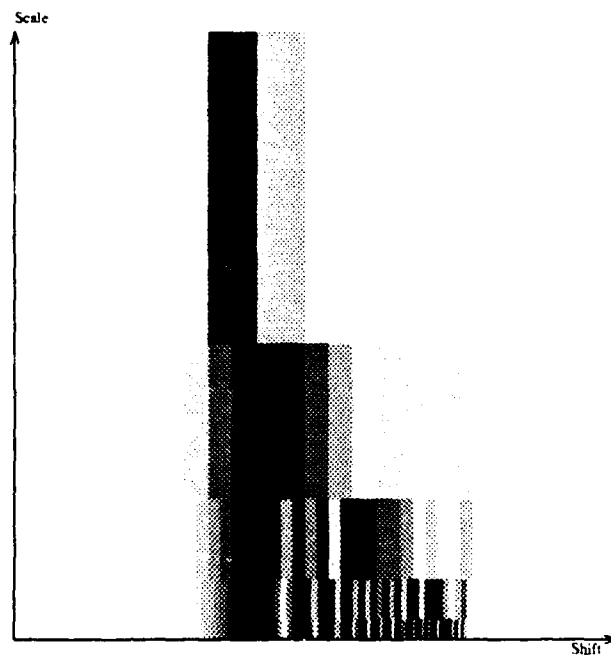


Figure 5.11. Grey Scale Representation of Chirp Function Approximation Coefficients for $M = 2$, $N = 2$, $p = 2$, $q = 1$, 5 levels.

This is a very important characteristic because it demonstrates the ability of the RRA to localize specific frequencies better than the corresponding MRA. The resolution in response of the MRA in Figure 5.9 does not allow a specific frequency or scale to be as accurately determined as with the RRA in this example. However, we must also point out that it takes two wavelets in this RRA case.

We should mention at this point that it is inaccurate to compare the decomposition images of the RRA and MRA for the same signal. We know that because the approximation spaces are not embedded for the RRA, the spaces spanned by the wavelets are not orthogonal between levels; the detail information is over-specified. Consequently, the decomposition images shown in this chapter must be interpreted with this in mind. For the most part, it does not pose a problem for getting the general characteristics from the images, but it becomes important when we make comparisons between the two types of analysis. To illustrate this, consider the effective sampling rates for the various levels of decomposition for the two wavelet analyses presented above. For the dyadic case, the effective sampling rate is given by $(1/2)^m$ whereas in the rational case the effective sampling rate is given by $(1/3)(2/3)^{m-1}$. For four levels of decomposition, this corresponds to $1/16$ for the dyadic and $8/81$ for the rational.

5.3 Speech Processing

We performed several experiments with speech signals to attempt to highlight differences between the MRA and the RRA. We also used these signals to compare the results of processing with different dilation factors. We sought to be able to determine whether speaker-dependent characteristics were present in the approximation and/or details of one decomposition versus another of a different dilation factor.

For these investigations, we used clean (without noise) sampled speech data from three speakers, 2 male and 1 female, from the TIMIT data base. The test sentence was

the same for each of the speakers. Each speech signal was originally sampled at 16 KHz, but was downsampled to 8 KHz to reduce the size of the data files. This made them more manageable and decreased processing time for the investigations performed.

Our first investigation involved trying to determine whether the RRA could separate the three speakers better than the MRA. The hypothesis was that the RRA provided a better set of features for identification than did the MRA. One of the complaints of the MRA is that significant information "fell between the cracks" of the detail and approximation spaces. That is, at a particular level of decomposition, a significant feature of a signal is projected partly into the detail space and partly into the approximation space. This diminishes its effectiveness as a feature because it could be overshadowed by other information which lies squarely in one space or the other, but would otherwise not be as significant. The RRA would not suffer from this as much because the resolution steps are finer and because the detail spaces at each level are not generally orthogonal with the detail spaces at other levels. Hence, if some important information fell "between" two detail spaces or a detail space and approximation space, another detail space would highlight it at either a previous or successive level of decomposition.

To investigate this, we assumed the information which was most significant for reconstruction was contained in the detail signals. By keeping some highest percentage of the detail coefficients, we could compare the resulting reconstruction to the original signal as a function of that percentage. The idea being that the reconstruction would be better with the RRA because the most important information would be redundantly represented in the detail coefficients and less affected by the thresholding.

In order to compare the reconstructions, we have used the metric defined by the l^2 norm. It has been pointed out by Anderson[1] that this may not be a valid metric for speech signals. However, we chose it because our goal for this test was reconstruction from

a mathematical standpoint. The l^2 norm is defined on sequences $a \in l^2(\mathbb{Z})$ to be:

$$\|a\| = \left(\sum_n |a_n|^2 \right)^{1/2} \quad (5.2)$$

and the corresponding metric (distance) for $a, b \in l^2(\mathbb{Z})$ is

$$D(a, b) = \left(\sum_n |a_n - b_n|^2 \right)^{1/2}. \quad (5.3)$$

For the purposes of comparison, we calculate normalized error by finding the distance between the reconstructed and original sequences and dividing by the norm of the original sequence.

For each speaker, the sentence was decomposed 3 levels for the MRA case and 5 levels for the RRA. The RRA used a dilation factor of 3/2 with $M = 3$ and $N = 2$ wavelets and scaling functions. The MRA also used $N = 2$ wavelets and scaling functions so that the regularity between the two would be comparable. In this investigation, the MRA and RRA were decomposed to different levels so that the effective sampling rates of the approximations at the lowest level were the same. The effective sampling rate is given by

$$r_a = (q/p)^m, \quad (5.4)$$

where m is the decomposition level. The sampling rate for the dyadic at $m = 3$ is 0.1250 and for the rational at $m = 5$ is approximately 0.1317. The threshold percent represents the number of overall detail coefficients kept in the reconstruction, independent of level. We mention this to avoid confusion with other thresholding techniques which are based on the values of the coefficients. In this investigation, the percent represents the percentage of all detail coefficients set to zero. A threshold of 90% implies that the top 10% of all coefficients are unchanged, the rest being set to zero.

Figures 5.12 and 5.13 present the results of this investigation. The results demon-

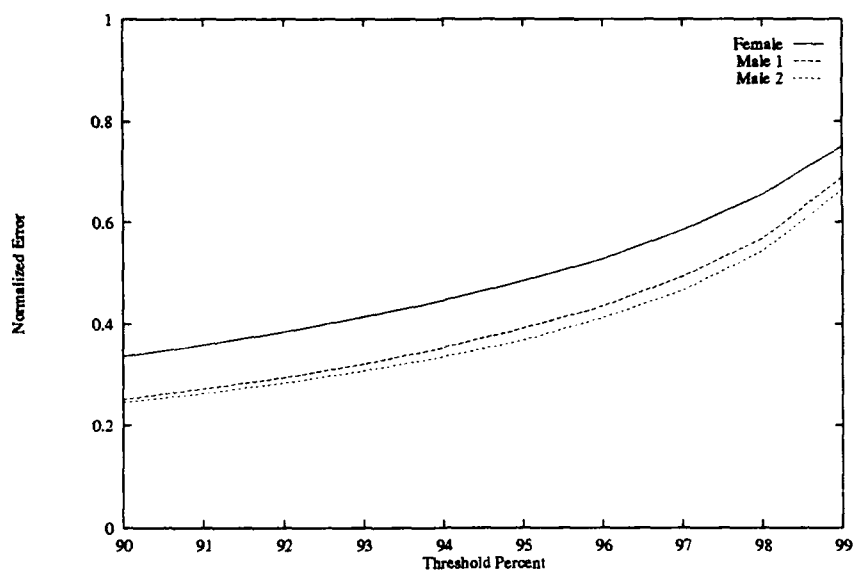


Figure 5.12. 5-level RRA Reconstruction Error for 3 Speakers

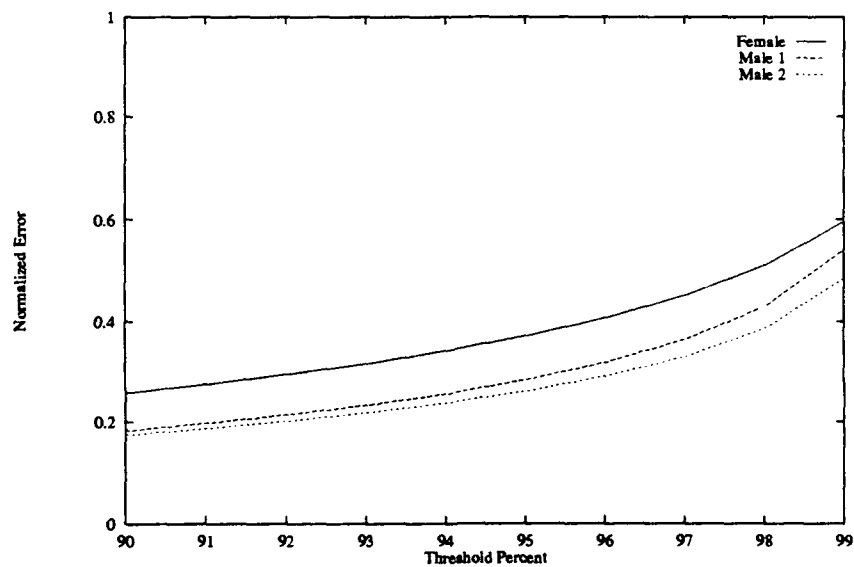


Figure 5.13. 3-level MRA Reconstruction Error for 3 Speakers

strate that both methods effectively separate the female speaker from the two males. However, the error for the RRA is worse than the MRA and the RRA does not appear to separate the speakers better or worse than does the MRA.

As a follow-on investigation, we performed the same processing except that the RRA was decomposed to 3 levels instead of 5. This is done so that the effective sampling rate of the detail coefficients is equivalent. For the RRA, the effective sampling rate of the detail coefficients is given by

$$r_d = (1/p) \cdot (q/p)^{m-1} \quad (5.5)$$

so that the effective sampling rate of the detail coefficient for the MRA and RRA for 3 levels of decomposition is 0.1250 and 0.1481 respectively. For the MRA, the effective sampling rate depends only on level and not whether we are considering the approximation and detail coefficients. This is caused by the symmetry of the decomposition. Figure 5.14 presents these results. These results are slightly better than those obtained with the

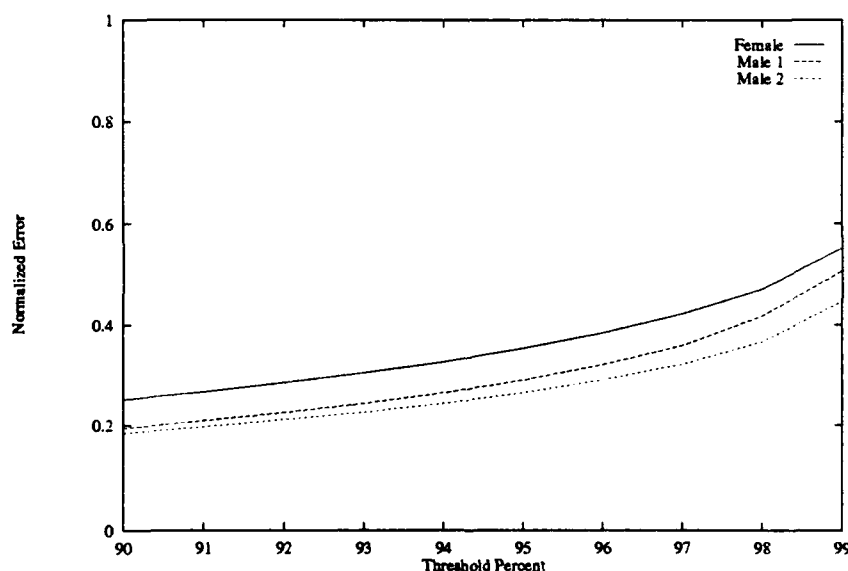


Figure 5.14. 3-level RRA Reconstruction Error for 3 Speakers

MRA. This indicates that overall reconstruction error might be linked more closely to the effective sampling rate reduction of the detail coefficients rather than the approximation coefficients.

These results are generally not encouraging, however. A possible explanation of the ability to separate speakers by sex is that female speech generally has higher frequencies than male speech. Consequently, it would make sense that the female speaker could be separated because more of her signal would be contained in the details of the decomposition. Since we are thresholding the detail coefficients, her speech is most affected, hence the difference in relative error compared to the male counterparts. However, we must be careful in drawing too many conclusions because we have used only three speakers in the comparison.

To illustrate the effects of the choice of dilation factor on the separation of speakers, we calculated the normalized reconstruction error for the female speaker and the first male speaker as a function of both the dilation factor and threshold percent. We used dilation factors of $q = 5$ with $p \in \{6, \dots, 9\}$ and $q = 6$ with $p \in \{7, \dots, 11\}$ which provides a relatively large set (9 points) of rational numbers between 1 and 2. The number of decomposition levels for each dilation factor was chosen so the effective sampling rate of the approximation coefficients was approximately 0.10. This resulted in as many as 15 levels of decomposition for $p/q = 7/6$ to as few as four for $p/q = 11/6$. The results are shown in Figure 5.15. Notice that we still see the obvious separation between the male and female speakers. We can make some other observations also. One reason we might fail to see any significant variation in two surfaces that might be used to distinguish speakers is the low regularity of the scaling functions and wavelets used in the analysis. Also, notice that the ripples in the surface indicate that the reconstruction error for dilations where $q = 5$ is generally less than those dilation factors where $q = 6$. However, the deviations are relatively small and for a given threshold percent, the error curve is generally constant

Male —
Female - - -

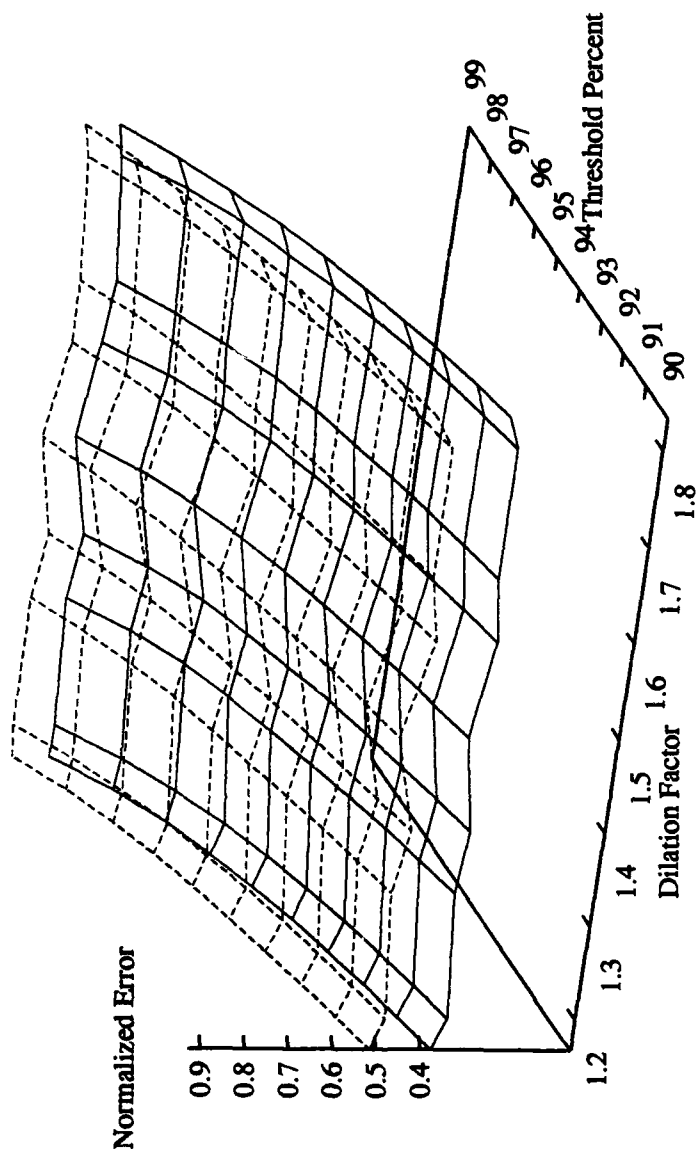


Figure 5.15. Reconstruction Error for Male and Female Speakers versus Dilation Factor and Threshold Level

across all the dilations. This is a significant result: from a coding standpoint, we can perform *arbitrary* rational sampling rate changes within the RRA framework and not significantly increase the relative error.

5.4 Impulse Response Error Analysis

In this section we investigate the error associated with choice of dilation factor. We want to determine general trends in reconstruction error as a function of the dilation factor. To do this, we decompose and reconstruct an impulse signal for various rational dilation factors and then calculate the relative error as a function of the dilation factor and the impulse position. The impulse position affects the error because for an analysis with rational dilation factor p/q , there will generally be p unique impulse responses and each will have unique error contributions.

The investigation focuses on rational dilation factors p/q between 1 and 2. We first investigate the case where we fix $q = 6$ and vary $p \in [7 \dots 11]$. We use $N = 2$ scaling functions and wavelets. Figure 5.16 presents the results. Notice that the error curve for each of the dilations generally has a minimum for impulse positions near the center of the range $[0 \dots p]$. Also notice that at the zeroth position, the dilation factors closer to unity have the least error and that the error at zero position is an upper bound for all the other errors. If this holds for all rational resolution analyses, then it becomes a very simple way to calculate the worst-case reconstruction error.

Now we fix $p = 11$ and vary $q \in [6 \dots 10]$. We again use $N = 2$ scaling functions and wavelets. Figure 5.17 presents the results. The same trend as the previous figure is observed. The dilation factors closer to unity yield the least error and almost perfect reconstruction can be obtained for impulses near 4 and 5.

We conclude with two comments on this analysis. First, a quick investigation of the individual error contributions of the wavelets and scaling functions yields identical results.

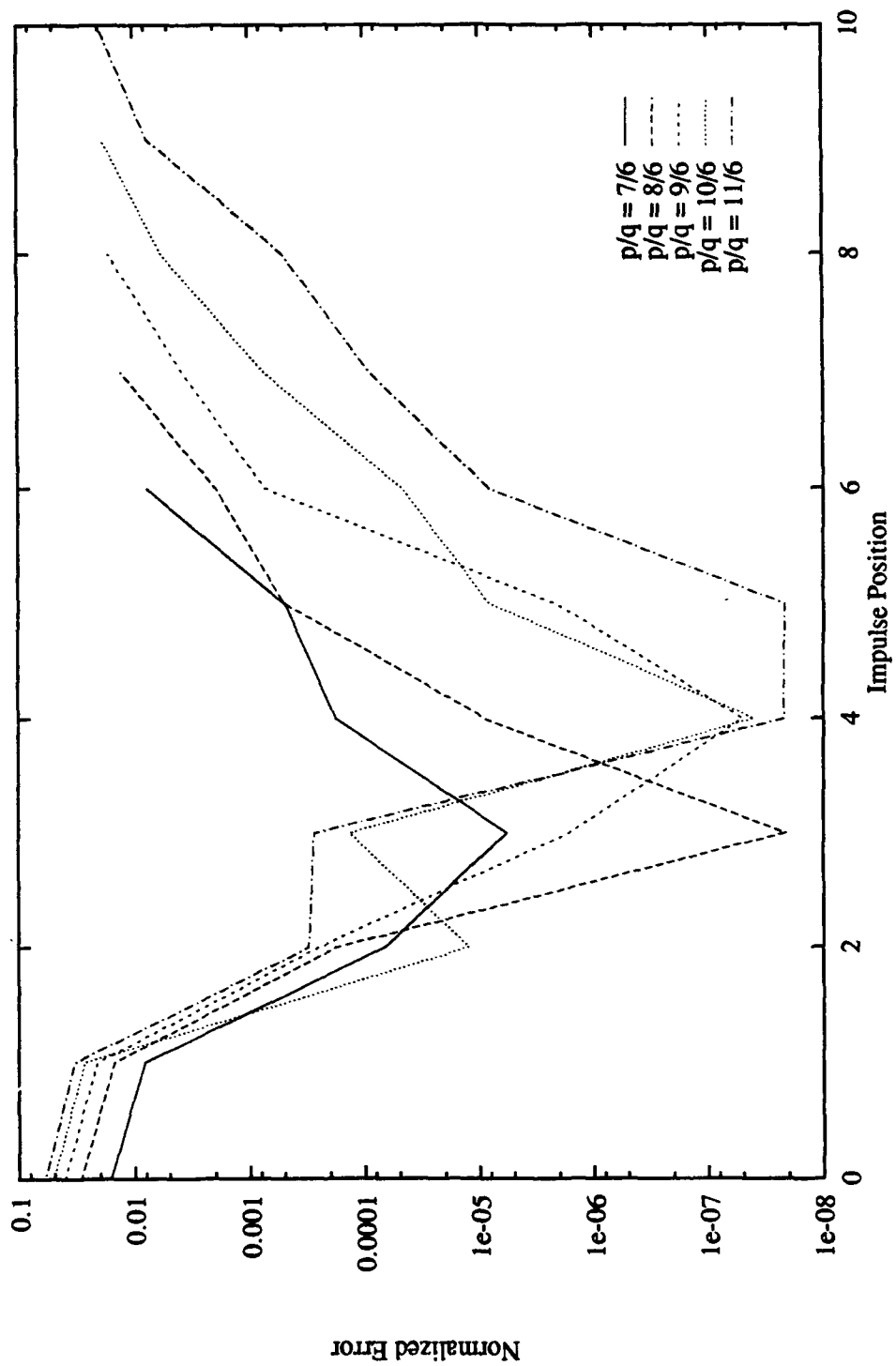


Figure 5.16. Comparison of Reconstruction Error for Dilation factors with Constant q

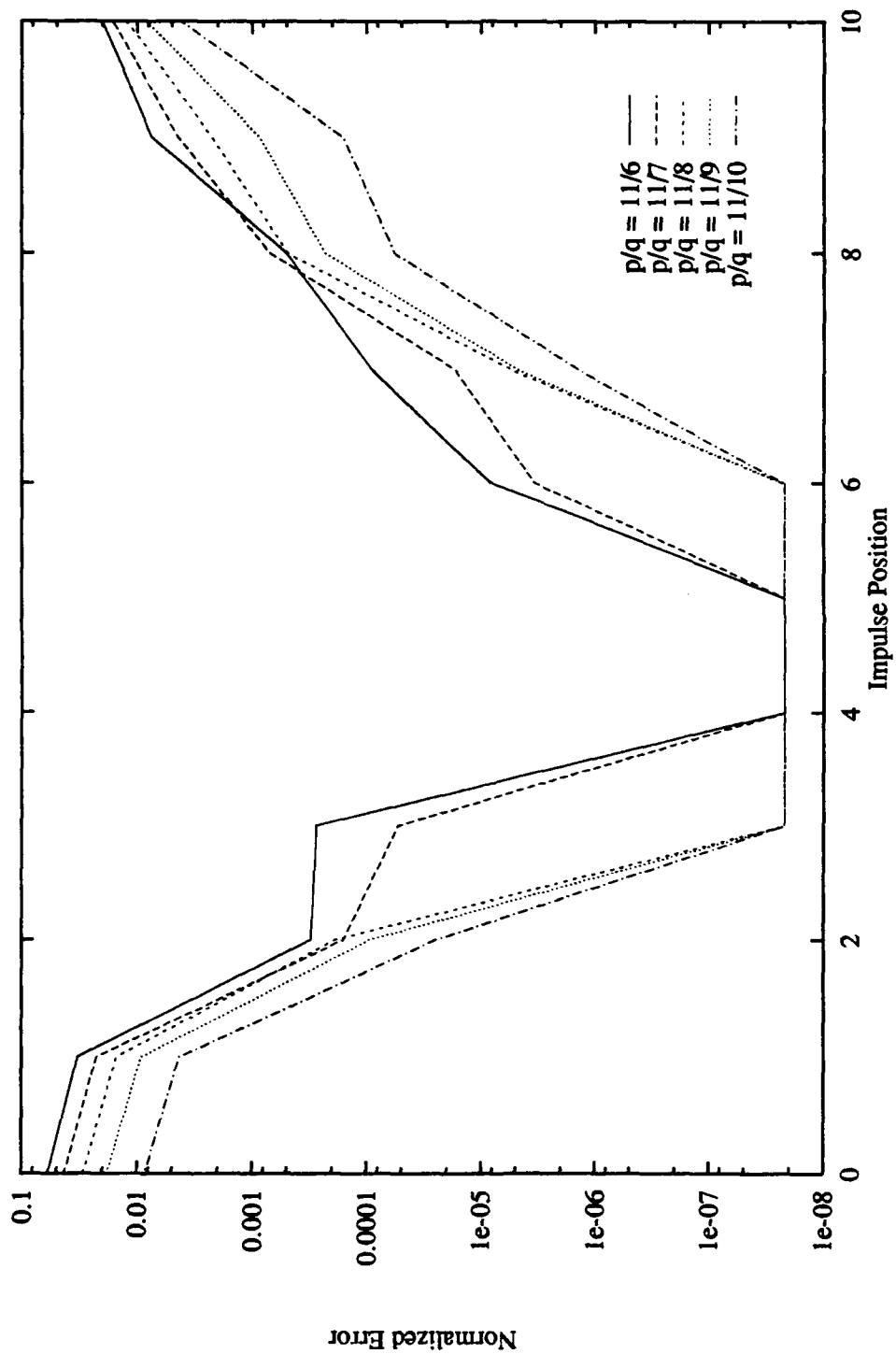


Figure 5.17. Comparison of Reconstruction Error for Dilation factors with Constant p

That is, when the RRA approximation coefficients projected from V_m are compared to the actual approximation coefficient projected from V_{m-1} , the errors were identical to those of the reconstructed signal. This indicates that the overall error is attributable only to the error in the projections from V_m to V'_m for the compactly-supported scaling functions in this thesis; the detail coefficients contribute nothing to the error.

Second, the flat portions of the error curves in Figure 5.17 exist as roundoff error. The machines used in this thesis have a 16-digit accuracy so that a squared error on the order of 10^{-16} gives errors on the order of 10^{-8} when the square root is taken.

5.5 Conclusions

In this chapter we presented the results of several investigations on various input signals including human speech. In general, we saw the performance of the RRA compare favorably with that of the MRA. Although, we did not get good results for the speech signals, we found a potential coding application in the relatively constant reconstruction errors for a wide range of dilation factors. We also saw that the reconstruction error of the MRA depended upon the choice of dilation factor and, in terms of the impulse responses, depended upon the position of the impulse. We saw that the upper bound on the reconstruction error was generally found for impulses at $n = 0$.

VI. Conclusions and Recommendations

6.1 Introduction

This chapter provides a conclusion to this thesis. We summarize the major points and evaluate how well the objectives of the thesis were met. Because most research efforts raise more questions than they answer, we conclude with a brief description of some of those issues and how they translate into areas for future research.

6.2 Major Points and Evaluation of Objectives

The main contribution of this thesis is the refinement of the theory and practical implementation of a rational-resolution analysis. We have also demonstrated a technique to generate families of compactly-supported scaling functions with an arbitrary degree of regularity and an arbitrary resolution base. Throughout this thesis we have worked in the domains of both the mathematical framework of multiresolution wavelet analysis and multirate digital signal processing, thereby showing the relationship between the two. Finally, we have presented some preliminary investigations into the applicability of the RRA.

We can express the results of the thesis in terms of the specific objectives enumerated in the first chapter. First, we have shown how the dyadic multiresolution analysis can be extended to an arbitrary integer dilation factor (or resolution base) using the theory of perfect-reconstruction multirate filter banks. We have shown the major difference between the two is the number of basis functions necessary to span $L^2(\mathbb{R})$. In the dyadic ($M = 2$) multiresolution analysis, there is a single wavelet whose dilations and translations form an orthonormal basis for $L^2(\mathbb{R})$. For an arbitrary integer multiresolution analysis, there are $M - 1$ wavelets dilated and translated by powers of M required to span $L^2(\mathbb{R})$.

The second objective was to see if a rational resolution analysis theory could be implemented. This thesis has demonstrated this objective. We have implemented a rational-resolution analysis which is similar to the dyadic multiresolution analysis in regard to its implementation. However, unlike multiresolution analyses (dyadic or arbitrary integer resolution base), the RRA implemented here does not require that the approximation spaces be embedded. In fact, it is this requirement that had thus far prevented a feasible RRA from being developed. We have described the perfect-reconstruction property of the RRA including a description of a class of scaling functions (the *B*-splines) which allows perfect reconstruction. We have demonstrated near-perfect reconstruction using the compactly-supported scaling functions.

The last objective was to determine the feasibility of the implementations of both integer and rational-resolution analyses and their applicability to real-world problems. The implementation of the integer-resolution analysis is effectively that of a perfect-reconstruction multirate filter bank. We have also cast the implementation of the RRA in terms of discrete-time filter operations with rational sampling rate changes. In both cases, the feasibility is automatic and also, the implementation is relatively fast and efficient. The application of the RRA to speech processing gave only mixed results at best. We attribute this not to a failure of the RRA, but to the way RRA was applied to the problem. There are many areas of speech processing which could possibly benefit from the RRA. Those areas become an area for further research.

6.3 Recommendations

There are several recommendations we can make concerning this research.

- For the classes of compactly-supported scaling functions generated in this thesis, we have shown that perfect reconstruction is not possible. It would be useful to investigate whether there exist compactly-supported scaling functions which do yield

perfect reconstruction and whether they can be generated. Perhaps the solution to this problem lies in generating scaling functions which are based not on a single dilation factor p , but on two dilation factors p and q .

- We did not demonstrate perfect reconstruction using the spline wavelets for lack of a technique to build the detail filters. For the compactly-supported scaling function, we used a modification of Vaidyanathan's technique which is applicable only to FIR filters. It would be useful to develop a technique to find the spline detail filters.
- We mentioned earlier that the choice of wavelets is not unique so that we are free to choose which wavelets we use in a particular analysis. This suggests that wavelet choice can be optimized with respect to some criteria. Vaidyanathan suggests an optimization based on the frequency content of the detail filters, but we can optimize the filters (and thus the wavelets) based on any criteria. Specifically, for a given resolution base and regularity, there might be a choice of wavelets better suited for one application than another. For example, in an image processing application, one set of wavelets might be better for segmenting out one object as opposed to another. This might have applications in target recognition.
- For the speech signals used in the previous chapter, it would be useful to do a listening test to get a more subjective evaluation of the reconstruction quality due to the various dilation factors and thresholding levels.
- Basis function regularity greatly impacts the coding and reconstruction of speech signals. In our examples on speech, we have used $N = 2$ scaling functions and wavelets. An obvious area for research is to investigate the effects of filter regularity on the reconstruction and coding.

6.4 *Conclusion*

The ultimate goal of this research was obtained. The theory of a multiresolution analysis based on an arbitrary rational dilation factor has been developed and implemented. Its main advantage over the dyadic multiresolution analysis is its flexibility in the choice of dilation factors and its ability to exploit information which might "fall between" the approximation and detail space in the dyadic case.

Appendix A. *Generating Scaling Functions and Wavelets*

A.1 *Introduction*

This appendix describes the generation of the compactly supported scaling functions and wavelets used in this thesis for inner product calculations and plotting. It is loosely based on the graphical construction technique described in Daubechies[6] and the reader is referred to her paper for a more rigorous treatment.

A.2 *Mathematical Foundations*

Recall the relationship between the scaling function ϕ and the scaling filter H :

$$\phi(M^{-1}t) = M^{1/2} \sum_n h(n)\phi(t - n) \quad (\text{A.1})$$

where M is the integer dilation factor and $H(f) = M^{-1/2} \sum_n h(n)\epsilon^{-i2\pi n f}$. In the frequency domain

$$\hat{\phi}(Mf) = H(f)\hat{\phi}(f) \quad (\text{A.2})$$

where $H(f) = M^{-1/2} \sum_n h(n)\epsilon^{-i2\pi n f}$. By iterating Equation A.2, we obtain an expression for $\hat{\phi}$ in terms of the infinite product:

$$\hat{\phi}(f) = \left(\prod_{j=1}^{\infty} H(M^{-j}f) \right) \hat{\phi}(0). \quad (\text{A.3})$$

With $\hat{\phi}(0) = \int \phi(t)dt = 1$, the scaling function is completely defined by the scaling filter. We can write a similar definition in the time domain by expressing Equation A.1 recursively.

Notice that the recursive definitions in both time and frequency domain imply that ϕ is defined by an infinite recursion. It is impossible to do this so we typically use a finite number of recursions to create an approximation, η , to the true scaling function ϕ . We

recursively define η in a manner similar to ϕ :

$$\eta_k(t) = M^{1/2} \sum_n h(n) \eta_{k-1}(Mt - n). \quad (\text{A.4})$$

By choosing an appropriate seed function η_0 , it can be shown that $\eta_\infty = \phi$. Daubechies[6] has shown this convergence when the seed function is the characteristic function $\chi_{[-1/2, 1/2]}$. There are other seed functions which work, but the characteristic function will be the most useful for the purposes of this thesis.

We can graphically show the construction of a scaling function by letting $\eta_0 = \chi_{[-1/2, 1/2]}$ and applying Equation A.4 for several iterations. Figure A.2 shows 2 levels of iteration for Daubechies' 4-coefficient scaling function. Notice that the basic structure of the scaling function begins to emerge at the first iteration. By choosing an appropriate level of recursion, the scaling function can be approximated with an arbitrary degree of accuracy. However, it is important to realize that we do not have a closed form for ϕ and the best we can do is approximate it with η . This is usually adequate for generating plots but can lead to problems when trying to perform inner products and other calculations.

The wavelet(s) ψ_i are generated in a similar manner as ϕ . Recall the definition of $\psi(t)$:

$$\psi(M^{-1}t) = M^{1/2} \sum_n g(n) \phi(t - n). \quad (\text{A.5})$$

By following a similar development as above, we can write an approximation for ψ by substituting η_k for ϕ in the above expression.

A.3 Scaling Function and Wavelet Support

The support of a particular compactly-supported scaling function depends on the dilation factor M and the length of the scaling filter. From Figure A.2, you can see the support of the function increases by M^{-k} for each iteration level k . This increase is

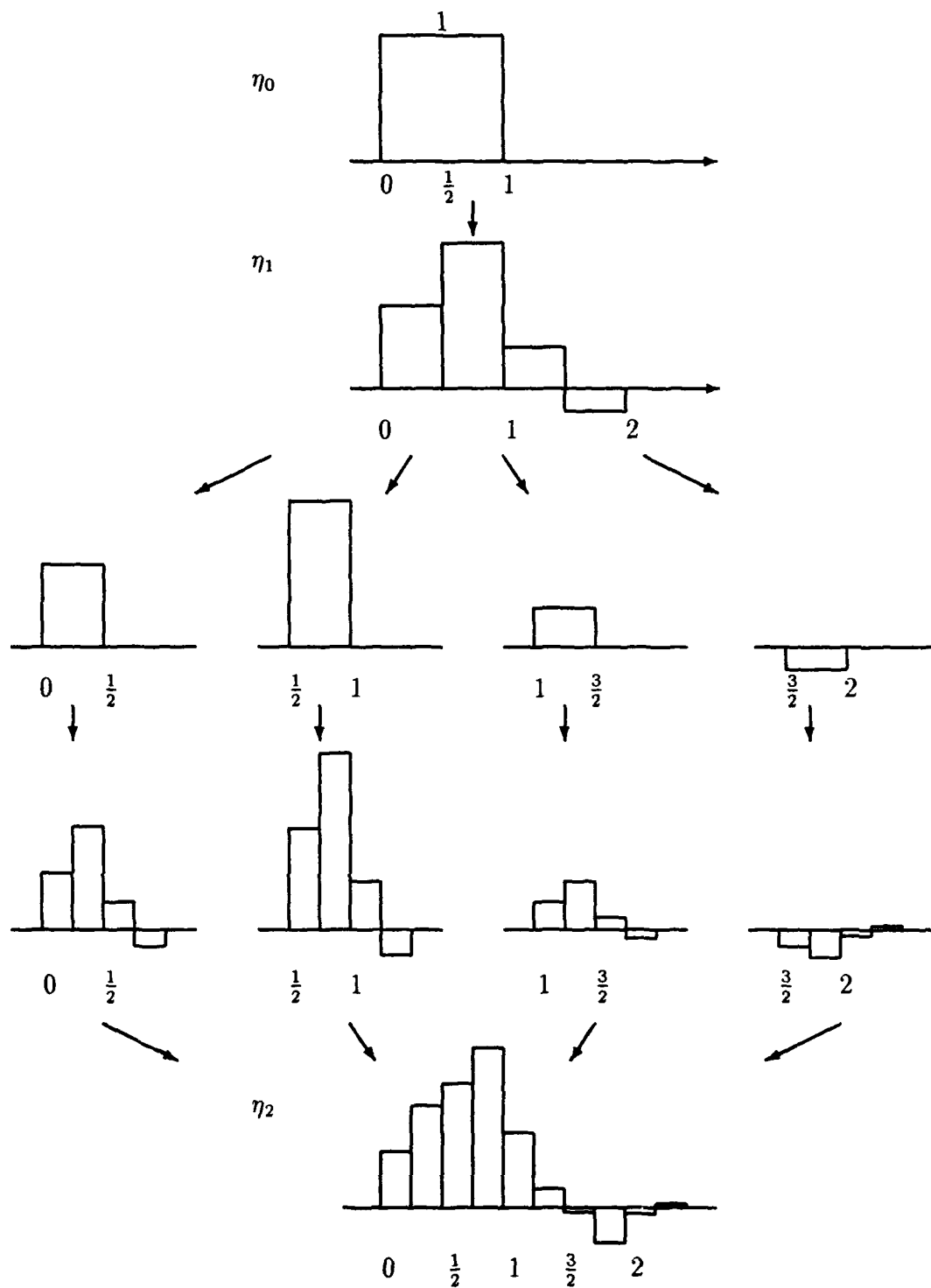


Figure A.1. Graphical Construction of a 4-Coefficient, $M=2$ Scaling Function

bounded in the limit by the following expression:

$$\text{supp}(\phi) \subset [0, s], \quad (\text{A.6})$$

where

$$s = 1 + (N - 1) \left(\sum_{k=0}^{\infty} M^{-k} \right) = \frac{N \cdot M - 1}{M - 1}, \quad (\text{A.7})$$

M is the (integer) dilation factor, and N is the degree of the zero of the scaling filter in the frequency domain. In general, N is the number of filter coefficients divided by the dilation factor. For example, the support of the scaling function in Figure A.2 with $M = 2$ and $N = 2$ will be 3.0, which agrees with Daubechies' result obtained in [6].

A.4 Plotting

An algorithm to calculate the η_k follows directly from the graphical construction method described in Figure A.2. The approximations at successive iteration levels are represented as arrays of points. Each point represents the amplitude of a characteristic function of a certain width. The width between each point is a function of the iteration level and the dilation factor. For example, the characteristic function corresponding to the zeroth iteration in Figure A.2 can be simply represented with a single element array. The next iteration would yield an array of 4 values and the width of each element would be one half the width of the previous element. In general, the element width ratio between iteration levels will be $1/M$ so that the width of an element at a particular iteration level is M^{-k} . Each iteration level will have an array of values corresponding to the η at that iteration.

For plotting purposes, it is usually sufficient to use 7 or 8 iterations. However, for inner product calculations, we want as many iterations as possible to improve accuracy. For large iteration levels, the implementation described above requires a great deal of computer

memory. The number of points at a particular iteration level is approximately exponential with the iteration level. Calculating η_k for large k can quickly exceed the memory capacity of a machine. One way to avoid this is to implement the processing recursively.

Equation A.4 can be implemented recursively so that the particular value of η_k can be calculated without explicitly calculating all values of η_{k-1} . For a given iteration level, both the number of points and the width of each element can be calculated. Let Δt_k be the elemental width of η_k and $l(\eta_k)$ be the number of points. Notice that

$$s_k = l(\eta_k) \cdot \Delta t_k \quad (\text{A.8})$$

with $l(\eta_k)$ recursively defined as

$$\begin{aligned} l(\eta_0) &= 1 \\ l(\eta_k) &= M \cdot (l(\eta_{k-1}) + N - 1) \end{aligned} \quad (\text{A.9})$$

and $\Delta t_k = M^{-k}$, so that the support of η_k is given by

$$\text{supp}(\eta_k) \subset [0, s_k]. \quad (\text{A.10})$$

If $\eta_k(i \cdot \Delta t_k)$ is evaluated for $i \in [0, l(\eta) - 1]$, these points are equivalent to those of η_k calculated in the non-recursive manner.

The recursive technique is not without its limitations. While the non-recursive technique is plagued with memory problems, the recursive technique requires a great deal of processing time. The amount is combinatorially dependent on the number of coefficients, the integer dilation factor, and the iteration level.

One possible solution to this dilemma is a hybrid technique which incorporates the best of both. Instead of recursively calculating every η_k , this technique retains an η_p in

computer memory so that during the recursive calculation of η_k , only $k - p$ recursion levels are required. In other words, the calculation recurses down to level p where the values are looked up in an array instead of any further time-consuming recursion. The level p can be determined by the amount of memory available on a particular machine. Notice that $p = 0$ would correspond to the total recursion technique.

While this technique would provide some speedup compared to the total recursion technique, it is not clear whether the amount of time still required would make it a practical alternative to the all-memory version. The amount of time required might depend more on the number of points to calculate rather than the levels of recursion.

Appendix B. Calculation of Inner Products

B.1 Introduction

This appendix discusses the procedure used in this thesis for calculating inner products between scaling functions of different dilations. This calculation is necessary in order to generate the coefficients of the filter operator which takes a function from one *rational* approximation space to the next. For the most part, filter coefficients corresponding to *integer* dilation factors are not found by calculating inner products between dilated scaling function. In general, their calculation can be done more efficiently and more accurately via solution of a set of filter constraint equations. For the rational dilation case, it is not apparent how to formulate a similar set of constraint equations; hence, the filter coefficients are found by the inner product method discussed below.

B.2 Scaling Function Approximations and Integration

The inner product between two functions in $L^2(\mathbb{R})$ is defined as

$$\langle f, g \rangle = \int_{-\infty}^{\infty} f(x)g^*(x)dx. \quad (\text{B.1})$$

The asterisk on $g(x)$ denotes complex conjugation. It is usually omitted when all the functions are assumed to be real, which they are in this thesis. To calculate inner products with scaling functions, we are forced to use the approximations η_k because it is generally not possible to calculate the compactly supported $\phi(t)$ exactly (see Appendix A). However, given

$$\lim_{k \rightarrow \infty} \eta_k = \phi \quad (\text{B.2})$$

we can pass the limit inside the inner product integral to obtain

$$\lim_{k \rightarrow \infty} \int_{-\infty}^{\infty} \eta_k(pt - n)\eta_k(qt - k)dt = \int_{-\infty}^{\infty} \phi(pt - n)\phi(qt - k)dt \quad (\text{B.3})$$

by use of the Lebesgue Dominated Convergence Theorem (LDCT)[22]. We can apply the LDCT because the scaling functions have finite energy, Equation B.2 holds pointwise, and we can always find another finite-energy function f such that

$$f(t) \geq |\eta_k(pt - n)\eta_k(qt - k)| \quad (\text{B.4})$$

for all k sufficiently large.

The approximation of ϕ discussed in Appendix A is very useful for the inner product calculations. It is a piecewise constant function with each piece having a constant width¹. This allows us to calculate integrals with the η_k exactly. The LDCT ensures that values of these integrals will converge to the values of the same integrals using the exact function ϕ .

B.3 Inner Products between Scaling Functions with Different Dilations

Filter coefficients are defined in terms of inner products between scaling functions of different dilations and integer shifts. For example, the coefficients for a particular scaling filter with an integer dilation factor M can be expressed as

$$h(n) = \langle \phi(\cdot), M^{-1/2}\phi(M^{-1} \cdot -n) \rangle. \quad (\text{B.5})$$

To implement this calculation, the scaling function approximation η and its dilated version are aligned and the corresponding piecewise products are summed. The result is divided by the width of a piece of the undilated version. This is illustrated in Figure B.3 for $M = 2$. The figure shows the first two elements of both the dilated and undilated η . The width of an undilated element is Δx . Notice that the boundaries of the elements in the figure are aligned. This will always be the case when the dilation factor is an integer and

¹The shape of the approximation of $\phi(t)$ will depend upon the generating function used to construct the approximation. For instance, if a piecewise linear function was used, the approximation of ϕ would also be piecewise linear. We assume the approximation is piecewise constant to simplify calculations. See Appendix A for a more detailed description of this.

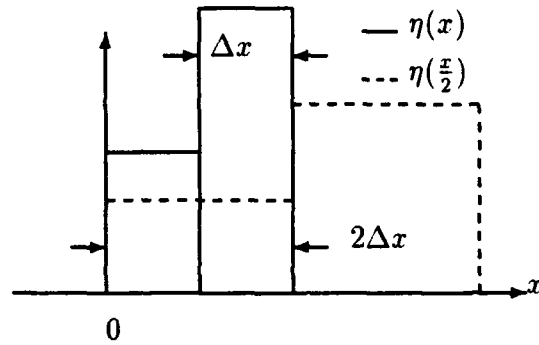


Figure B.1. Graphical Representation of Inner Product Calculation (Integer Dilation)

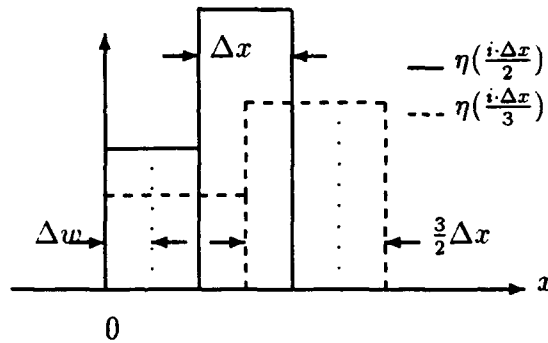


Figure B.2. Graphical Representation of Inner Product Calculation (Rational Dilation)

it allows you to set the elemental width for the summation to be the elemental width of the undilated η .

When the dilation factor is not an integer, the calculation becomes slightly more complicated. Figure B.3 shows the first two elements in an inner product calculation when the dilation factor is $\frac{3}{2}$. Notice that the boundaries of the two scaling functions are generally not aligned. In order to do the calculation, either the boundaries must be aligned or the sum taken over a new elemental width. It is more practical to sum over a new elemental width when the dilation factor is a rational number.

This width is Δw in Figure B.3. For an arbitrary rational dilation factor p/q , $\Delta w = \Delta x/q$ so that an integral number "fits" exactly within Δx and $p/q \Delta x$ (q and

p respectively). The width Δx will depend entirely upon the resolution of the particular η approximation of ϕ . The calculation of the inner product can be done now by multiplying the two η 's pointwise at integer multiples of Δw , summing those products, then dividing the sum by Δw . It is a good idea to evaluate η at a small offset to avoid numeric problems at the edges between elements. Specifically, if $\epsilon = \Delta w/2$, evaluating $\eta(i \cdot \Delta w + \epsilon)$ will ensure you are "in the middle" of the width of each elemental piece.

Appendix C. *Compactly-Supported Scaling Function Coefficients*

This Appendix contains the filter coefficients which correspond to the compactly-supported scaling functions described in this thesis. M is the dilation factor of the filter and N is the degree of the zero in the frequency domain. In general, the number of coefficients equals $N \cdot M$.

Table C.1. $M = 3$ Scaling Function Coefficients

N	n	$h(n)$	N	n	$h(n)$
$N = 1$	0	0.5773502691896258	$N = 6$	12	-0.004390717677049114
	1	0.5773502691896258		13	-0.0117630392913734
	2	0.5773502691896258		14	0.005939350606862516
$N = 2$	0	0.3383860972838639		0	0.04641991275107735
	1	0.5308361870137393		1	0.1639465729921871
	2	0.7232862767436145		2	0.4066715005201326
	3	0.2389641719057618		3	0.5656198750350017
	4	0.0465140821758866		4	0.5822303477386939
$N = 3$	5	-0.1459360075539887		5	0.2439043899487991
	0	0.2031351458445597		6	-0.03360979671294295
	1	0.4231503391080737		7	-0.2535074168509084
	2	0.707315562281546		8	-0.0827402704145488
	3	0.4462253778312972		9	-0.001567872609927079
	4	0.1986450810341451		10	0.1160507314856822
	5	-0.1772352755829245		11	0.003460975861427684
	6	-0.07201025448623133		12	0.0004017081380376375
	7	-0.04444515095259269		13	-0.03676774192974475
	8	0.04726998249100431		14	0.00823961325938988
$N = 4$	0	0.123406981953495		15	0.0000864425883298631
	1	0.3178956389295323		16	0.005397775753665225
	2	0.6213168633509574	$N = 7$	17	-0.002185939985627229
	3	0.5614260707071095		0	0.02863469944250044
	4	0.3689078320251187		1	0.1145779336727611
	5	-0.0862580790830778		2	0.3130369746334096
	6	-0.1277798008064663		3	0.5052370391891819
	7	-0.1337592046407223		4	0.6066049784880124
	8	0.05875903404126836		5	0.389300653623506
	9	0.02029701733548439		6	0.0928372491743659
	10	0.02430600287569403		7	-0.2229533413299443
	11	-0.01646754911952597		8	-0.1671131569370772
$N = 5$	0	0.07550761756142822		9	-0.07162196707431434
	1	0.2308607082172001		10	0.1226804243338364
	2	0.5130453503201613		11	0.04678622725673165
	3	0.5926979649102604		12	0.02814719913757102
	4	0.5034315642711169		13	-0.05893429635971259
	5	0.07274582768780658		14	-0.002075105196602145
	6	-0.1155977613104273		15	-0.006590670189590142
	7	-0.2180464638838977		16	0.01777849645238094
	8	0.006923562601957478		17	-0.003400563925014199
	9	0.02913316570543634		18	0.0007067195113203001
	10	0.07286749987660257		19	-0.00240392606630167
	11	-0.02130382202713998		20	0.00081523973607586

Table C.2. $M = 4$ Scaling Function Coefficients

N	n	$h(n)$	N	n	$h(n)$
$N = 1$	0	0.5	$N = 6$	2	0.261409705243678
	1	0.5		3	0.4621234160454917
	2	0.5		4	0.5034896944442804
	3	0.5		5	0.4974275790863239
$N = 2$	0	0.2697890493972125		6	0.3582663910214228
	1	0.3947890493972125		7	0.02935921938985153
	2	0.5197890493972127		8	-0.06205420421900776
	3	0.6447890493972127		9	-0.1720416625275725
	4	0.2302109506027876		10	-0.1653977530653066
	5	0.1052109506027876		11	0.0311291404573808
	6	-0.01978904939721243		12	0.01081024188096791
$N = 3$	7	-0.1447890493972125		13	0.05413053935774315
	0	0.1508314546357131		14	0.05420808584702153
	1	0.2819260000350612		15	-0.0299790295109188
	2	0.4442705454344095		16	-0.001415646351253019
	3	0.6378650908337577		17	-0.0086466114650548
	4	0.4102152723259671		18	-0.00848642904691611
	5	0.2730261815272712		19	0.007367253618095049
	6	0.07333709072857486		0	0.02837982990998122
	7	-0.1888520000701211		1	0.084920390919197
	8	-0.06104672696167835		2	0.1894452880035414
	9	-0.05495218156233073		3	0.3634158417256748
$N = 4$	10	-0.01760763616298289		4	0.4630341033971846
	11	0.05098690923636504		5	0.521603688112835
	0	0.0857141205095909		6	0.4581682609563594
	1	0.1931389929529531		7	0.1884297474496925
	2	0.3491797139433843		8	0.03064209572041676
	3	0.5616487834808844		9	-0.151511509208909
	4	0.49550221952709		10	-0.2217355640601113
	5	0.4145659963852793		11	-0.04963847654759235
	6	0.2190322276022618		12	-0.03004065049723437
	7	-0.1145365868219623		13	0.06148349926787944
	8	-0.0952932238298487		14	0.1006557092799305
	9	-0.1306953948763132		15	-0.01252355607606148
	10	-0.0827500202815714		16	0.00916526414636643
	11	0.07198039995437733		17	-0.01940336450539526
	12	0.01407688379316929		18	-0.03095839677252821
$N = 5$	13	0.02299040553808251		19	0.01321015681716564
	14	0.01453807873592691		20	-0.001180642679889488
	15	-0.01909259661329754		21	0.00290729541121007
$N = 5$	0	0.04916991424491036		22	0.004424702589612802
	1	0.1291301555484611		23	-0.002893713372051781

Table C.3. $M = 5$ Scaling Function Coefficients

N	n	$h(n)$	N	n	$h(n)$
$N = 1$	0	0.4472135954999579	$N = 5$	8	0.1287274768405204
	1	0.4472135954999579		9	-0.1279100395776194
	2	0.4472135954999579		10	-0.07629704034654595
	3	0.4472135954999579		11	-0.1133335965818052
	4	0.4472135954999579		12	-0.1071173925933397
$N = 2$	0	0.2291122486958535		13	-0.0469153020891433
	1	0.3185549677958451		14	0.07800580122278156
	2	0.4079976868958367		15	0.01065157792180793
	3	0.4974404059958284		16	0.01919978418230139
	4	0.5868831250958201		17	0.01929325164155149
	5	0.2181013468041045		18	0.007354271535558496
	6	0.1286586277041128		19	-0.02019486489967753
	7	0.03921590860412127		0	0.0369295857643589
$N = 3$	8	-0.05022681049587032		1	0.0864822003896527
	9	-0.1396695295958619		2	0.1630385669708455
	0	0.1226418655699167		3	0.2735816072515638
	1	0.2115096557509954		4	0.4258097847282368
	2	0.3182659897520724		5	0.4434891758283
	3	0.4429108675731478		6	0.4572821120709057
	4	0.5854442892142215		7	0.4051300667360689
	5	0.3779406579655435		8	0.2626790616132943
	6	0.2896477967033775		9	0.002712951480869918
	7	0.1655778478012153		10	-0.03555071825051925
	8	0.00573081125905639		11	-0.1281179958592347
	9	-0.1898933129230993		12	-0.1669842966509591
	10	-0.05336892803550154		13	-0.1209852164559706
$N = 4$	11	-0.05394385695441473		14	0.04533689941226271
	12	-0.03663024205332937		15	0.002437098513524916
	13	-0.001428083332245672		16	0.0374251056022139
	14	0.05166261920883635		17	0.0548109596566571
	0	0.06693186642815647		18	0.03745650892140251
	1	0.1364344418138782		19	-0.03475938322425875
	2	0.2322802998208425		20	-0.0000915463544155504
	3	0.3580471492130495		21	-0.005857826702287961
	4	0.5173126987544992		22	-0.0088018375203643
	5	0.4459271914965655		23	-0.005518365829028025
	6	0.4049129660856119		24	0.00811334310413951
	7	0.3027574366309285			

Table C.4. $M = 5$ Scaling Function Coefficients (continued)

N	n	$h(n)$	N	n	$h(n)$
$N = 6$	0	0.02051980444910794		15	-0.04003381202512913
	1	0.05415134428079754		16	0.02688551062236399
	2	0.1114576256922577		17	0.07989589044878187
	3	0.2012850535192487		18	0.0805790774016231
	4	0.3342197800496445		19	-0.02258740257607172
	5	0.3996119866793481		20	0.01213573568549719
	6	0.4564050600513028		21	-0.00839671639398176
	7	0.4578850077299457		22	-0.02516131296018287
	8	0.369949626302656		23	-0.02371218660701047
	9	0.1505135168490312		24	0.01623310032102943
	10	0.05658960992477092		25	-0.001609729213060351
	11	-0.0831415456624427		26	0.00130994260250239
	12	-0.1805630929152357		27	0.003699477504981466
	13	-0.1841525577767697		28	0.003264582660787288
	14	-0.02785215868011903		29	-0.003313240462983433

Table C.5. $M = 6$ Scaling Function Coefficients

N	n	$h(n)$	N	n	$h(n)$
$N = 1$	0	0.4082482904638631	$N = 4$	12	-0.04779458872577158
	1	0.4082482904638631		13	-0.05069209412595289
	2	0.4082482904638631		14	-0.04224936923547141
	3	0.4082482904638631		15	-0.02246641405432692
	4	0.4082482904638631		16	0.00865677141748031
$N = 2$	5	0.4082482904638631		17	0.0511201871799504
	0	0.2018407738385801		0	0.05572988604737748
	1	0.2698821555825572		1	0.1050926383523982
	2	0.3379235373265344		2	0.1705385816962569
	3	0.4059649190705117		3	0.2539577544607309
	4	0.474006300814489		4	0.3572401950275974
	5	0.542047682558466		5	0.4822759417786338
	6	0.2064075166252832		6	0.4080354889061076
	7	0.1383661348813059		7	0.3847969539507332
	8	0.07032475313732867		8	0.3246490761695098
$N = 3$	9	0.002283371393351552		9	0.2219217404171019
	10	-0.06575801035062568		10	0.07094483154818399
	11	-0.1337993920946029		11	-0.1339517655825801
	0	0.1049238332330833		12	-0.06405884983625399
	1	0.1700677095768791		13	-0.0976286550965853
	2	0.2465518162113377		14	-0.1056293478217274
	3	0.3343761531364593		15	-0.082390812866354
	4	0.4335407203522437		16	-0.02224293508512964
	5	0.5440455178586907		17	0.0804844006672756
	6	0.3511190459565507		18	0.00854176534668483
	7	0.2888726750129367		19	0.01598735325736644
	8	0.2039458434879964		20	0.01868998041987424
	9	0.0963385513817303		21	0.01475960845243124
	10	-0.0339492013058611		22	0.002306198973259885
	11	-0.1869174145747785		23	-0.02056028639941723

Table C.6. $M = 6$ Scaling Function Coefficients (continued)

N	n	$h(n)$	N	n	$h(n)$
$N = 5$	0	0.02995834418878171		3	0.02209470468778374
	1	0.06414562072724588		4	0.02957020047325365
	2	0.1142831722968498		5	0.040995665474175
	3	0.1839227287556434		6	0.001156942247115822
	4	0.2769310263586415		7	0.006300234219310142
	5	0.3974898077578217		8	0.02078210190349239
	6	0.4003041010582172		9	0.04385725021651865
	7	0.4188327209012286		10	0.07316259259029323
	8	0.3995957157224446		11	0.1044547456409219
	9	0.3302762044714527		12	0.2746019565327771
	10	0.1972972805099502		13	0.3407764197133076
	11	-0.01417798838814122		14	0.388698033710682
	12	-0.02066311814903798		15	0.4155336801713361
	13	-0.0968092105655529		16	0.4210558109178919
	14	-0.1440198478127712		17	0.408167458610194
	15	-0.1466547658878028		18	0.1924213371475503
	16	-0.0871836624059057		19	0.0966050895763715
	17	0.05381380339945708		20	0.006591282579620384
	18	-0.00193543121123696		21	-0.07235329535143365
	19	0.0260631696830913		22	-0.1369374131080576
	20	0.04568663517974514		23	-0.1863704076244232
	21	0.04839816099185513		24	-0.07963276184528923
	22	0.02440091724472992		25	-0.05654629332141781
	23	-0.03736195152418986		26	-0.02979290274345203
	24	0.0005843945785826144		27	-0.002277800234288918
	25	-0.003984010280720485		28	0.02376657637685398
	26	-0.007297384920941675		29	0.04704306688550553
	27	-0.007694037865814324		30	0.01015052096474545
	28	-0.003197271242108155		31	0.00806437466981969
	29	0.00848461922037111		32	0.00499665091764906
$N = 6$	0	0.00955029551298974		33	0.00139375107012385
	1	0.01304846570266636		34	-0.002369476690216469
	2	0.0169731241919911		35	-0.006042238426359006

Table C.7. $M = 7$ Scaling Function Coefficients

N	n	$h(n)$	N	n	$h(n)$
$N = 1$	0	0.3779644730092272	$N = 4$	14	-0.04356647929253521
	1	0.3779644730092272		15	-0.04724346368787514
	2	0.3779644730092272		16	-0.04320688740955714
	3	0.3779644730092272		17	-0.03145675045758156
	4	0.3779644730092272		18	-0.01199305283194779
	5	0.3779644730092272		19	0.01518420546734398
$N = 2$	6	0.3779644730092272		20	0.05007502444029371
	0	0.1820860761697475		0	0.04827799192057586
	1	0.2360810008853514		1	0.0855454129896321
	2	0.2900759256009553		2	0.1334565988935662
	3	0.3440708503165593		3	0.1931134868714732
	4	0.3980657750321632		4	0.2656180141624482
$N = 3$	5	0.4520606997477671		5	0.3520721180055859
	6	0.5060556244633709		6	0.4535777356399815
	7	0.1958783968394797		7	0.3781248366224261
	8	0.141883472123876		8	0.3639696092803986
	9	0.087888547408272		9	0.3255966481074033
	10	0.03389362269266805		10	0.259700141386153
	11	-0.02010130202293581		11	0.1629742773993588
	12	-0.07409622673853972		12	0.03211324442974472
	13	-0.1280911514541436		13	-0.136188769239979
	0	0.0926794040869014		14	-0.05556962380363828
	1	0.1429973444071671		15	-0.0850665076111028
	2	0.2010288454010908		16	-0.0980592182612519
	3	0.2667739070686723		17	-0.0912419440368151
	4	0.340232529409912		18	-0.06130887322050606
	5	0.4214047124248097		19	-0.004954194095036613
	6	0.5102904561133648		20	0.0811279050568761
	7	0.3288515482148742		21	0.007131268270212489
	8	0.2822105922899487		22	0.01351595835064323
	9	0.2201425150177076		23	0.01697044426986016
	10	0.1426473163981501		24	0.01639278878876893
	11	0.04972499643127694		25	0.01068105466827485
	12	-0.0586244448829132		26	-0.001266695330717368
	13	-0.1824010075444182		27	-0.02055239844730261

Table C.8. $M = 7$ Scaling Function Coefficients (continued)

N	n	$h(n)$	N	n	$h(n)$
$N = 5$	0	0.02547293891079519		18	-0.1243336643910737
	1	0.05075013025828832		19	-0.06176006119987676
	2	0.0863334949637646		20	0.05893353785482703
	3	0.1342373567811073		21	-0.004424054994927929
	4	0.1966334590697807		22	0.01835674396538422
	5	0.2758509647948308		23	0.03670396212991989
	6	0.374376456526889		24	0.04586611620041481
	7	0.367489241888185		25	0.04046204445618074
	8	0.3863341750310027		26	0.01448090675427949
	9	0.3813604927362881		27	-0.0387178154705925
	10	0.3456128372275629		28	0.000960375347910158
	11	0.2715061723060899		29	-0.002727828570636248
	12	0.1508257833507116		30	-0.005802376452088698
	13	-0.02527272268198999		31	-0.007350881781635344
	14	-0.01153402814983906		32	-0.006303538438884565
	15	-0.07474874768192308		33	-0.00143312069786309
	16	-0.1206311003758032		34	0.00864501677298443
	17	-0.1404009554253633			

Table C.9. $M = 8$ Scaling Function Coefficients

N	n	$h(n)$	N	n	$h(n)$
$N = 1$	0	0.3535533905932738	$N = 3$	0	0.083658276085724
	1	0.3535533905932738		1	0.1240047617351233
	2	0.3535533905932738		2	0.1698755191125425
	3	0.3535533905932738		3	0.2212705482179815
	4	0.3535533905932738		4	0.2781898490514403
	5	0.3535533905932738		5	0.3406334216129192
	6	0.3535533905932738		6	0.4086012659024174
$N = 2$	7	0.3535533905932738		7	0.4820933819199369
	0	0.1669973759042		8	0.310134941408303
	1	0.2111915497283592		9	0.273636143933663
	2	0.2553857235525184		10	0.2260888030029839
	3	0.2995798973766775		11	0.1674929186162655
	4	0.3437740712008368		12	0.0978484907735067
	5	0.3879682450249959		13	0.0171555194747075
	6	0.4321624188491552		14	-0.07458599528013066
	7	0.4763565926733144		15	-0.1773760534910087
	8	0.1865560146890733		16	-0.04023982690075423
	9	0.1423618408649142		17	-0.04408751507551423
	10	0.098167667040755		18	-0.04241093152225384
	11	0.05397349321659584		19	-0.03521007624097416
	12	0.00977931939243665		20	-0.02248494923167421
	13	-0.03441485443172254		21	-0.004235550494354479
	14	-0.0786090282558817		22	0.01953811997098512
	15	-0.1228032020800409		23	0.04883606216434463

Table C.10. $M = 8$ Scaling Function Coefficients (continued)

N	n	$h(n)$	N	n	$h(n)$
$N = 4$	0	0.04294578648476931		4	0.1484062411512839
	1	0.07231622565417008		5	0.2041722742290823
	2	0.1091519993131062		6	0.2724989773770527
	3	0.1541436414275804		7	0.3549676353333151
	4	0.2079816859635952		8	0.3415248451795527
	5	0.2713566668871534		9	0.3593172076325466
	6	0.3449591181642582		10	0.3610197867070042
	7	0.4294795737609114		11	0.3423790453483093
	8	0.3538254217040411		12	0.2987961795188312
	9	0.344771731160197		13	0.2253271181980097
	10	0.3188463088757665		14	0.1166825233822948
	11	0.2739775529527471		15	-0.03277220991492413
	12	0.2080938614931327		16	-0.005574944858665277
	13	0.1191236325988996		17	-0.05883618537589542
	14	0.00499526437204878		18	-0.1008959954806414
	15	-0.1363628450854222		19	-0.1264098705399874
	16	-0.0493475787629123		20	-0.1295154054463694
	17	-0.07515734135924746		21	-0.1038322946179448
	18	-0.0896196439430277		22	-0.04246233199825156
	19	-0.0906628846162363		23	0.0620105889436502
	20	-0.07621546148086722		24	-0.005921533591333628
	21	-0.0442057726389109		25	0.01297857285096882
	22	0.007437783807644039		26	0.02935037430356146
	23	0.0807868097568001		27	0.04032140164366638
	24	0.006129761167490422		28	0.04267391876561533
	25	0.01162277513827403		29	0.03284492258067218
	26	0.01517472634754502		30	0.006926143017217612
	27	0.01609508082929956		31	-0.03933595697940006
	28	0.01369330461753471		32	0.001180822955390681
	29	0.007278863746248116		33	-0.001860270686163901
	30	-0.003838775750562934		34	-0.004583404946991721
	31	-0.02035014783890116		35	-0.006443096037894503
$N = 5$	0	0.02234420088043657		36	-0.006807543423931084
	1	0.04195406614387475		37	-0.00495862982441625
	2	0.06866262998244083		38	-0.0000919212129218486
	3	0.1037059101512808		39	0.00868333318272398

Table C.11. $M = 9$ Scaling Function Coefficients

N	n	$h(n)$	N	n	$h(n)$
$N = 1$	0	0.3333333333333333		0	0.07669971772284562
	1	0.3333333333333333		1	0.1099696509754184
	2	0.3333333333333333		2	0.1473548105654401
	3	0.3333333333333333		3	0.1888551964929107
	4	0.3333333333333333		4	0.2344708087578302
	5	0.3333333333333333		5	0.2842016473601987
	6	0.3333333333333333		6	0.3380477123000158
	7	0.3333333333333333		7	0.3960090035772827
$N = 2$	8	0.3333333333333333		8	0.4580855211919972
	0	0.1550206443672593		9	0.2941781119756248
	1	0.1920576814042964		10	0.2646752825075191
	2	0.2290947184413335		11	0.2269420003645157
	3	0.2661317554783706		12	0.1809782655466145
	4	0.3031687925154077		13	0.1267840780538147
	5	0.3402058295524447		14	0.06435943788611809
	6	0.3772428665894819		15	-0.006295654956474995
	7	0.414279903626519		16	-0.085181200473968
	8	0.4513169406635559		17	-0.1722971986663575
	9	0.1783126889660744		18	-0.03754449636510948
	10	0.1412756519290373		19	-0.04131160014957614
	11	0.1042386148920001		20	-0.04096347759659503
	12	0.06720157785496318		21	-0.03650012870616426
	13	0.03016454081792608		22	-0.02792155347828484
	14	-0.006872496219111069		23	-0.01522775191295661
	15	-0.04390953325614811		24	0.001581275989820552
	16	-0.0809465702931852		25	0.02250553023004668
	17	-0.1179836073302223		26	0.04754501080772171

Table C.12. $M = 9$ Scaling Function Coefficients (continued)

N	n	$h(n)$	N	n	$h(n)$
$N = 4$	0	0.03892712901139129		5	0.1584149525921297
	1	0.06282088728945303		6	0.2083742732387508
	2	0.0921852462314366		7	0.2679952819291707
	3	0.1274774532081674		8	0.3383370222704727
	4	0.1691547555904707		9	0.3203417820901251
	5	0.2176744007491718		10	0.3367135860399202
	6	0.273493636055095		11	0.3416453392429375
	7	0.3370697088790671		12	0.3323742199103918
	8	0.4088598665919126		13	0.3059341851997885
	9	0.3336128405188941		14	0.2591559712148808
	10	0.3276278770097143		15	0.1886670930056198
	11	0.3093463378461969		16	0.0908918445684606
	12	0.2773964809158649		17	-0.03794870115413573
	13	0.2304065641062465		18	-0.001501570187173229
	14	0.1670048453048523		19	-0.047038872731207
	15	0.0858195823992283		20	-0.0849120904563847
	16	-0.01452096672311143		21	-0.111662861735681
	17	-0.1353885441746527		22	-0.1235279933617903
	18	-0.04459211799952101		23	-0.116439460546701
	19	-0.06726642877848832		24	-0.0860244069216378
	20	-0.0817593902405704		25	-0.02760514453757423
	21	-0.0866992602732459		26	0.06380084613539339
	22	-0.0807142967640679		27	-0.006854205878511266
	23	-0.06243275760055767		28	0.00910862314756855
	24	-0.03048290067022208		29	0.0235492389364822
	25	0.01650701613939987		30	0.03461931444124389
	26	0.07990873494078699		31	0.04026730156110148
	27	0.005385481800848524		32	0.03823843114160752
	28	0.01015099781094619		33	0.02607471297461927
	29	0.01356113949455029		34	0.001114935798149474
	30	0.01515865948083395		35	-0.03950533270343115
	31	0.01448631039897341		36	0.00131381514356832
	32	0.01108684487814215		37	-0.001241865601837588
	33	0.004503015547515254		38	-0.00362791614216551
	34	-0.005722424963732404		39	-0.005496566558387706
	35	-0.02004672402642617		40	-0.006449241668042838
$N = 5$	0	0.02003351220860843		41	-0.006036561025236143
	1	0.03579186252225289		42	-0.003758338920641535
	2	0.05667876179579384		43	0.000936415618498908
	3	0.0834992273191487		44	0.00864949882837498
	4	0.117109081645667			

Table C.13. $M = 10$ Scaling Function Coefficients

N	n	$h(n)$	N	n	$h(n)$
$N = 1$	0	0.3162277660168379	$N = 3$	0	0.07114422411477666
	1	0.3162277660168379		1	0.0991820366045694
	2	0.3162277660168379		2	0.1303821267545305
	3	0.3162277660168379		3	0.1647444945646601
	4	0.3162277660168379		4	0.2022691400349579
	5	0.3162277660168379		5	0.2429560631654242
	6	0.3162277660168379		6	0.2868052639560583
	7	0.3162277660168379		7	0.3338167424068614
	8	0.3162277660168379		8	0.3839904985178331
$N = 2$	9	0.3162277660168379		9	0.4373265322889726
	0	0.1452331793562896		10	0.2803921713759507
	1	0.1768559559579734		11	0.2559393229980493
	2	0.2084787325596571		12	0.2251619192998104
	3	0.240101509161341		13	0.1880599602812358
	4	0.2717242857630247		14	0.1446334459423229
	5	0.3033470623647084		15	0.0948823762830742
	6	0.3349698389663924		16	0.03880675130348887
	7	0.3665926155680761		17	-0.02359342899643391
	8	0.3982153921697598		18	-0.0923181646166933
	9	0.4298381687714437		19	-0.1673674555572879
	10	0.170994586660548		20	-0.03530862947389135
	11	0.1393718100588643		21	-0.03889359358578215
	12	0.1077490334571807		22	-0.0393162800375042
	13	0.07612625685549679		23	-0.03657668882905862
	14	0.04450348025381313		24	-0.03067481996044419
	15	0.01288070365212923		25	-0.02161067343 66179
	16	-0.01874207294955454		26	-0.0093842492427107
	17	-0.05036484955123827		27	0.006004452606408584
	18	-0.0819876261529221		28	0.02455543211569622
	19	-0.1136104027546058		29	0.04626868928515226

Table C.14. $M = 10$ Scaling Function Coefficients (continued)

N	n	$h(n)$	N	n	$h(n)$
$N = 4$	0	0.0357790693211718		20	-0.04083679928820061
	1	0.05569749441044538		21	-0.06088758428431618
	2	0.07976433639592423		22	-0.07481767391215044
	3	0.1082958230436259		23	-0.0816783848736904
	4	0.1416081821195683		24	-0.080521033870852
	5	0.1800176413897692		25	-0.07039693760558663
	6	0.2238404286202469		26	-0.05035741277986717
	7	0.2733927715770168		27	-0.01945377609560594
	8	0.3289908980260989		28	0.02326265574523489
	9	0.3909510357335097		29	0.0787405660407039
	10	0.3164731351805834		30	0.004812360804177019
	11	0.3124322783456108		31	0.00898557754597906
	12	0.2991084484822011		32	0.01217265505175558
	13	0.2755529622923021		33	0.0140573655554852
	14	0.2408171364778582		34	0.01432348129115213
	15	0.1939522877408066		35	0.01265477449273811
	16	0.1340097327831202		36	0.00873501739422478
	17	0.060040788306722		37	0.002247982229594825
	18	-0.02890322898644371		38	-0.007122558767169427
	19	-0.1337710023944041		39	-0.01969283336208572

Table C.15. $M = 10$ Scaling Function Coefficients (continued)

N	n	$h(n)$	N	n	$h(n)$
$N = 5$	0	0.01825316481863816	25	-0.1166304281090333	
	1	0.03126076932886969	26	-0.1033012088451528	
	2	0.04811319371493264	27	-0.0708559174025254	
	3	0.06935979201581777	28	-0.01599842954738051	
	4	0.0955815410471259	29	0.06475711561415665	
	5	0.1273910404010694	30	-0.007445332551242246	
	6	0.1654325124464666	31	0.006246811439950762	
	7	0.2103818023287509	32	0.0189848166178308	
	8	0.2629463779699623	33	0.02951995012477937	
	9	0.3238653300687631	34	0.03647698799679233	
	10	0.3026435480071967	35	0.0383542151631957	
	11	0.3175769936723825	36	0.0335234254470862	
	12	0.3240477251715959	37	0.02022992156497594	
	13	0.3201745541150132	38	-0.003407484872944622	
	14	0.3039498010062402	39	-0.03939647336298435	
	15	0.2732392952426608	40	0.001394609585293693	
	16	0.225782375115017	41	-0.000788523372513339	
	17	0.1591918878076512	42	-0.002881124130846402	
	18	0.0709541893986625	43	-0.004650066416809651	
	19	-0.04157085514071924	44	-0.005830601180903728	
	20	0.001381776241089483	45	-0.006126356597019323	
	21	-0.03806828496760772	46	-0.005209338062436231	
	22	-0.07203684527235055	47	-0.002719928197824462	
	23	-0.0981764637378433	48	0.001733113152756642	
	24	-0.1139499627682312	49	0.00857264892185734	

Table C.16. $M = 11$ Scaling Function Coefficients

N	n	$h(n)$	N	n	$h(n)$
$N = 1$	0	0.3015113445777636	$N = 3$	0	0.06658894719044639
	1	0.3015113445777636		1	0.0906314685753338
	2	0.3015113445777636		2	0.1171658192542526
	3	0.3015113445777636		3	0.146191999227203
	4	0.3015113445777636		4	0.1777100084941847
	5	0.3015113445777636		5	0.2117198470551982
	6	0.3015113445777636		6	0.2482215149102427
	7	0.3015113445777636		7	0.2872150120593191
	8	0.3015113445777636		8	0.328700335502427
	9	0.3015113445777636		9	0.3726774942395661
$N = 2$	10	0.3015113445777636		10	0.4191464792707365
	0	0.1370506111717107		11	0.2683404520246002
	1	0.1644607334060529		12	0.2476655314891714
	2	0.191870855640395		13	0.2220069523656809
	3	0.2192809778747371		14	0.1913647146541253
	4	0.2466911001090792		15	0.155738818354509
	5	0.2741012223434214		16	0.1151292634668275
	6	0.3015113445777635		17	0.06953604999108532
	7	0.3289214668121057		18	0.01895917792727797
	8	0.3563315890464477		19	-0.03660135272459009
	9	0.3837417112807897		20	-0.0971455419645233
	10	0.4111518335151321		21	-0.1626733897925181
	11	0.1644607334060526		22	-0.03341805463723713
	12	0.1370506111717105		23	-0.03678565548669566
	13	0.1096404889373683		24	-0.03766142704212383
	14	0.0822303667030263		25	-0.0360453693035192
	15	0.05482024446868417		26	-0.031937482270884
	16	0.02741012223434192		27	-0.02533776594421677
	17	0.0		28	-0.01624622032351841
	18	-0.02741012223434225		29	-0.004662845408788307
	19	-0.05482024446868439		30	0.00941235879997315
	20	-0.0822303667030265		31	0.02597939230276605
	21	-0.1096404889373686		32	0.04503825509959048

Table C.17. $M = 11$ Scaling Function Coefficients (continued)

N	n	$h(n)$	N	n	$h(n)$
$N = 4$	0	0.03323835505706048		22	-0.03779289273231257
	1	0.05016659207376368		23	-0.05565017827871089
	2	0.07032818481276115		24	-0.06879105524616591
	3	0.0939496632098697		25	-0.07653593382727309
	4	0.121257557200906		26	-0.07820522421456389
	5	0.1524783967216869		27	-0.0731193366005698
	6	0.1878387117080287		28	-0.06059868117788625
	7	0.227565032095749		29	-0.03996366813902341
	8	0.271883887820664		30	-0.01053470767655185
	9	0.3210218088185881		31	0.02836779001698986
	10	0.3752053250253446		32	0.07742341474905601
	11	0.3017075461484975		33	0.004358336098835736
	12	0.2989488945135434		34	0.00804603626346712
	13	0.2889820050056997		35	0.01099220999978634
	14	0.2711272878174995		36	0.01297032737197767
	15	0.2447051531415028		37	0.01375385844422716
	16	0.2090360111702481		38	0.01311627328071552
	17	0.1634402720963095		39	0.01083104194562656
	18	0.1072383461122186		40	0.006671634503144009
	19	0.03975064341049972		41	0.0004115210174506223
	20	-0.03970242581623751		42	-0.00817582844727006
	21	-0.1318004513754971		43	-0.01931694382683486

Table C.18. $M = 11$ Scaling Function Coefficients (continued)

N	n	$h(n)$	N	n	$h(n)$
$N = 5$	0	0.01683606451412131		28	-0.1080661539025414
	1	0.02780185466777634		29	-0.0909617062960706
	2	0.04173632948946605		30	-0.05800772206475813
	3	0.0590287091320898		31	-0.006807099400134576
	4	0.080088807379088		32	0.06516082529043388
	5	0.1053470316444427		33	-0.007820367758597513
	6	0.1352543829726773		34	0.004080497357108471
	7	0.1702824560388567		35	0.01536517929480397
	8	0.2109234391485835		36	0.02515638725060398
	9	0.2576901142380059		37	0.03249445589852939
	10	0.311115856873819		38	0.03633734539059219
	11	0.287574313682633		39	0.03556064135665338
	12	0.3011717418651756		40	0.02895755490425245
	13	0.3083085027372334		41	0.01523892261882054
	14	0.3076542456231692		42	-0.006966793436390617
	15	0.2977962453251734		43	-0.03911350572021632
	16	0.2772394021232571		44	0.001442821356839374
	17	0.2444062417753798		45	-0.0004481680813412936
	18	0.1976369155170801		46	-0.002292714917654592
	19	0.1351892000620296		47	-0.003928128935157815
	20	0.05523849760157873		48	-0.005171126286359851
	21	-0.04412216419524384		49	-0.00581782949323717
	22	0.003478512959986801		50	-0.00564376744721784
	23	-0.03109458105382146		51	-0.004403875409191849
	24	-0.06160595184871909		52	-0.0018324950095088
	25	-0.0863998683156524		53	0.002356625752024798
	26	-0.1036970375613464		54	0.00847033250614304
	27	-0.1115946049100103			

Appendix D. *Plots of Compactly-Supported Scaling Functions*

This Appendix contains the plots of η_k which correspond to the scaling function coefficients in Appendix C. In some of the plots, it appears the function does not go to zero at its rightmost point. This is caused by using a finite iteration k . At higher iterations, the function would converge toward zero, however, the number of plotting points required would be impractical. In all of the following plots, $\phi(t)$ is on the vertical axis and t is on the horizontal axis.

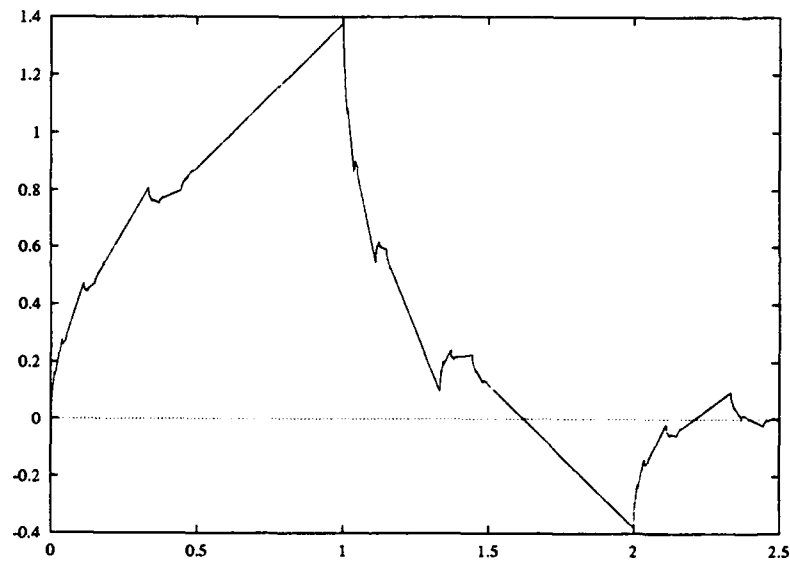


Figure D.1. Scaling Function (η_7) for $M = 3$ and $N = 2$

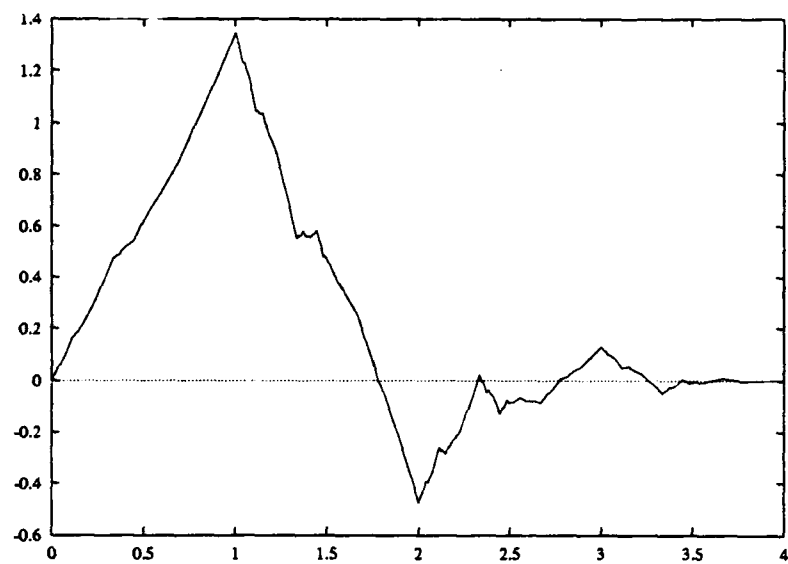


Figure D.2. Scaling Function (η_7) for $M = 3$ and $N = 3$

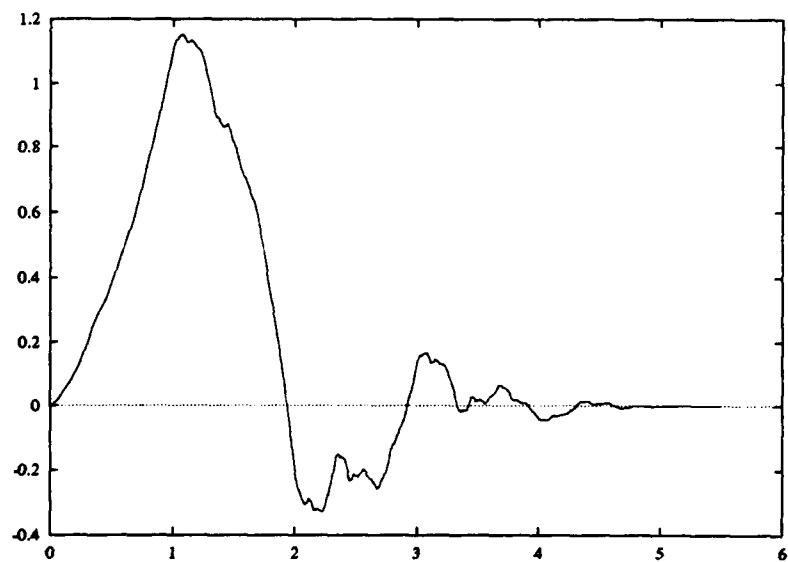


Figure D.3. Scaling Function (η_7) for $M = 3$ and $N = 4$

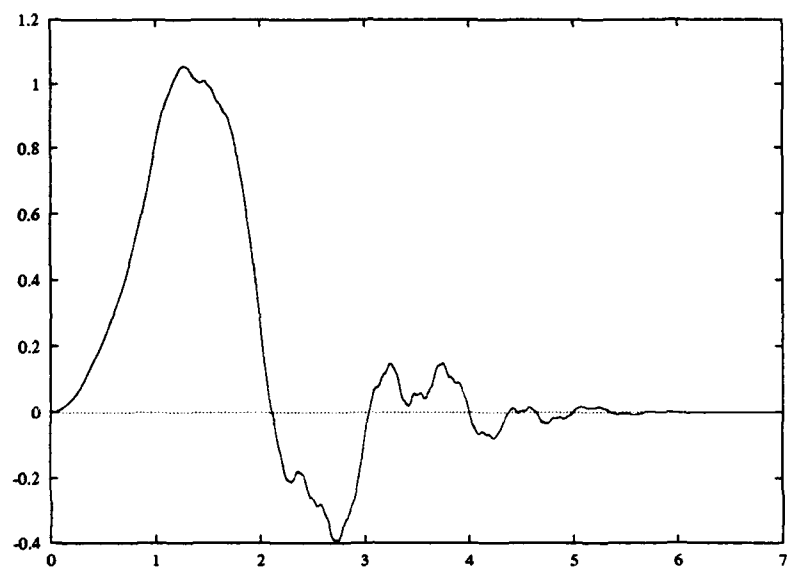


Figure D.4. Scaling Function (η_τ) for $M = 3$ and $N = 5$

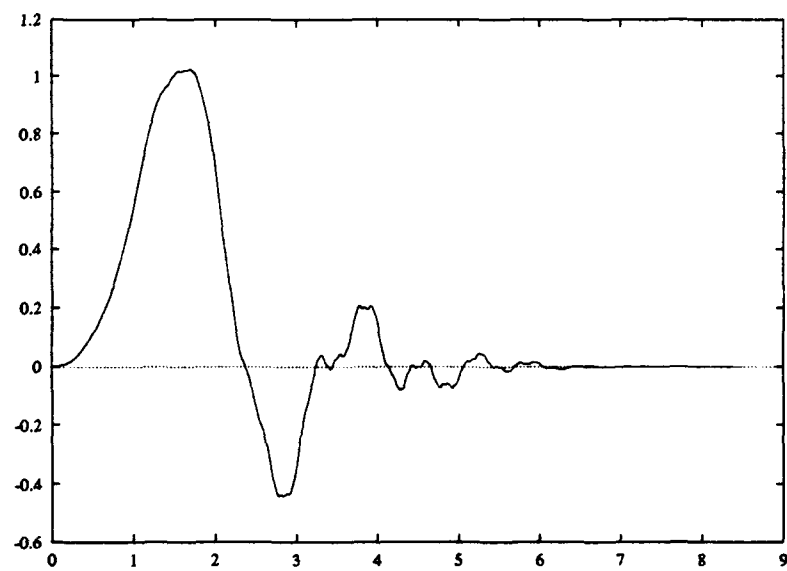


Figure D.5. Scaling Function (η_τ) for $M = 3$ and $N = 6$

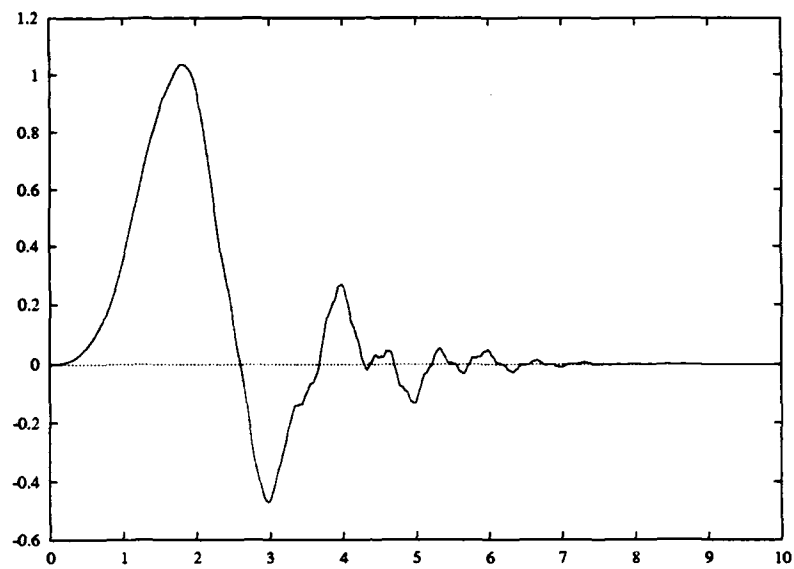


Figure D.6. Scaling Function (η_τ) for $M = 3$ and $N = 7$

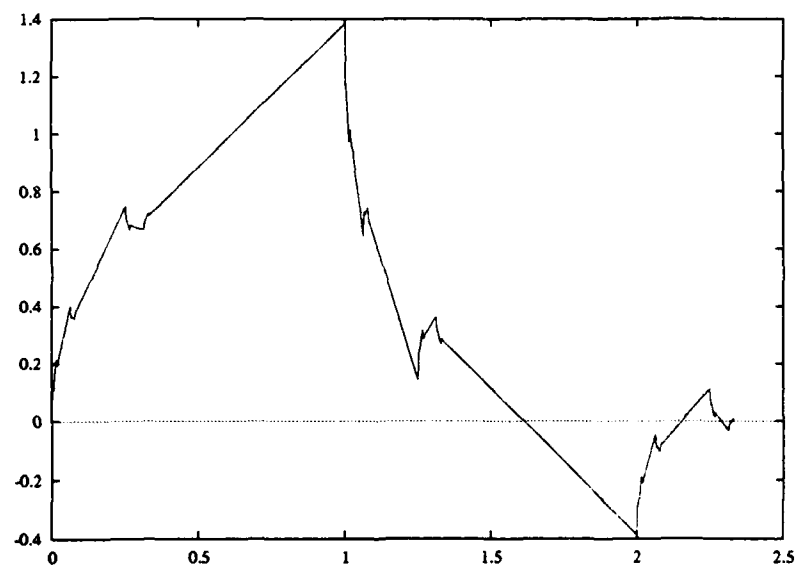


Figure D.7. Scaling Function (η_5) for $M = 4$ and $N = 2$

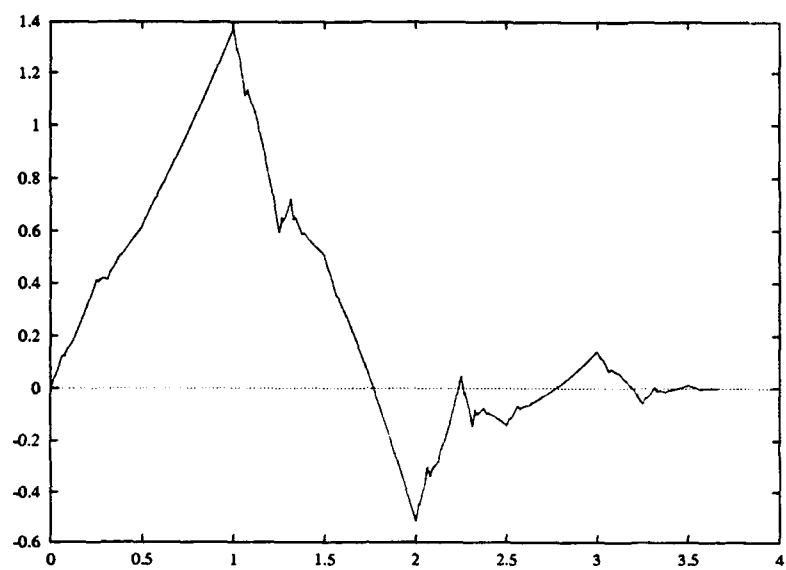


Figure D.8. Scaling Function (η_5) for $M = 4$ and $N = 3$

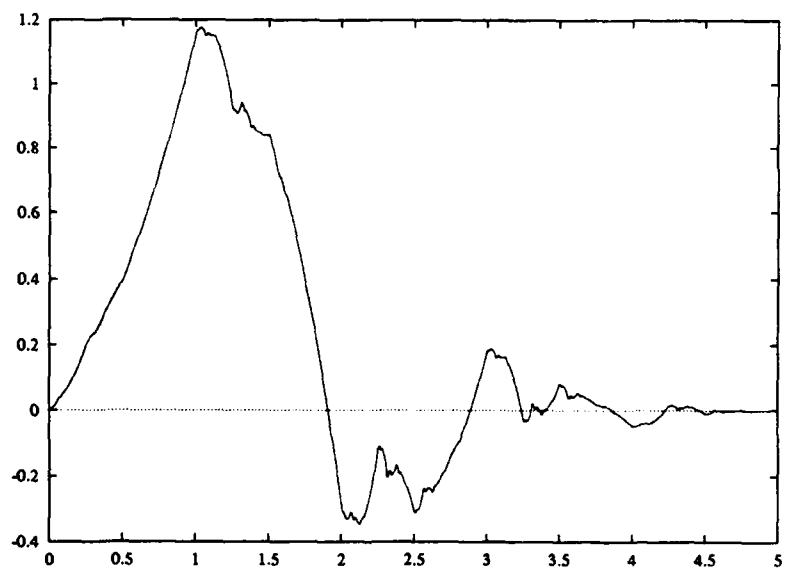


Figure D.9. Scaling Function (η_5) for $M = 4$ and $N = 4$

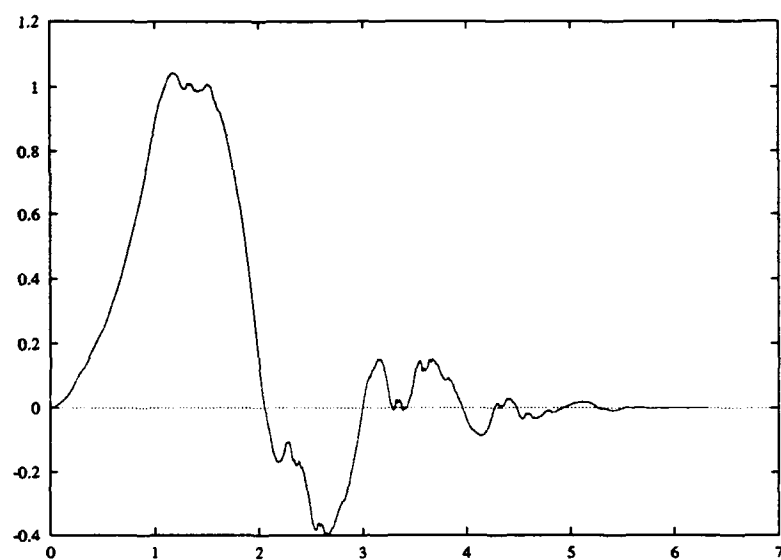


Figure D.10. Scaling Function (η_5) for $M = 4$ and $N = 5$

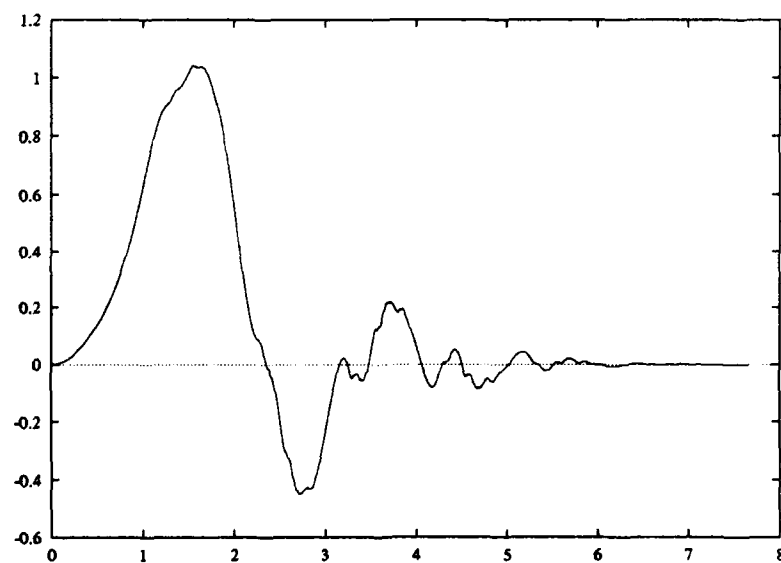


Figure D.11. Scaling Function (η_5) for $M = 4$ and $N = 6$

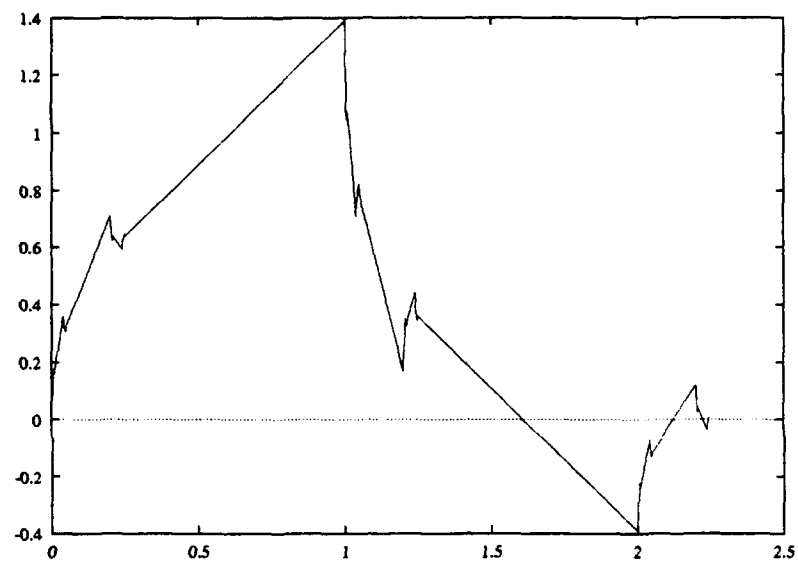


Figure D.12. Scaling Function (η_4) for $M = 5$ and $N = 2$

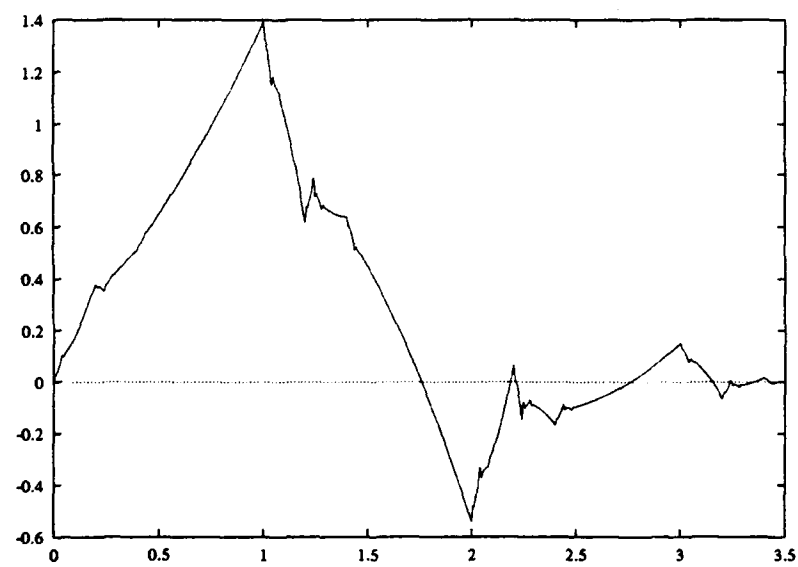


Figure D.13. Scaling Function (η_4) for $M = 5$ and $N = 3$

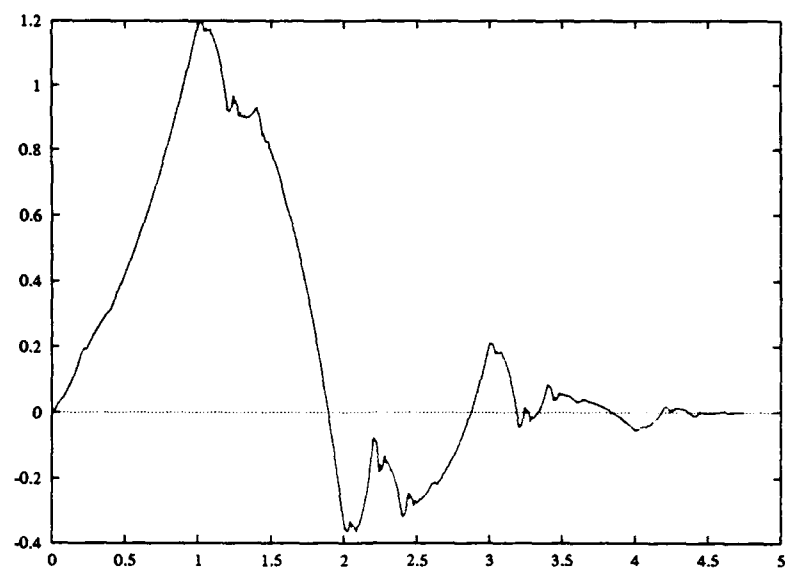


Figure D.14. Scaling Function (η_4) for $M = 5$ and $N = 4$

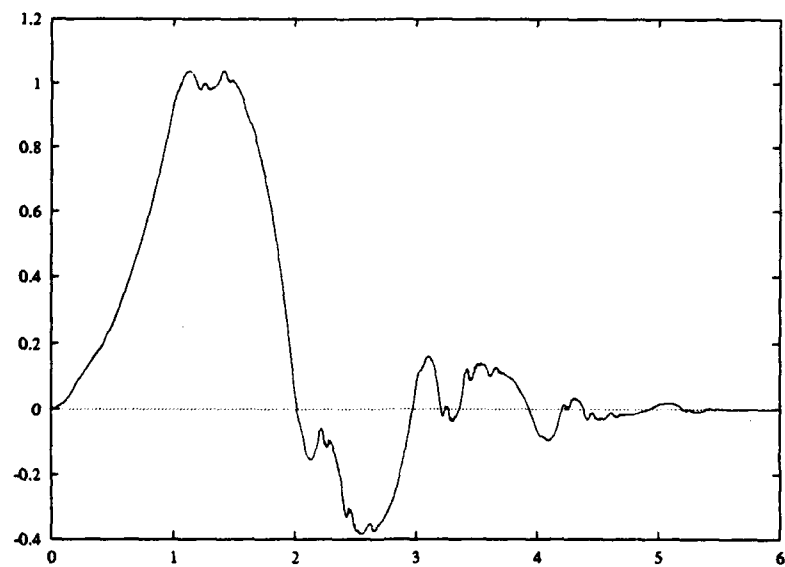


Figure D.15. Scaling Function (η_4) for $M = 5$ and $N = 5$

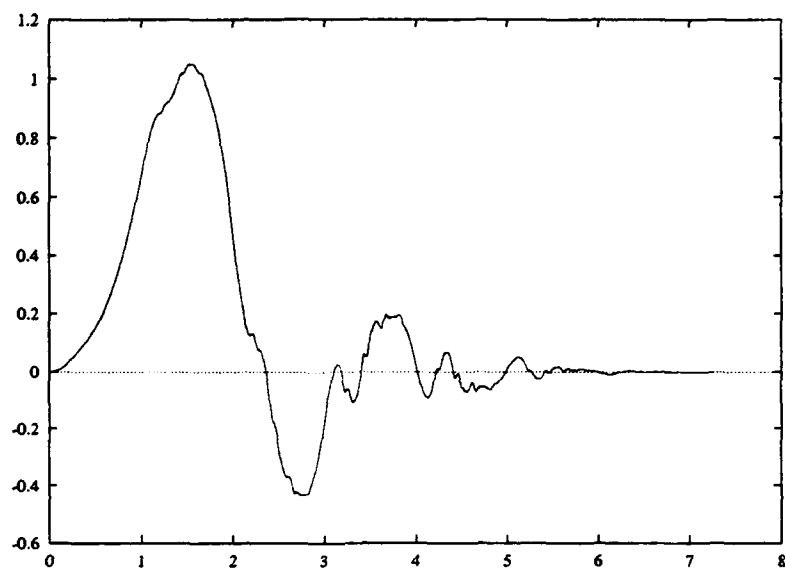


Figure D.16. Scaling Function (η_4) for $M = 5$ and $N = 6$

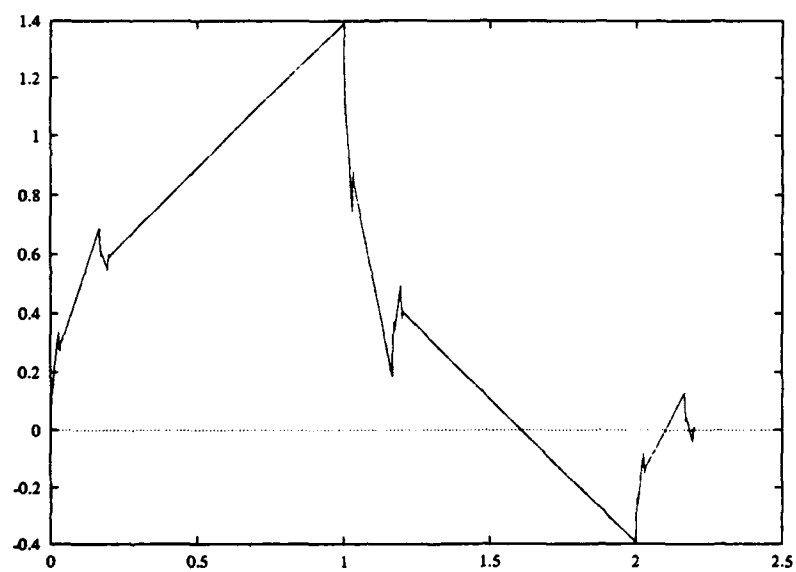


Figure D.17. Scaling Function (η_4) for $M = 6$ and $N = 2$

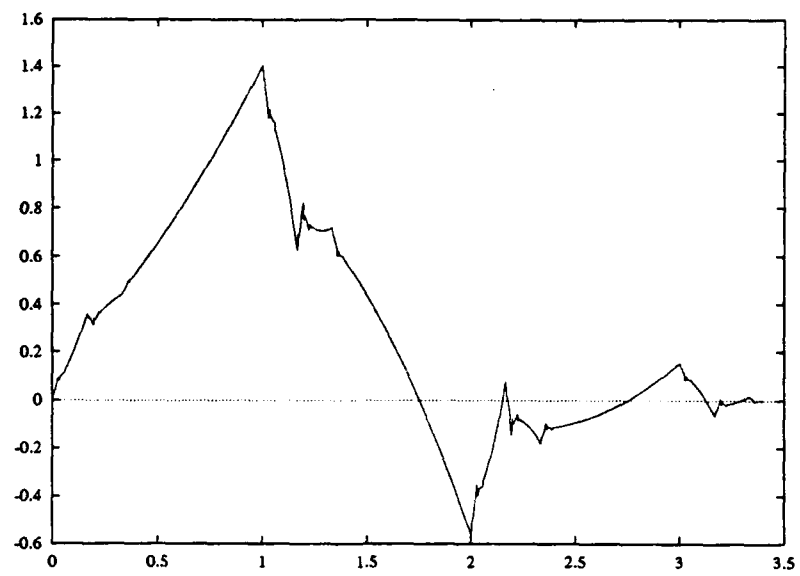


Figure D.18. Scaling Function (η_4) for $M = 6$ and $N = 3$

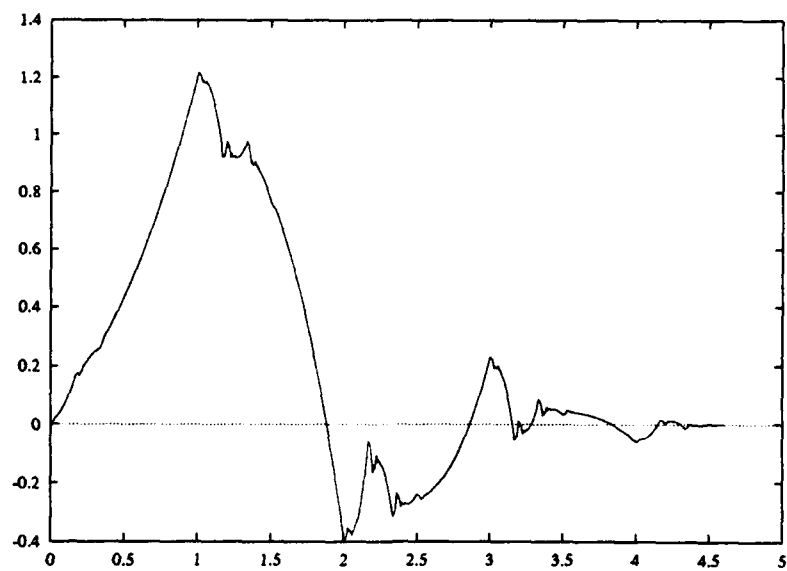


Figure D.19. Scaling Function (η_4) for $M = 6$ and $N = 4$

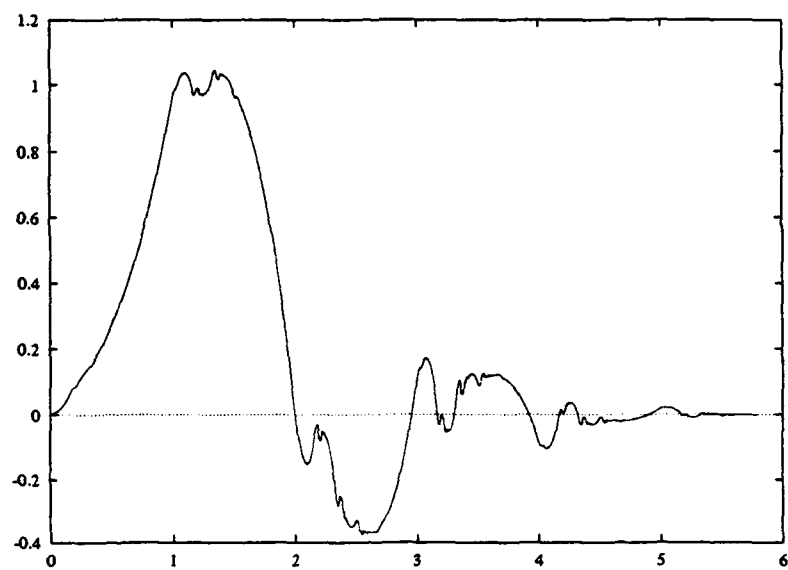


Figure D.20. Scaling Function (η_4) for $M = 6$ and $N = 5$

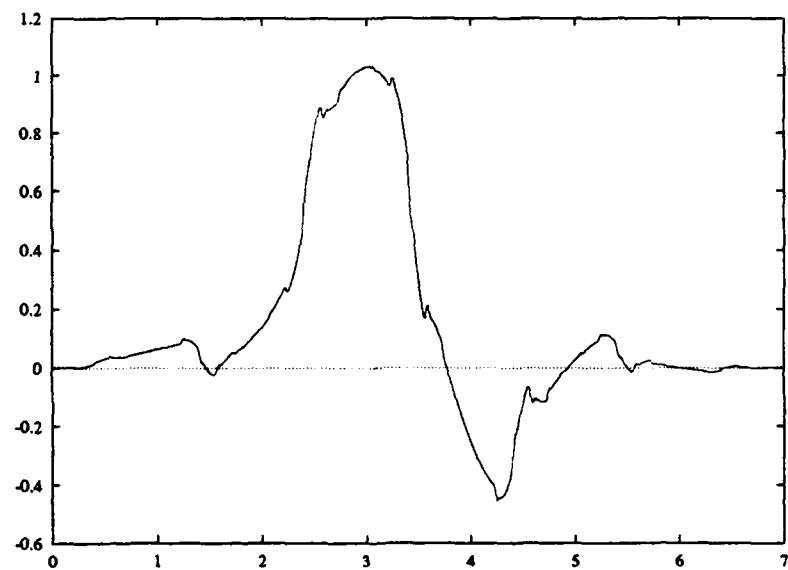


Figure D.21. Scaling Function (η_4) for $M = 6$ and $N = 6$

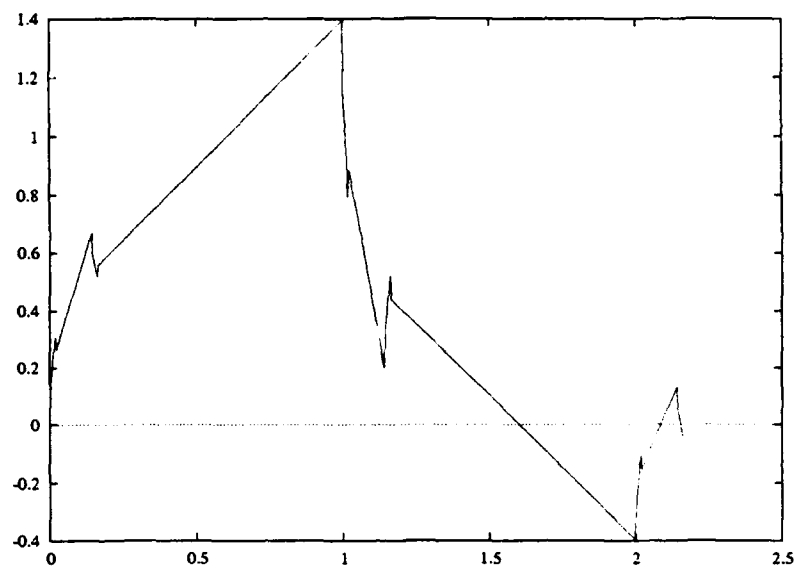


Figure D.22. Scaling Function (η_3) for $M = 7$ and $N = 2$

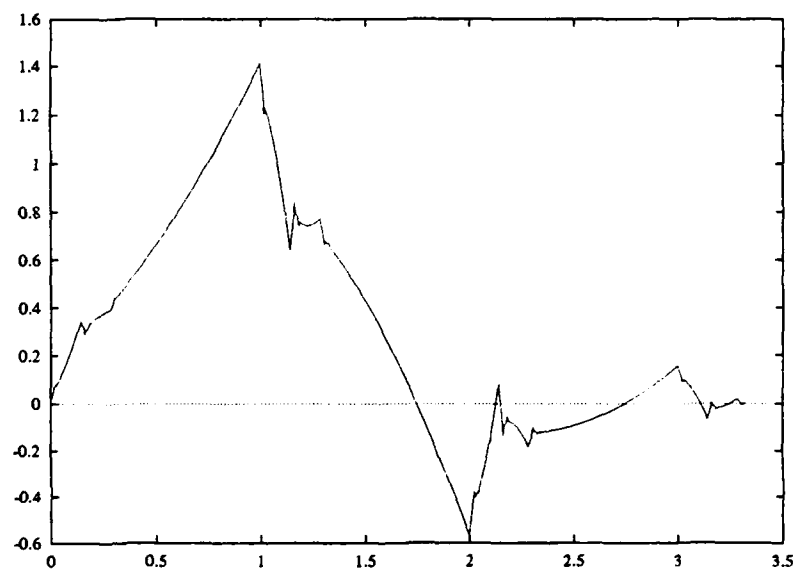


Figure D.23. Scaling Function (η_3) for $M = 7$ and $N = 3$

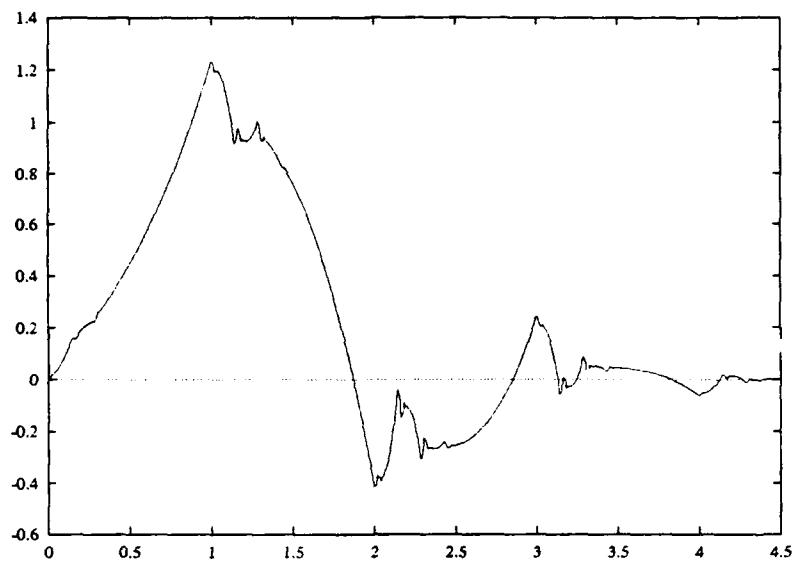


Figure D.24. Scaling Function (η_3) for $M = 7$ and $N = 4$

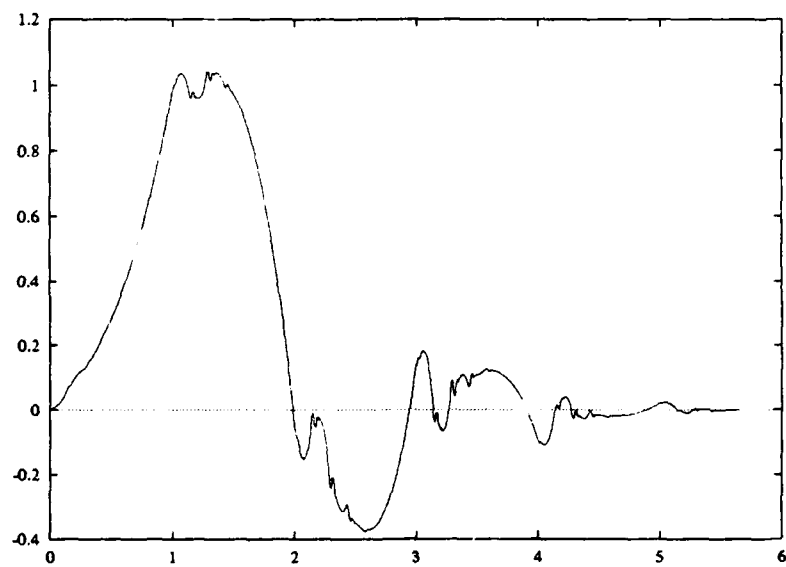


Figure D.25. Scaling Function (η_3) for $M = 7$ and $N = 5$

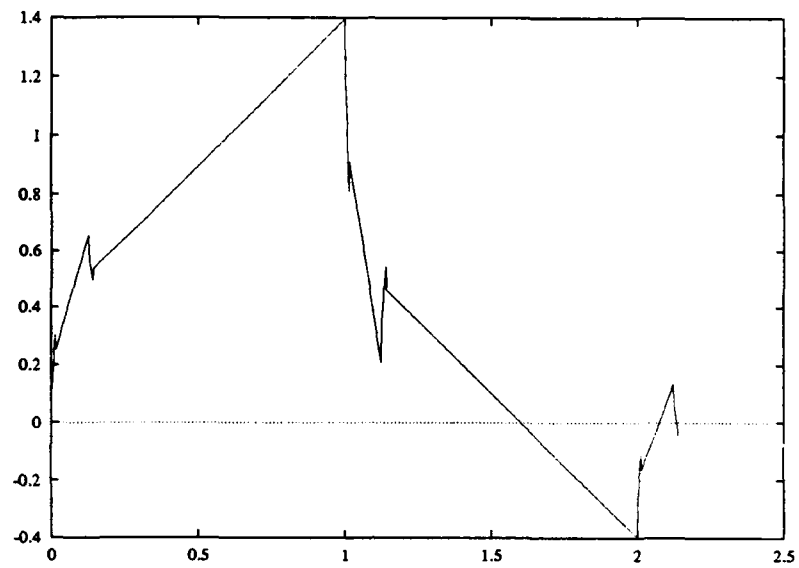


Figure D.26. Scaling Function (η_3) for $M = 8$ and $N = 2$

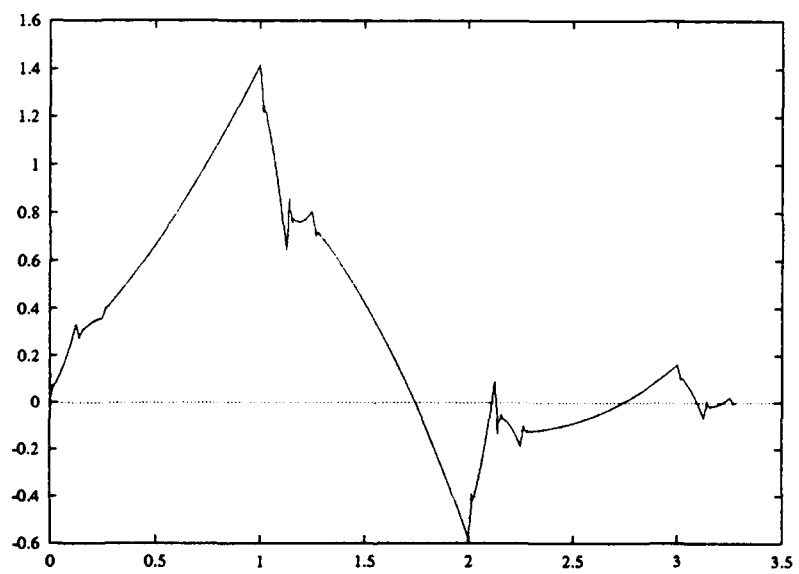


Figure D.27. Scaling Function (η_3) for $M = 8$ and $N = 3$

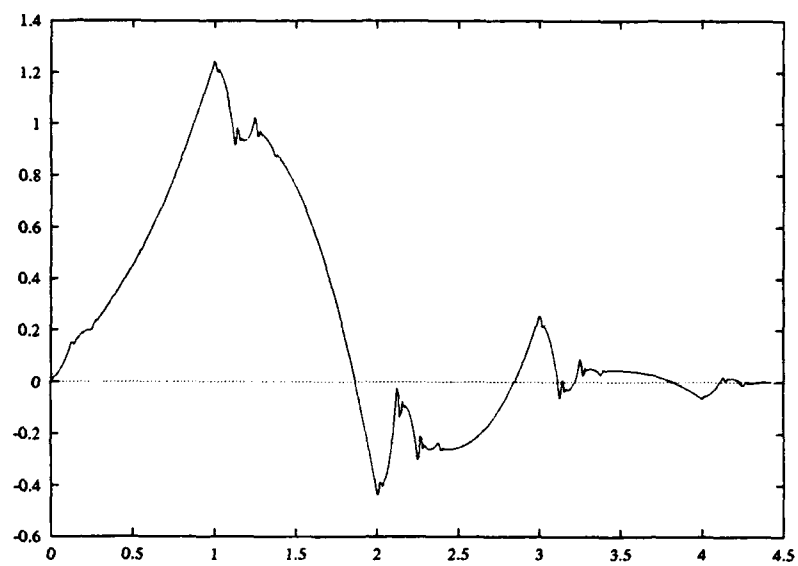


Figure D.28. Scaling Function (η_3) for $M = 8$ and $N = 4$

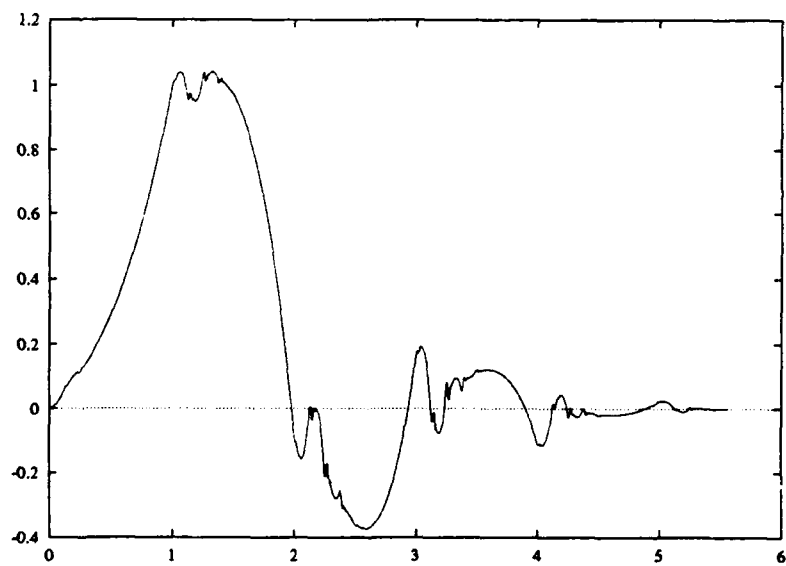


Figure D.29. Scaling Function (η_3) for $M = 8$ and $N = 5$

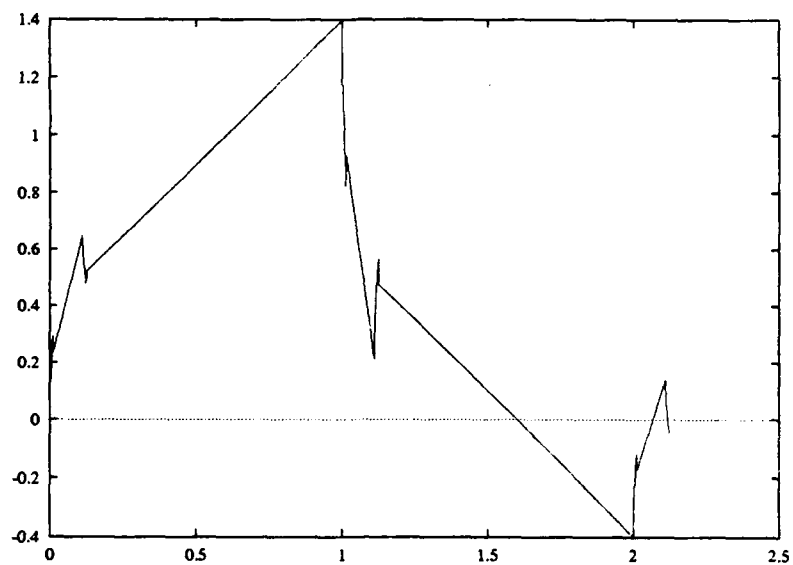


Figure D.30. Scaling Function (η_3) for $M = 9$ and $N = 2$

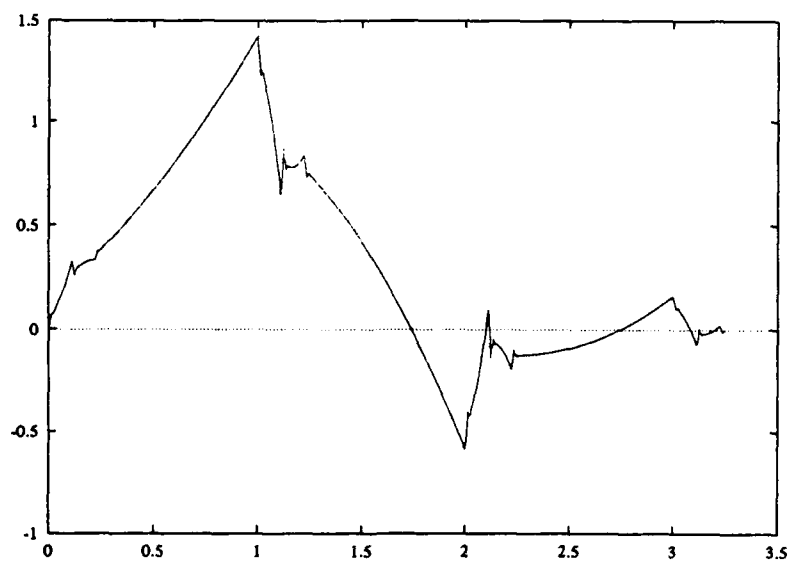


Figure D.31. Scaling Function (η_3) for $M = 9$ and $N = 3$

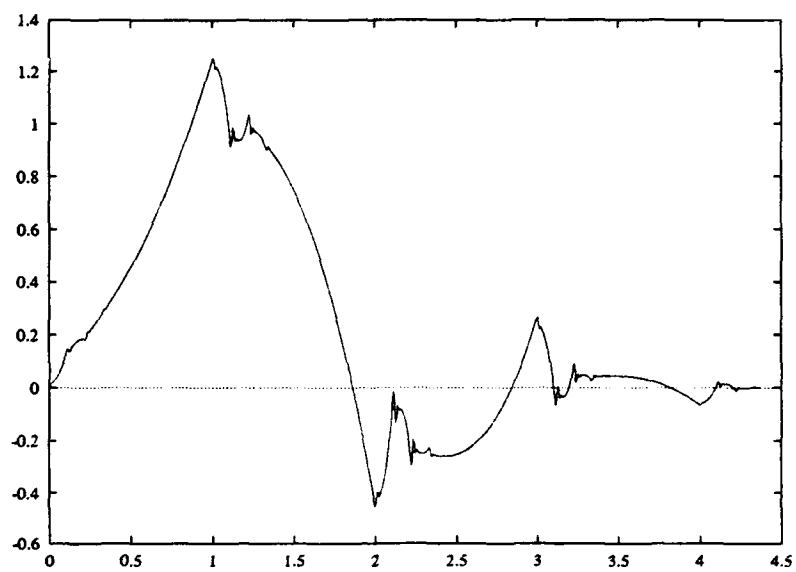


Figure D.32. Scaling Function (η_3) for $M = 9$ and $N = 4$

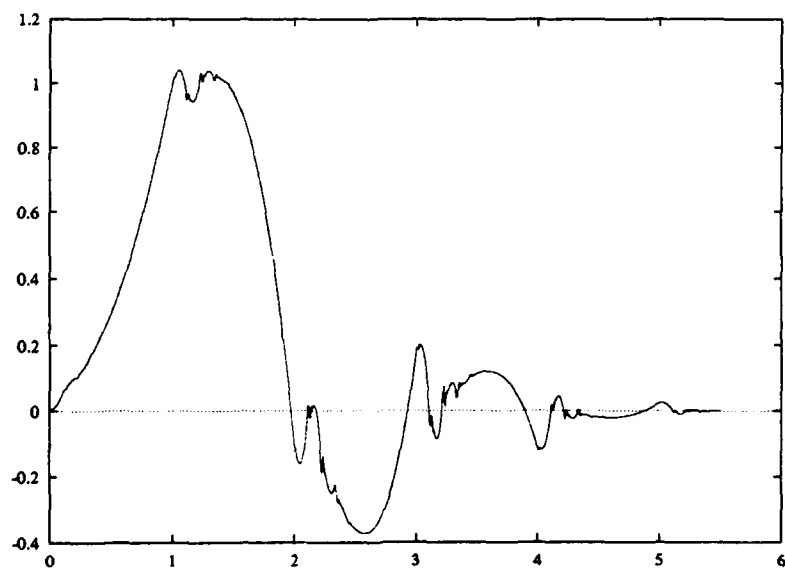


Figure D.33. Scaling Function (η_3) for $M = 9$ and $N = 5$

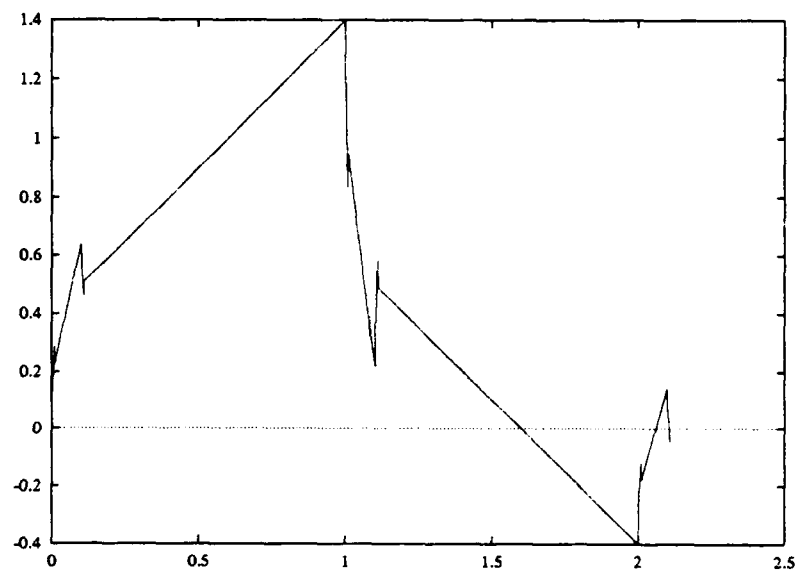


Figure D.34. Scaling Function (η_3) for $M = 10$ and $N = 2$

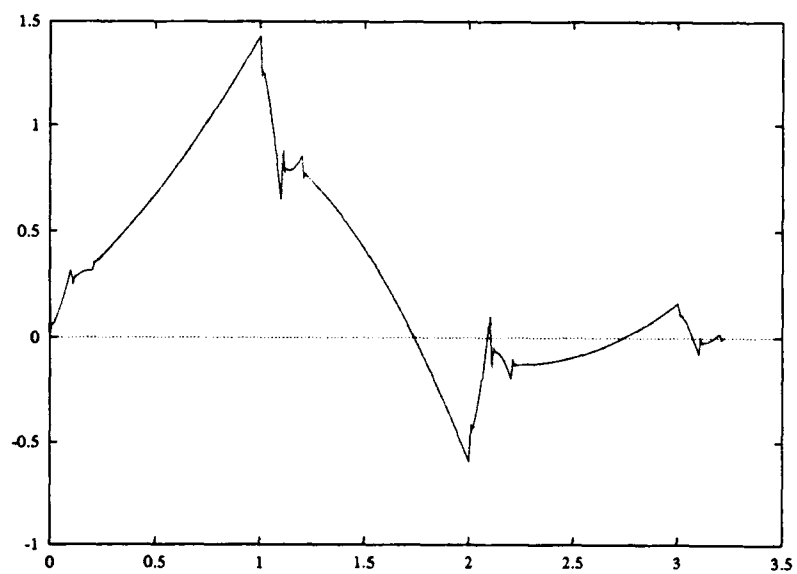


Figure D.35. Scaling Function (η_3) for $M = 10$ and $N = 3$

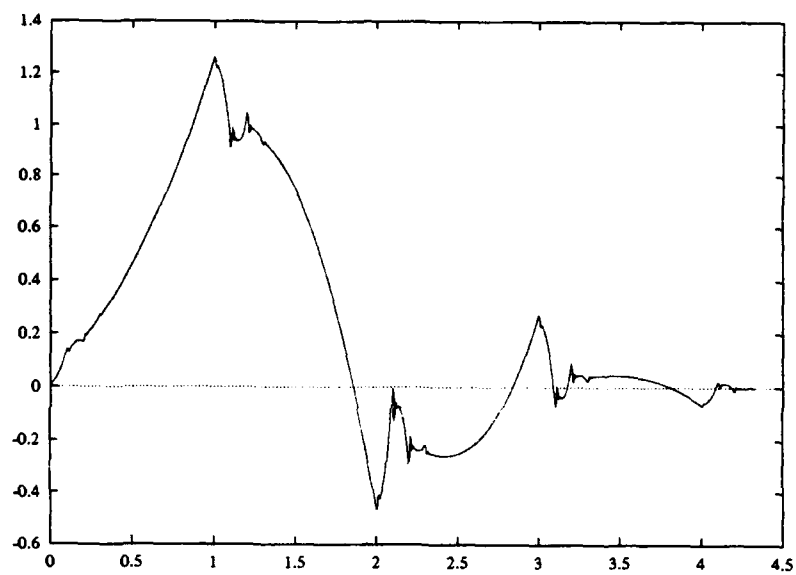


Figure D.36. Scaling Function (η_3) for $M = 10$ and $N = 4$

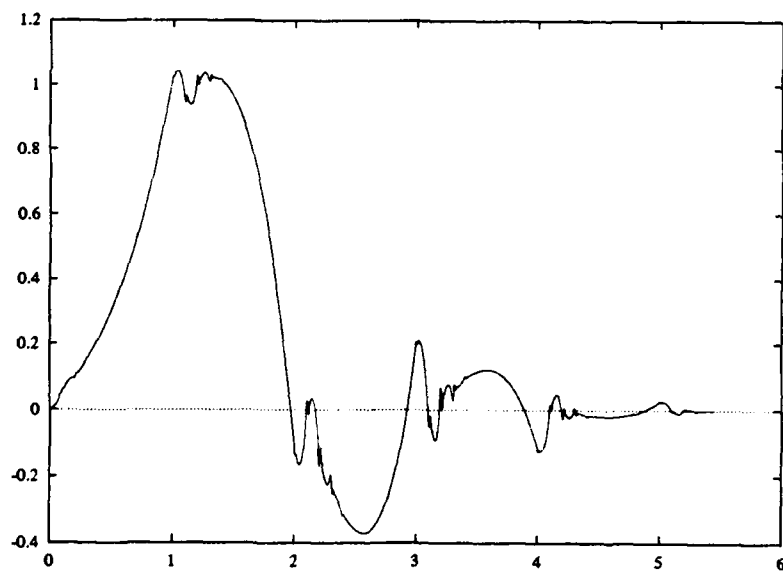


Figure D.37. Scaling Function (η_3) for $M = 10$ and $N = 5$

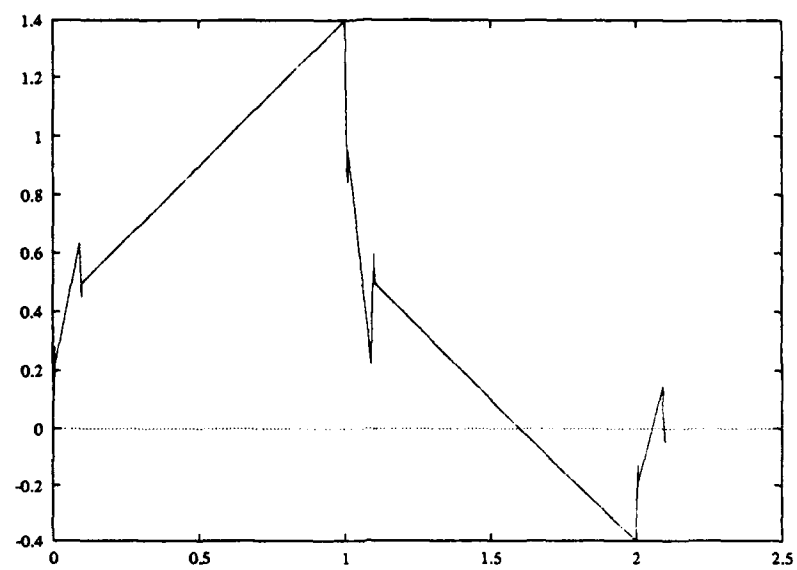


Figure D.38. Scaling Function (η_3) for $M = 11$ and $N = 2$

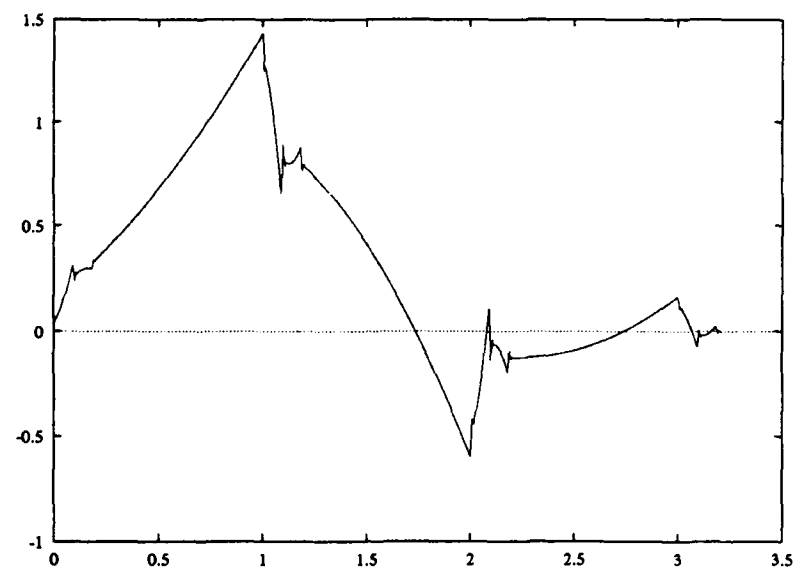


Figure D.39. Scaling Function (η_3) for $M = 11$ and $N = 3$

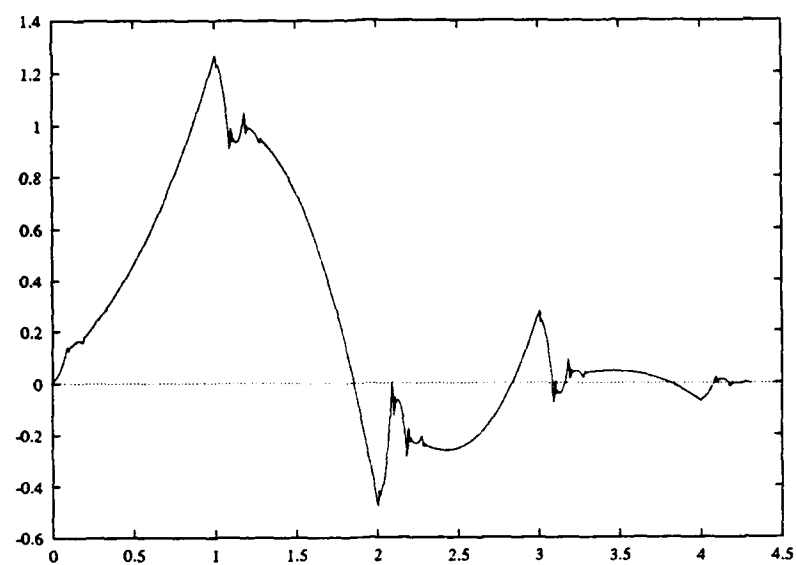


Figure D.40. Scaling Function (η_3) for $M = 11$ and $N = 4$

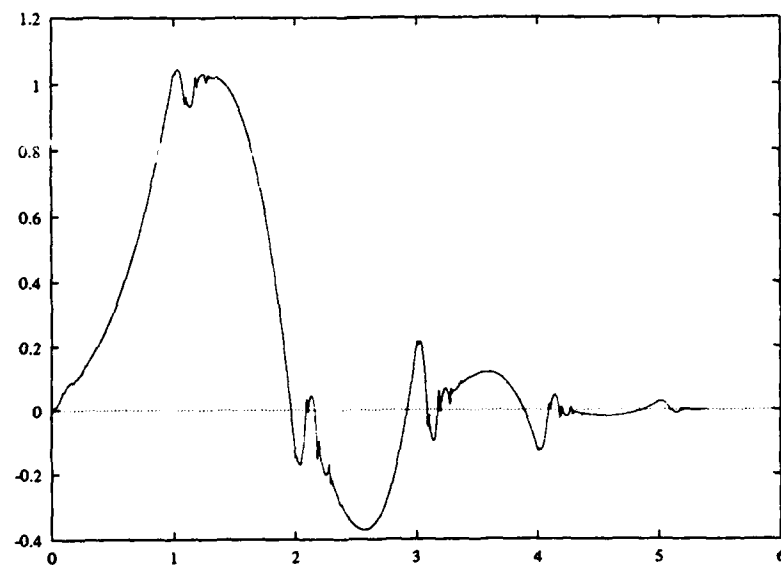


Figure D.41. Scaling Function (η_3) for $M = 11$ and $N = 5$

Vita

Captain Bruce Patrick Anderson was born May 30, 1965 in Roswell, NM. He graduated from Woodbridge High School, Woodbridge VA, in 1983 after which he attended the University of Virginia. He graduated with a Bachelor of Science in Electrical Engineering in 1987 and received an ROTC commission as a Second Lieutenant in the United States Air Force.

His first assignment was to the 31 Test and Evaluation Squadron (SAC), Edwards AFB CA. He was initially responsible for conducting maintainability evaluations on B-1B operational and support software. He was reassigned as an operations engineer in 1989 where he was responsible for planning, scheduling, and conducting B-1B test missions in support of several national-priority test efforts. He was selected for AFIT in residence in April, 1991.

Captain Anderson is engaged to be married to Ms. Julie Phipps of Pittsfield MA.

Permanent address: 10851 Meadow Pond Lane
Oakton, Virginia 22124

Bibliography

1. Anderson, Timothy, PhD. Personal interview, October 1992.
2. Auscher, Pascal. *Ondelettes Fractales et Applications*. PhD dissertation, Université de Paris-Dauphine, 1988.
3. Ausher, P. "Wavelet Bases for $L^2(\mathbb{R})$ with Rational Dilation Factor." *Wavelets and their Applications* edited by M. B. Ruskai and others, Jones and Barlett, 1992.
4. Burt, P. and E. Adelson. "The Laplacian Pyramid as a Compact Image Code," *IEEE Transactions on Communications*, 31:217-236 (1983).
5. Carey, John. "Wavelets Are Causing Ripples Everywhere," *Business Week* (3 February 1992).
6. Daubechies, Ingrid. "Orthonormal Bases of Compactly Supported Wavelets," *Commun. Pure. Appl. Math.*, 41:909-996 (November 1988).
7. Daubechies, Ingrid. "The Wavelet Transform, Time-Frequency Localization and Signal Analysis," *IEEE Transactions on Information Theory*, 36(5):961-1003 (September 1990).
8. Daubechies, Ingrid. *Ten Lectures on Wavelets*. Society of Industrial and Applied Mathematics, 1992.
9. Grossman, A. and J. Morlet. "Decomposition of Hardy Functions into Square Integrable Wavelets of Constant Shape," *SIAM Journal Math. Anal.*, 15(4):723-736 (July 1984).
10. Grossman, Alexander, "The History of Wavelets." Banquet presentation. The Role of Wavelets in Signal Processing Applications, 12 March 1992.
11. Kovačević, Jelena and Martin Vetterli. "Perfect Reconstruction Filter Banks with Rational Sampling Rates in One and Two Dimensions," *Proc. SPIE Conf. on Visual Communications and Image Processing*, 1199 (November 1989).
12. Mallat, Stephane G. "Multiresolution Approximations and Wavelet Orthonormal Bases of $L^2(\mathbb{R})$," *Transactions of the American Mathematical Society*, 315(1):69-87 (September 1989).
13. Mallat, Stephane G. "A Theory for Multiresolution Signal Decomposition: The Wavelet Representation," *IEEE Transactions on Pattern Analysis and Machine Intelligence*, 11(7):674-693 (July 1989).
14. Meyer, Yves. *Ondelettes et Operateurs*. Paris, France: Hermann, 1988.
15. Meyer, Yves. "Orthonormal Wavelets." *Wavelets, Time-Frequency Methods, and Phase Space* edited by J. A. Combes and Ph. Tchamichian, 21-37, Berlin: Springer-Verlag, 1989.

16. Nguyen, Truong Q. and P. P. Vaidyanathan. "Maximally Decimated Perfect-Reconstruction FIR Filter Banks with Pairwise Mirror-Image Analysis (and Synthesis) Frequency Responses," *IEEE Transactions on Acoustics, Speech and Signal Processing*, 36(5):693-706 (May 1988).
17. Oppenheim, Alan V. and Ronald W. Schaffer. *Discrete Time Signal Processing*. Englewood Cliffs, NJ: Prentice-Hall, 1989.
18. Parsons, Thomas. *Voice and Speech Processing*. McGraw-Hill, 1987.
19. Rioul, Oliver and Martin Vetterli. "Wavelets and Signal Processing," *IEEE Signal Processing Magazine*, 14-38 (October 1991).
20. Smith, Mark J. T. and Thomas P. Barnwell. "Exact Reconstruction Techniques for Tree-Structured Subband Coders," *IEEE Transactions on Acoustics, Speech and Signal Processing*, 34(3):434-441 (June 1986).
21. Smith, M.J.T. and III T.P. Barnwell. "A unifying framework for analysis/synthesis systems based on maximally decimated filter banks," *ICASSP Proceedings*, 521-524 (March 1985). Tampa, FL.
22. Stakgold, Ivar. *Green's Functions and Boundary Value Problems*. John Wiley & Sons, 1979.
23. Vaidyanathan, P. P. "Theory and Design of M-Channel Maximally Decimated Quadrature Mirror Filters with Arbitrary M, Having the Perfect-Reconstruction Property," *IEEE Transactions on Acoustics, Speech and Signal Processing*, 35(4):476-492 (April 1987).
24. Vaidyanathan, P. P. "Multirate Digital Filters, Filter Banks, Polyphase Networks, and Applications: A Tutorial," *Proceedings of the IEEE*, 78(1):56-93 (January 1990).
25. Vaidyanathan, P. P. *Multirate Digital Signal Processing*. 1992. unpublished draft copy.
26. Vaidyanathan, P. P. and others. "Improved Technique for Design of Perfect Reconstruction FIR QMF Banks with Lossless Polyphase Matrices," *IEEE Transactions on Acoustics, Speech and Signal Processing*, 37(7):1042-1056 (July 1989).
27. Vetterli, Martin and Didier Le Gall. "Perfect Reconstruction FIR Filter Banks: Some Properties and Factorizations," *IEEE Transactions on Acoustics, Speech and Signal Processing*, 37(7):1057-1071 (July 1989).
28. Vetterli, Martin and Cormac Herley. "Wavelets and Filter Banks: Theory and Design," *IEEE Transaction on Signal Processing*, 40(9):2207-2232 (September 1992).

REPORT DOCUMENTATION PAGE

Form Approved
OMB No. 0704-0188

Public reporting burden for this collection of information is estimated to average 1 hour per response, including the time for reviewing instructions, searching existing data sources, gathering and maintaining the data needed, and completing and reviewing the collection of information. Send comments regarding this burden estimate or any other aspect of this collection of information, including suggestions for reducing this burden, to Washington Headquarters Services, Directorate for Information Operations and Reports, 1215 Jefferson Davis Highway, Suite 1204, Arlington, VA 22202-4302, and to the Office of Management and Budget, Paperwork Reduction Project (0704-0188), Washington, DC 20503.

1. AGENCY USE ONLY (Leave blank)		2. REPORT DATE December 1992	3. REPORT TYPE AND DATES COVERED Master's Thesis	
4. TITLE AND SUBTITLE Theory and Implementation of Wavelet Analyses in Rational Resolution Decompositions			5. FUNDING NUMBERS	
6. AUTHOR(S) Bruce P. Anderson, Captain, USAF				
7. PERFORMING ORGANIZATION NAME(S) AND ADDRESS(ES) Air Force Institute of Technology, WPAFB OH 45433-6583			8. PERFORMING ORGANIZATION REPORT NUMBER AFIT/GE/ENC/92D-1	
9. SPONSORING/MONITORING AGENCY NAME(S) AND ADDRESS(ES) Department of Defense R571 Ft. Meade, MD 20755 Contract Number: H98230-R5-92-9740			10. SPONSORING/MONITORING AGENCY REPORT NUMBER	
11. SUPPLEMENTARY NOTES				
12a. DISTRIBUTION/AVAILABILITY STATEMENT Approved for public release; distribution unlimited.			12b. DISTRIBUTION CODE	
13. ABSTRACT (Maximum 200 words) The multiresolution analysis (MRA) developed by Mallat and Meyer and further discussed by Daubechies is a useful tool in the analysis of sampled signals such as images and speech. This thesis develops the theory and implementation of a rational-resolution analysis (RRA) as an extension of the dyadic MRA for arbitrary rational dilation factors. We present a method to calculate families of compactly-supported scaling functions and wavelets based on arbitrary integer dilation factors and provide examples. The perfect-reconstruction properties of the RRA are discussed and it is demonstrated that the compactly-supported scaling functions and wavelets do not yield perfect-reconstruction. However, the approximate-reconstruction is demonstrated and families of basis functions which do lead to perfect reconstruction are characterized. Finally, comparisons are made between RRAs and conventional MRAs and illustrated with speech signals.				
14. SUBJECT TERMS Wavelets, Multiresolution Analysis, Multirate Digital Signal Processing			15. NUMBER OF PAGES 160	
			16. PRICE CODE	
17. SECURITY CLASSIFICATION OF REPORT UNCLASSIFIED	18. SECURITY CLASSIFICATION OF THIS PAGE UNCLASSIFIED	19. SECURITY CLASSIFICATION OF ABSTRACT UNCLASSIFIED	20. LIMITATION OF ABSTRACT UL	